Vpr-Controlled Manipulation of T Cell Physiology: NF-AT Activation and Protein Degradation as Key Mechanisms for HIV-1 Pathogenesis

Dissertation

der Mathematisch-Naturwissenschaftlichen Fakultät

der Eberhard-Karls-Universität zu Tübingen

zur Erlangung des Grades eines

Doktors der Naturwissenschaften

(Dr. rer. nat.)

vorgelegt von

M.Sc. Carlos Alberto Vanegas Torres

aus Baja California, Mexiko

Tübingen

2025

Gedruckt mit Genehmigung der Mathematisch-Naturwissenschaftlichen Fakultät der Eberhard-Karls-Universität zu Tübingen.

Tag der mündlichen Qualifikation: 21.05.2026

Dekan:	Prof. Dr. Thilo Stehle
1. Berichterstatter/-in:	Prof. Dr. Michael Schindler
2. Berichterstatter/-in:	Prof. Dr. Daniel Sauter
3. Berichterstatter/-in:	Prof. Dr. Rosa Lozano Durán

El Mar

Tan arduamente el mar,
tan arduamente,
el lento mar inmenso,
tan largamente en sí, cansadamente,
el hondo mar eterno.
Lento mar, hondo mar,
profundo mar inmenso…

Tan lenta y honda y largamente y tanto
insistente y cansado ser cayendo
como un llanto, sin fin,
pesadamente,
tenazmente muriendo…

Va creciendo sereno desde el fondo,
sabiamente creciendo,
lentamente, hondamente, largamente,
pausadamente,
mar,
arduo, cansado mar,
Padre de mi silencio.

Idea Vilariño Romani (1942)

«Poemas recobrados»
(Biblioteca Nacional 2020 | ISBN 978-9974-726-13-0)

Table of Contents

I List of Abbreviations

Abbreviation	Meaning
AIDS	Acquired Immunodeficiency Syndrome
AP	Alkaline Phosphatase
APS	Ammonium Persulfate
BSA	Bovine Serum Albumin
BP	Biological Process
cGAS-STING	Cyclic GMP-AMP synthase – Stimulator of Interferon Genes pathway
CoIP	Co-immunoprecipitation
crRNA	CRISPR RNA
DAPI	4',6-diamine-2-phenylindol
DEG	Differentially expressed gene
DMSO	Dimethylsulfoxide
DMEM	Dulbecco's modified Eagle's medium
dNTP	Deoxynucleoside triphosphate
DPBS	Dulbecco's phosphate buffered saline)
DSB	Double-strand break
DTT	Dithiothreitol
EDTA	Ethylenediaminetetraacetic acid
FANA ASO	2′-deoxy-2′-fluoro-D-arabinonucleic acid antisense oligonucleotide
FBS / FCS	Fetal Bovine Serum / Fetal Calf Serum
FDR	False Discovery Rate
FRET	Förster's Resonance Energy Transfer
GO	Gene ontology
HA	Haemagglutinin
HAART	Highly active antiretroviral therapy
HDAC	Histone Deacetylase
HEPES	4-(2-hydroxyethyl)-1-piperazineethanesulfonic acid)
hpi	Hours post-infection
hpt	Hours post-transfection
IF	Immunofluorescence
IL-2	Interleukin-2
IP	Immunoprecipitation
IRF	Interferon regulatory factor
ISG	Interferon-stimulated gene
kb	kilobase
KD/KO	Knockdown/Knockout

KG	Kusabira Green
LTNP	Long-term non-progressor
LTR	Long terminal repeat
MA	Matrix
MFI	Mean fluorescence intensity
NaCit	Sodium Citrate
NaPyr	Sodium Pyruvate
NC	Nucleocapsid
NF-κB	Nuclear Factor 'kappa-light-chain-enhancer' of activated B cells
NF-AT	Nuclear Factor of Activated T cells
NLS	Nuclear Localization Signal
ORF	Open reading frame
PCA	Principal component analysis
PEI	Polyethylenimine
PFA	Paraformaldehyde
PHA	*Phaseolus vulgaris* Leucoagglutinin
PI	Propidium Iodide
PIC	Pre-integration complex
PRR	Pattern Recognition Receptors
RNP	Ribonucleoprotein
RLR	Retinoic acid-inducible gene-I-like receptor
RT	Reverse transcription / reverse transcriptase
SDS	Sodium Dodecyl Sulfate
SEAP	Secreted Alkaline Phosphatase
SG	Stress Granule
SIVcpz	Simian Immunodeficiency Virus, chimpanzee lineage
SSB	Single-strand break
tracrRNA	trans-activating CRISPR RNA
TEMED	N,N,N',N'tetramethylenethylenediamine
TLR	Toll-like receptor
T_{FH}	T follicular helper cells
T_{RM}	T resident memory cells
VLP	Virus-Like Particles
Vpr	Viral protein R
vDNA	Viral DNA
WB	Western Blot
WRE	Wnt-responsive element

II Abstract (English)

Human immunodeficiency virus type 1 (HIV-1), the lentiviral pathogen behind the global AIDS pandemic, preferentially infects $CD4^+$ T lymphocytes, leading to their progressive depletion via both direct viral cytotoxicity and through increased rates of apoptosis. To achieve full pathogenicity *in vivo*, HIV-1 encodes multiple accessory proteins, most of which play defined roles at various steps of the viral replication cycle. In contrast, the 96-amino acid Viral Protein R (Vpr) is implicated in disrupting host cell physiology through a variety of mechanisms, such as facilitating the nuclear import of viral pre-integration complexes, as well as significantly boosting viral production by enhancing the transcriptional activity of viral LTRs. Further, Vpr is actively encapsidated into HIV-1 virions, allowing its direct delivery into host cells upon *de novo* infection. Collectively, these characteristics epitomize Vpr as a crucial supporting element in the establishment of a productive HIV-1 infection. Nevertheless, multiple gaps exist in the understanding of the mechanisms whereby Vpr allows HIV-1 to exert control over its host cell at various organizational levels, and many studies still fail to answer these questions in physiologically relevant models, such as donor-derived $CD4^+$ T lymphocytes. To address these issues, HIV-1 infection assays employing inhibitors for various signaling pathways were performed on T cell-derived models and primary $CD4^+$ T cells alike, focusing on Vpr's role in the induction of NF-AT signaling. Consecutively, a thorough bioinformatic analysis was executed on an RNA-Seq dataset derived from HIV-1-infected primary T lymphocytes, aiming to identify how Vpr presence can influence the transcriptomic footprint left by HIV-1 on its host. Finally, Vpr's ability to hijack and redirect its host's proteasomal activity was studied in the context of two putative protein targets previously identified through non-targeted proteomics: TCF7 and G3BP1.

The present work demonstrated that the role virion-delivered Vpr plays in supporting the establishment of a productive HIV-1 infection is highly reliant on its ability to induce the activation of NF-AT, as artificially inhibiting this transcriptional factor completely curtailed Vpr's characteristic boost in viral productivity and spread. The aforementioned bioinformatic analyses revealed that Vpr-mediated NF-AT induction leads to the transcriptional reprogramming of the host T cell, differentially affecting a variety of physiological processes, including cell cycle progression, ribosome assembly, protein translation, immune & inflammatory function, intracellular signaling, and cell proliferation, amongst others. In addition, this study established the mechanism whereby Vpr leads to the proteasomal degradation of TCF7, a *trans*-acting factor of central relevance towards T cell development, differentiation, and survival. Taken together, these results establish Vpr-mediated NF-AT activation as a central mechanism through which HIV-1 reprograms T cell physiology to enhance viral replication, expanding Vpr's array of virus-supporting roles and illustrating their eventual outcome on T cell physiology. Future work ought to prioritize validating many of these phenomena in primary $CD4^+$ T cells, in parallel exploring the downstream effects of Vpr-targeted protein degradation on T cell differentiation, exhaustion, as well as in the establishment and reactivation of potential HIV-1 reservoir populations.

III Zusammenfassung (Deutsch)

Das Humane Immundefizienz-Virus Typ 1 (HIV-1) ist ein lentiviraler Erreger, der für die AIDS-Pandemie verantwortlich ist. Es infiziert bevorzugt $CD4^+$ T-Lymphozyten und führt durch direkte virale Zytotoxizität sowie erhöhte Apoptoseraten zu deren allmählichen Erschöpfung. Um seine volle Pathogenität zu entfalten, kodiert HIV-1 eine Reihe von Hilfsproteinen, von denen das kleine, aber vielseitige Virusprotein R (Vpr) eine besondere Rolle einnimmt. Vpr ist an mehreren Mechanismen beteiligt, die die Wirtszellphysiologie stören, z. B. durch die Erleichterung des Kernimports viraler Prä-Integrationskomplexe, die Verstärkung der Transkriptionsaktivität viraler LTRs, und die direkte Einschleusung in Wirtszellen über die Einbettung in Virionen. Diese Eigenschaften machen Vpr zu einem entscheidenden Faktor für die Etablierung einer produktiven HIV-1-Infektion. Dennoch bestehen weiterhin offene Fragen zu den molekularen Mechanismen, mit denen Vpr die Kontrolle über die Wirtszelle auf verschiedenen Ebenen ausübt, insbesondere in physiologisch relevanten Modellen wie primären $CD4^+$ T-Lymphozyten. Um diese Wissenslücken zu adressieren, wurden in dieser Arbeit HIV-1-Infektionsexperimente mit Inhibitoren gegen verschiedene Signalwege sowohl in T-Zell-Linien als auch in primären $CD4^+$ T-Zellen durchgeführt. Im Fokus stand dabei die Rolle von Vpr bei der Induktion der NF-AT-Signalübertragung. Ergänzend erfolgte eine umfassende bioinformatische Analyse von RNA-Seq-Datensätzen aus HIV-1-infizierten primären T-Zellen, die es ermöglichte, den transkriptomischen Fußabdruck von Vpr detailliert zu charakterisieren, wobei sowohl bekannte als auch neue Zielgene identifiziert wurden, die durch Vpr beeinflusst werden – darunter Gene, die mit der Zellzyklusprogression, der Ribosomenbiogenese, der Proteintranslation, der Immun- und Entzündungsfunktion sowie der Zellproliferation in Verbindung stehen. Zusätzlich wurde der Einfluss von Vpr auf den Abbau von spezifischen Zielproteinen untersucht, die zuvor durch Proteomikanalysen als potenzielle Interaktionspartner identifiziert wurden. Besonderes Augenmerk lag dabei auf den Proteinen TCF7 und G3BP1. Die Ergebnisse zeigten, dass Vpr den proteasomalen Abbau von TCF7 effizient induziert, was tiefgreifende Auswirkungen auf die T-Zell-Homöostase und Funktion haben kann. Die vorliegende Arbeit zeigt, dass die Rolle von Vpr bei der Etablierung einer produktiven HIV-1-Infektion maßgeblich von seiner Fähigkeit abhängt, die NF-AT-Aktivierung zu induzieren. Die chemische Hemmung von NF-AT unterdrückte vollständig die für Vpr charakteristische Steigerung der viralen Produktion und Ausbreitung. Die Kombination aus experimentellen und bioinformatischen Ansätzen offenbarte, dass Vpr-vermittelte NF-AT-Aktivierung zu einer umfassenden transkriptionellen Reprogrammierung der T-Zelle führt, die zahlreiche zelluläre Prozesse beeinflusst. Zudem konnte der Mechanismus aufgeklärt werden, durch den Vpr den proteasomalen Abbau von TCF7 einleitet. Insgesamt erweitern diese Ergebnisse das Funktionsspektrum von Vpr und unterstreichen seine zentrale Bedeutung für die Manipulation der T-Zell-Physiologie zugunsten der viralen Replikation. Künftige Studien sollten die Validierung dieser Phänomene in primären $CD4^+$ T-Zellen weiter vorantreiben und die Auswirkungen von Vpr-gesteuerter Proteindegradation auf T-Zell-Differenzierung, Erschöpfung und die Etablierung von HIV-1-Reservoiren untersuchen.

IV Introduction

IV.I Classification & History of HIV-1

Retroviruses are a family of RNA viruses able to replicate by subjecting their RNA genome to reverse transcription and integrating the resulting DNA intermediate into the host cell's genome, enabling persistent infection and replication. Therein, the *Lentivirus* genus - as alluded to by its name - is notorious for eliciting diseases with long incubation periods, infecting both dividing and non-dividing cells. Human Immunodeficiency Virus Type 1 (HIV-1) is the type species of the *Lentivirus* genus and the primary causative agent of the acquired immunodeficiency syndrome (AIDS) [1,2].

Nearly 100 years ago, a single transmission event between chimpanzees (*Pan troglodytes*) and humans in West Central Africa marked the emergence of HIV-1. Originally a strain of SIV, this infectious agent adapted to its new host population, quickly spreading and eventually giving rise to HIV-1 group M, responsible for the AIDS pandemic of the 20th and 21st centuries [3–6]. Other SIV strains have undergone similar interspecies jumps, namely from gorillas (HIV-1 group O) [7] and sooty mangabeys (HIV-2) [8], though their epidemiological significance is mostly confined to reduced human populations and/or small regions within central Africa [7–9].

AIDS is characterized by opportunistic infections, uncommon neoplasias, and the immune deficiency from which the syndrome derives its name [10]. The development of drugs targeting various individual steps of HIV-1's replication cycle, particularly in combination (HAART), has ultimately proven invaluable in controlling the morbidity and mortality of AIDS, helping prevent viral transmission and dramatically improving the life quality of HIV-1^{+} patients [11,12]. Nevertheless, neither a vaccine nor a cure for HIV-1 are yet available, and this virus continues to pose a sizeable burden on healthcare systems worldwide, particularly in sub-Saharan Africa [13].

IV.II Virion structure & genome organization

HIV-1's structural and genomic features grant it various advantages that define its biochemical nature and underpin its efficiency in driving the progression of AIDS. The structure of HIV-1 virions consists of a highly condensed dimeric RNA genome bound by multiple viral proteins, including proteases (p14), integrases (p31), and reverse transcriptase (p66/p51). This RNA-protein complex is stabilized by nucleocapsid proteins (p7) and enclosed within an icosahedral/conic capsid composed of ~2000 copies of the p24 protein. Surrounding this assemblage is a p17-based matrix, which not only provides structure to the virion, but also stabilizes its envelope by serving as a docking surface for both lipids and envelope glycoproteins (gp120/gp41) [1,6]. The resulting viral particles are characterized by a spherical morphology and a diameter of 80-100 nm, exhibiting 8 nm-long glycoprotein protrusions [2,14]. HIV-1 possesses a complex yet compact genome consisting of two identical, positive-sensed, 5'-capped, 3'-polyadenylated RNA strands. It is composed of three hallmark ORFs - each encoding a single polyprotein - which give rise to all nine essential retroviral components upon maturation: the group-

specific antigen (*gag*), polymerase (*pol*), and envelope (*env*) genes, in a 5'-to-3' order. [1,6] However, HIV-1 takes advantage of alternative splicing and ribosomal frameshifting to encode six additional genes: *tat*, *rev*, *nef*, *vif*, *vpu*, and *vpr*.

IV.III HIV-1 accessory proteins

Whilst Tat and Rev have been described to play a crucial role in ensuring the correct spatiotemporal expression of the viral genome across HIV-1's life cycle, the remaining gene products are termed "accessory proteins", as they were initially sh own to be dispensable for HIV-1 infection and replication in cell lines, though still necessary for the virus to achieve full pathogenicity *in vivo*. Nowadays, these virulence factors have been demonstrated to excel at subverting metabolic pathways, countering restriction factors, and aiding immune evasion, favoring the establishment of a productive HIV-1 infection by fine-tuning the intracellular conditions of the host [15–18]. For instance, Vpu has been described to antagonize Tetherin, a restriction factor that inhibits the diffusion of budding virions [19], whilst Nef elicits the downregulation of MHC-I and CD4 surface levels [20]. Similarly, Vif has been demonstrated to counteract various restriction factors of the APOBEC family [21].

Vpr is a 14 kDa, 96 aa protein featuring an unstructured N-terminal domain and three amphipathic α-helices [22]. A hydrophobic center, comprised of sterically convergent hydrophobic residues from helices α1 and α3, grants its tertiary structure a high degree of stability [23]. In contrast to other HIV-1 accessory proteins, however, Vpr does not possess a single hallmark function, instead relying on its established capability to interact with a broad array of protein targets by hijacking the E3 ubiquitin ligase adaptor DCAF1/VprBP [22,24]. This takes place through the crosstalk between multiple regions of DCAF1's β-propeller and Vpr's α1- and α3-helices, its unstructured domain further stabilizing this interaction [23,25,26]. As a result, Vpr can manipulate the substrate specificity of the DDB1-CRL4-DCAF1 E3 ubiquitin ligase complex, thereby granting HIV-1 the possibility to remodel the host's proteome to its own advantage [24,27,28]. Additionally, Vpr is HIV-1's only accessory protein to be consistently incorporated into the viral particle, being recruited during virion assembly through Gag's p6 moiety. As such, Vpr is delivered into the host's cytosol directly upon viral entry, allowing it to coordinate the subversion of various physiological processes to ensure the establishment of a productive infection [22,29].

IV.IV HIV-1's replication cycle and the role of Vpr therein

Triggered by the interaction between virion-associated gp120 and host surface CD4 receptors, viral entry is aided by the presence of co-receptor proteins CCR5/CXCR4, for which different HIV-1 strains possess variable affinities [30–32]. Thereupon, the viral envelope fuses with the host cell membrane, releasing its payload unto the cytosol. Whilst progressively uncoating, the viral capsid advances towards the cell nucleus, shielding the viral genome concomitantly undergoing RT in its core [33–36]. Already at this step, virion-delivered Vpr interacts with UNG2 to improve the fidelity of this process

by reducing its overall mutation rate [23,26,37–40], additionally targeting the potentially harmful APOBEC3G [41,42], Exo1 [43], and HLTF [38,44–46] proteins for degradation.

Upon reaching the nuclear membrane, Vpr helps bridge the interaction between the now complete PIC and the nuclear pore complex, granting the viral genome entry into the nucleus [17,33–35,47]. Once therein, the viral capsid fully disassembles, poising the viral integrase to mediate the insertion of HIV-1 DNA into actively transcribed regions of the host's chromatin [48]. Vpr indirectly supports this step by degrading expression-modulating factors like SRSF1 [49], CTIP2 [50], and PHF13 [51], preventing the viral genome from becoming transcriptionally silent [52,53]. Flanking the integrated – and thus linearized – viral genome, LTR promoters feature diverse *cis*-acting regulatory elements upstream of the proviral CATA box [54], amongst them Sp-, NF-κB-, NF-AT-, and AP-1-binding sites, along with a Tat-responsive region [55,56]. At this step, Vpr enhances viral transcription by transactivating the LTRs through the recruitment of various Sp transcription factor family isoforms [57–59], upregulating genes that either promote viral survival or downregulate antiviral immune responses.

The host‘s cell cycle also plays a vital role in the physiology of HIV-1, as it has been observed that its arrest at the G2/M checkpoint optimizes LTR transcriptional activity [60,61]. This likely occurs due to IRES-dependent initiation being favored over cap-dependent translation, and vRNA transcripts are known to harbor such a feature in their 5‘-leader sequence [62]. Cell cycle arrest at the G2/M checkpoint is commonly induced as a response to DNA damage, eliciting the recruitment of DNA repair machinery [63]. Vpr's involvement in this process is one of its longest-studied activities, and the most recent evidence in this field indicates that Vpr can engage the DNA damage response by selectively degrading proteins involved in the structural, transcriptional, and epigenetic maintenance of the genome [64–72].

Rapidly after its synthesis, the $p55^{Gag}$ precursor is targeted via its myristoylated MA domain to cholesterol-rich lipid rafts on the cell membrane, serving as the structural framework for virion assembly. The CA and SP1 domains drive Gag-Gag interactions, allowing a curved hexameric lattice to form, and providing a matrix where Gag-Pol monomers can co-associate. Rev-exported gRNA dimers associate to Gag's NC domain through their Ψ-sequence, ensuring their correct incorporation and serving as the foundational core of the nascent virion. Furin then cleaves the gp160 Env precursor in the Golgi apparatus, with the resulting gp120-gp41 trimers localizing to viral assembly sites; the transmembrane gp41 protein can then associate with Gag's MA domain, granting the virion an entry receptor for the next round of infection [1].

Vpr supports this process by degrading LAPTM5, a restriction factor that reroutes gp120 for lysosomal degradation [73], as well as by sequestering Lysyl RNA synthetase, preventing the aminoacylation of $tRNA^{Lys3}$ that later serves as a primer for RT [74,75]. Gag's p6 domain not only allows the recruitment of Vpr into virions, but is additionally responsible for co-opting the host's ESCRT machinery, which enables viral progeny to be released from the host cell [76,77]. Once the new virion is separated from the

host's membrane, an autocatalytic cleavage event by the Gag-Pol polyprotein yields a mature protease within the virion, triggering its dimerization and the proteolytic maturation of the Gag polyprotein into MA, CA, NC, and p6 proteins, together with the processing of Gag-Pol into RT, protease, and integrase; this crucial step is the main determinant for viral infectivity, and defects therein lead to non-infectious viral progeny [1].

IV.V The interplay between host cell signaling and HIV-1

In addition to its multiple roles in the replication cycle of HIV-1, Vpr has long been suspected to actively subvert T cell function by disrupting signaling pathways involved in immune activation, inflammation, and proliferation [78–81]. Such is the case of the NF-kB signaling cascade, whose manipulation by Vpr has been demonstrated to play a crucial role in HIV-1 latency reversal [82,83], but still remains only partially characterized due to the inconsistent nature of its supporting evidence: some studies have implicated Vpr in sabotaging NF-κB-mediated gene activation [84,85] by preventing its nuclear translocation [86,87], while others reveal that it can elicit the phosphorylation of TAK1 [88] and IKKα/β [89], activating NF-κB signaling instead. A third line of evidence has even linked G2 cell cycle arrest and the DNA damage response with the activation of NF-κB signaling through the atypical pathway [90,91], resulting in increased viral genome transcription [92].

Analogously, the JAK-STAT signaling pathway is responsible for translating surface cytokine-receptor interactions into transcriptional changes involved in regulating immunity and cell cycle progression [93,94]. Within the context of HIV-1 infection, the activation of this pathway boosts the host's immune responses [95,96], an effect HIV-1 interferes with by subduing the expression of TLRs, IRFs, and multiple antiviral proteins, including OAS-1, MxA, and Tetherin [97]. HIV-1 Vif has also been observed to sabotage the activation of this pathway by preventing the phosphorylation of STAT1 [98] and strategically targeting various STAT family members for proteasomal degradation [99]. As such, elucidating the roles of NF-κB and JAK-STAT signaling in the context of HIV-1 infection remains a highly active research topic.

The β-Catenin signaling pathway regulates cell proliferation, differentiation, and survival by transducing the interaction between external stimulatory molecules (i.e. Wnt ligands) and Frizzled surface receptors into the deactivation of protein machinery responsible for degrading β-Catenin in the cytosol [100,101]. The accumulation and nuclear translocation of β-Catenin allows it to engage various *trans*-regulatory elements of the TCF/LEF family, eliciting the transcriptional activation of hundreds of genes featuring WREs [102]. β-Catenin signaling has been demonstrated to exert a clear restrictive effect towards HIV-1 replication, namely by binding TCF4 sites on the viral LTR [101,103–106]. This notwithstanding, HIV-1 employs various mechanisms to counteract β-Catenin-mediated restriction; Nef serves as a decoy for activated β-Catenin by virtue of its tertiary structure resembling endogenous β-Catenin ligands [107], whilst Tat can sequester TCF4 to prevent β-Catenin from interfering with viral

gene expression [105,108]. Nevertheless, whether Vpr plays a role in helping HIV-1 bypass this signaling pathway remains unknown.

Various transcriptional factors involved in regulating lymphocyte physiology are known to be influenced by Vpr. Such is the case of IRF3, a signaling component at the crossroads between innate immune activation and inflammation [81]. Not only is this protein targeted for proteasomal degradation through the presence of both Vpr and Vif [109], but its nuclear localization is additionally prevented by Vpr's ability to sequester and degrade KPNA1 [87]. NF-AT, a transcriptional factor essential towards T cell activation, proliferation, differentiation, and survival, is also heavily influenced by Vpr [81,110]. Canonically, NF-AT undergoes nuclear translocation as a response to the activation of membrane-coupled receptors and the subsequent mobilization of Ca^{2+} ions [110,111]; however, virion-delivered Vpr can bypass upstream stimulation events to directly activate NF-AT, boosting LTR transcription and consequently aiding the establishment of a productive HIV-1 infection in $CD4^{+}$ T lymphocytes [112].

Tightly linked to the triggering of pathways governing innate immunity, stress granules are biomolecular hydrogel condensates containing stalled mRNAs and proteins, forming through a liquid-liquid phase separation phenomenon [113,114] as a response to cellular stressors, including viral infections [115]. The assembly of these structures resembles prion-like domain-mediated aggregation [116,117], requiring the presence of RNA-biding SG nucleator proteins such as UBAP2L [117,118], G3BP1/2 [119–124], TIA-1, and TIAR [117,125], amongst various others. Mechanistically, stress granules prevent the translation of viral mRNAs whilst simultaneously stabilizing RLRs [126,127] and protein kinase R, enhancing the sensing of exogenous nucleic acids in the cytosol and boosting the induction of type I interferons [128,129]. Due to their critical role in viral sensing, stress granule formation frequently represents a target of viral immune evasive countermeasures; for instance, HCV's core protein disrupts SG assembly by sequestering TIA-1 and TIAR, whilst West Nile virus induces the disassembly of already nucleated SGs to promote viral protein synthesis at later timepoints in its replication cycle [115,130,131]. Stress granules play a complex, context-dependent role in the replicative cycle of HIV-1, with Gag preventing their assembly by recruiting eEF2 and concomitantly sequestering G3BP1 through its capsid domain [132]. Opposingly, the nucleocapsid protein has been demonstrated to interact with Staufen1, inducing SG nucleation and host mRNA translation arrest [133]. Nevertheless, whether any of HIV-1's accessory proteins influences SG assembly is yet to be determined.

IV.VI Aims of the thesis

As previously postulated, Vpr is a multifaceted accessory protein of central importance towards the pathophysiology of HIV-1, exerting a proven effect on its host at the transcriptional, translational, and signaling levels, amongst others. Using both donor-derived primary $CD4^+$ T cells and T-derived mammalian cell lines, the present thesis sought to explore the effects virion-delivered Vpr may exert on the JAK-STAT and NF-κB pathways, as well as on the activation of ISGs, and on the upregulation of surface markers associated with a T_{RM} phenotype.

Previous work by our group demonstrated that virion-delivered Vpr induces the activation of NF-AT by increasing intracellular Ca^{2+} levels whilst interfering with the export kinase GSK3β, correlating with the establishment of a productive infection in primary $CD4^+$ T lymphocytes [112]. This thesis explored a potential connection between these two phenomena through an array of infection assays aimed at studying how the NF-AT inhibitor FK-506 affects the infection rates and viral titers achieved by native HIV-1 viral stocks in a broad cohort of donor-derived primary $CD4^+$ T cells over the course of multiple timepoints. Further, a transcriptomic dataset corresponding to donor-derived HIV-1-infected CD4+ T lymphocytes at 48 hours post-infection, as generated by Dr. Anthea Darius, was scrutinized with the help of various bioinformatic tools in order to reveal whether a link exists between Vpr-mediated NF-AT activation, host cell transcriptional dysregulation, and the alteration of T cell physiology.

Further, a non-directed proteomic screening assay on HIV-1-infected primary $CD4^+$ T cells revealed that the overall abundance of a large array of protein targets decreases as a consequence of Vpr presence at 24 and 48 hours post-infection, amongst them TCF7 and G3BP1. Due to TCF7's central role in T cell biology, the present work sought to establish a TCF7 KO/KD protocol in primary $CD4^+$ T cells using various readily available methods, as well as to delineate the molecular mechanism whereby Vpr elicits TCF7 degradation. Additionally, the subcellular localization of this phenomenon was studied, along with its impact on β-Catenin signaling. Finally, a live cell imaging approach was developed in order to study the impact of Vpr on G3BP1's biological role in the assembly of stress granules within the context of HIV-1 infection.

V Materials & Methods

V.I Materials

V.I.I Equipment

Device / Instrument	Model(s)	Manufacturer
Agarose gel electrophoresis system	HE33 Mini	Hoefer
Cell imaging multi-mode reader	Cytation3	Biotek / Agilent
Centrifuges	5810R 5417R	Eppendorf
Flow Cytometer	MACSQuant VYB	Miltenyi Biotec
Gel/Membrane Imager	FcOdyssey	LI-COR
Incubators	NU-5810E Steri-Cult 200	Nuaire Labotect Göttingen
Laminar flow hoods	HeraSafe MSC Advantage	Heraeus Thermo Fisher Scientific
Live Cell Analyzer	IncuCyte	Sartorius
Microscopes	Axiovert 100 Axiovert 200 Observer.Z1 / Apotome2	Zeiss
Microvolume Spectrophotometer	NanoDrop ND-1000	Thermo Fisher Scientific
Multi-mode Reader	TriStar² S LB 942	Berthold Technologies
SDS gel electrophoresis and Western blot system	Mini PROTEAN Tetra Mini Trans-Blot Module Powerpac Universal	Bio-Rad
Thermal cyclers	Light Cycler 480 PTC-200 Peltier	Roche MJ Research
Thermal mixer	ThermoMixer F2	Thermo Fisher Scientific
Vortexer	Reax Top	Heidolph

V.I.II Software

Software	Version / Packages	Company/Website
BioRender	N/A	https://app.biorender.com/
CorelDraw 2024	v25.0.0.230	Cascade Parent Limited
FlowLogic	v8.3	Inivai Technologies / https://inivai.com/
Fluorescence SpectraViewer	N/A	Thermo Fischer Scientific/ https://www.thermofisher.com/order/fluorescence-spectraviewer/#!/

Galaxy Web Platform	v24.1.0/ DESeq2 (v1.40.2)	https://usegalaxy.org/
Gen5	v3.12	Biotek
GraphPad Prism	v10.1.1	GraphPad LLC
ICE	v1.0.9.8	Berthold Technologies
Image Studio	v6.0	LI-COR
IncuCyte Software	2022B Rev2	Sartorius
Light Cycler 480 Software	v1.5.1.62	Roche
Mendeley	v1.19.5	Elsevier / https://www.mendeley.com/
NanoDrop 1000	v3.8.1	Thermo Fisher Scientific
R Studio	v3.6.0+/ ggplot2 (v3.5.0) [134] enrichplot (v1.22.0) [135] clusterProfiler (v4.10.1) [136–139] EnhancedVolcano (v1.20.0)	Posit PBC
Serial Cloner	v2.6	SerialBasics
Zen Desk	v3.10	Zeiss

V.I.III Reagents

Reagent	Catalog number	Company
Acetic acid	100063	Merck Millipore
Acrylamide Solution (30%)	A3626	AppliChem
Agar	30391023	Thermo Fisher Scientific
Agarose	50004L	Lonza
Fast AP	EF0654	Thermo Fisher Scientific
APS	A3678	Sigma-Aldrich
Ampicillin	A0839	AppliChem
β-mercaptoethanol	21985023	Gibco
Benzonase	70746-4	Merck Millipore
Biotin powder	B4639	Sigma-Aldrich
Blasticidin	ant-bl-05	Invivogen
BSA	0216006991	MP Biomedicals
Bromophenol blue	A2331	AppliChem
Calcium chloride dihydrate	2382	Merck Millipore
Coelenterazine	102171	PJK Biotech
DAPI	D9542-1MG	Sigma-Aldrich

Reagent	Catalog number	Company
DMSO	D2438	Sigma-Aldrich
DTT	A3668	AppliChem
DNA loading dye	R0611	Thermo Fisher Scientific
DNAse Set - RNAse-Free	79254	Qiagen
dNTP-Mix (10 mM each)	R0192	Thermo Fisher Scientific
DMEM, high glucose, GlutaMAX supplement	61965026	Thermo Fisher Scientific
Doxorubicin	S1208	SelleckChem
DPBS	14190136	Gibco
Edit-R Human TCF7 crRNA (sequences 1-5)	CM-019735-0X-0010	Horizon Discovery
Edit-R CRISPR-Cas9 Synthetic tracrRNA	U-002005-05	Horizon Discovery
Edit-R Cas9 Nuclease protein NLS 20µM	CAS11201	Horizon Discovery
Ethanol 99%	ETO-5000-99-1	SAV liquid production
Ethidium bromide	97064-970	VWR
EDTA	A1103	AppliChem
FANA ASO, TCF7 Knockdown 25 nmol, for in vitro use	AUMsilence	AUM Biotech
FANA ASO, GFP-Labeled Scramble 25 nmol, for in vitro use	AUMscrlab	AUM Biotech
FANA ASO, Positive Control 25 nmol, for in vitro use	AUMposctrl	AUM Biotech
FastDigest, Green Reaction Buffer 10x	B72	Thermo Fisher Scientific
FastDigest Restriction Enzymes	FD-	Thermo Fisher Scientific
FBS / FCS	A31605	Gibco
Ficoll-Paque PLUS	11768538	Thermo Fisher Scientific
FK-506	F4679	Sigma-Aldrich
GeneRuler 1 kb plus DNA ladder	SM1331	Thermo Fisher Scientific
L-Glutamine	K0282	Merck Millipore
Glycerol	3783.2	Carl Roth
Glycine	A1067	AppliChem
H_2SO_4	124240025	Thermo Fisher Scientific
HEPES 1 M	15630056	Gibco
HIV-1 p24 antigen	ab43037	Abcam

Reagent	Catalog number	Company
HCl	1.00317	Merck Millipore
IL-2 (Recombinant, Human)	78036.1	StemCell Technologies
Isopropanol	33539	Honeywell
Kanamycin	A1493	AppliChem
KCl	P8041	Sigma-Aldrich
KH_2PO_4	104873	Merck Millipore
K_2HPO_4	P749.2	Carl Roth
KPL SureBlue TMB Microwell Peroxidase Substrate	5120-0076	LGC Seracare R&D
LB Medium (Lennox)	X964.3	Carl Roth
Lipofectamine RNAiMAX Transfection Reagent	13778030	Thermo Fischer Scientific
D-Luciferin	102112	PJK Biotech
MACS Quant Calibration Beads	130-093-607	Miltenyi Biotec
MACSQuant Running Buffer	130-111-747	Miltenyi Biotec
MACSQuant Storage Solution	130-092-748	Miltenyi Biotec
MACSQuant Washing Buffer Solution	130-092-749	Miltenyi Biotec
Methanol	322415	Sigma-Aldrich
$MgCl_2$	63068	Sigma-Aldrich
$MgSO_4$	M7506	Sigma-Aldrich
MG-132	AG-CP3-0011-M001	AdipoGen Life Sciences
Milk powder (non-fat)	A0830	AppliChem
$NaAsO_2$	S7400-100G	Sigma-Aldrich
NaCl	27810.295	VWR
NaCit	S-4641	Sigma
$Na_2HPO_4 \circ H_2O$	131678	AppliChem
NaOH pellets	1.06482	Merck Millipore
NaPyr	11360039	Life Technologies
Non-essential amino acids	11140035	Gibco
IGEPAL CA-630	I8896	Sigma-Aldrich
Opti-MEM	31985062	Life Technologies
HIV-1 p24 protein	ab127888	Abcam
PEI	23966-1	Polysciences

Reagent	Catalog number	Company
Penicillin-Streptomycin solution	P0781	Sigma-Aldrich
PFA	0335.2	Carl Roth
PHA	R30852801	Thermo Fisher Scientific
PhosSTOP phosphatase inhibitor tablets	4906845001	Sigma-Aldrich
Phusion High-Fidelity DNA Polymerase	F530S	Thermo Fisher Scientific
PI	A2261	AppliChem
QUANTI-Luc 4 Lucia/Gaussia solution	rep-qlc4lg1	Invivogen
QUANTI-Blue solution	rep-qbs3	Invivogen
Sigma FAST Protease Inhibitor	S8830	Sigma-Aldrich
Liquid RNase A	740397	Macherey-Nagel
RosetteSep Human $CD4^+$ T Cell Enrichment Cocktail	15062	Stemcell Technologies
RPMI-1640 Medium, GlutaMAX Supplement	R2405	Sigma-Aldrich
Ruxolitinib	17190212	StemCell Technologies
Saponin	A4518,0100	AppliChem
SDS-PAGE Page Ruler prestained protein ladder	26617	Thermo Fisher Scientific
SN-50	HY-P0151	MedChemExpress
SDS Pellets	CN30.2	Carl Roth
Sucrose	S0389	Sigma-Aldrich
T4 DNA ligase	EL 0014	Thermo Fisher Scientific
TEMED	17919	Thermo Fisher Scientific
Tris Base	A1086	AppliChem
Tris-HCl	A3452	AppliChem
Triton X-100	T9284	Sigma-Aldrich
Trypsin	T4174	Sigma-Aldrich
Tween 20	A4974	AppliChem
VectaShield	H-1000-10	VectorLabs
Yeast Extract	2363.3	Carl Roth
Zeocin	ant-zn-1	Invivogen
z-VAD-FMK	sc-3067	Santa Cruz

V.I.IV Kits

Kit	Application	Company
JetPRIME Transfection System	Transfection	Polyplus
Luna Universal qPCR Master Mix (2x)	RT-PCR	New England Biolabs
Neon transfection system	Electroporation	Invitrogen
NucleoSpin Gel and PCR Cleanup Kit	Gel extraction	Macherey-Nagel
PureYield Plasmid Midiprep System	Plasmid Isolation	Promega
QIAprep Miniprep Kit	Plasmid Isolation	Qiagen
QuantiTect Reverse Transcription Kit	Reverse Transcription	Qiagen
RNeasy Mini Kit	RNA Isolation	Qiagen
Anti-Rabbit IgG IP Beads (TrueBlot) 2.5 ml	Co-Immunoprecipitation	Rockland

V.I.V Buffers & Solutions

Buffer	Composition
FACS Buffer	1% FCS in PBS
HBS (10x)	1.4 M NaCl, 250 mM HEPES, 14 mM Na_2HPO_4, fill up with ddH_2O, dilute to 2x HBS and adjust pH to 7.23
IL-2	10 ng/µl in PBS with 0.1% BSA
Luciferase assay buffer	100 mM K_2HPO_4/KH_2PO_4 pH 7.8, 15 mM $MgSO_4$, 5 mM ATP
Luciferase lysis buffer	100 mM K_2HPO_4 / KH_2PO_4 pH 7.8, 1 % Triton-X-100, add fresh 1 mM DTT
Luciferase substrate buffer	1 mM D-Luciferin or Coelenterazine in assay buffer
PBS (10x)	26.8 mM KCl, 1.37 M NaCl, 81 mM Na_2HPO_4 * 12 H_2O, 14.7 mM KH_2PO_4, fill up with dH_2O and adjust pH to 7.4
PHA	stock 1 µg/µl in dH_2O
PI staining solution	50 µg/ml PI, 0.1 % Sodium citrate, 0.1 % Triton in PBS, add fresh RNase A (0.33 mg/ml)
6x SDS Loading dye	0.2 % bromophenol blue, 30 % glycerol, 10 % SDS, 0.6 M DTT, 0.5 M Tris, fill up with dH_2O and adjust pH to 6.8
SDS Running Buffer (10x)	250 mM Tris base, 1.92 M glycine, 1 % SDS, fill up with dH_2O, adjust pH to 8.3
TAE (50x)	2 M Tris base, 0.05 M EDTA, 1 M acetic acid, fill up with dH_2O
TBS (10x)	500 mM Tris, 1.5 M NaCl, fill up with dH_2O and adjust pH to 7.5
TBS-T	TBS 1x + 0.05 % Tween 20
Transfer Buffer (10x)	250 mM Tris base, 1.92 M glycine, 1 % SDS, fill up with dH_2O and adjust pH to 8.1 – 8.5, for 1x Transfer Buffer add 20 % Methanol

Western blot lysis buffer	50 mM Tris-HCl (pH 6,8), 2 % SDS, 10 % Glycerol, 1 % Triton X-100, add fresh Protease Inhibitor
Stacking gel buffer	0.5 M Tris-HCl, adjust pH to 6.8, fill up to 1L with dH_2O.
Separation gel buffer	1.5 M Tris Base, adjust pH to 8.8, fill up to 1L with dH_2O.
CoIP lysis buffer	50 mM HEPES, 150 mM NaCl, 0,3 % IGEPAL CA-630, adjust pH to 7.5, fill up to 1L with dH_2O. Add Benzonase and protease / phosphatase inhibitors directly before using.
PBS-T	PBS + 0.05 % Tween 20
PBS-TT	PBS-T + 0.05 % Triton X-100
IF Buffer	PBS + Glycine 10 %
PI working solution	PBS + 50 µg/ml propidium iodide + 0.33 µg/ml RNase A

V.I.VI Culture media & Nutrient solutions

Medium	Composition
HEK/293T	DMEM with L-Glutamine + 10 % FCS + 100 µg/ml Penicillin / Streptomycin
U-2 OS (G3BP1-GFP)	DMEM with L-Glutamine + 10 % FCS + 100 µg/ml Penicillin / Streptomycin + 1 µg/ml of Puromycin
Jurkat-Dual	RPMI-1640 with L-Glutamine + 10 % FCS + 100 µg/ml Penicillin / Streptomycin + 100 µg/ml Zeocin + 10 µg/ml Blasticidin
Primary human $CD4^+$ T cells	RPMI-1640 with L-Glutamine + 10 % FCS + 100 µg/ml Penicillin / Streptomycin + 10 ng/ml IL-2
Infection Medium	RPMI-1640 with L-Glutamine + 1 % FCS + 100 µg/ml Penicillin / Streptomycin + 10 ng/ml IL-2
KO Medium	RPMI-1640 with L-Glutamine + 10 ng/ml IL-2
Bacterial medium (LB)	20 g/L LB Medium (Lennox), fill up with dH_2O
Bacteria agar plates	20 g/L LB Medium (Lennox), 2% agar. Fill up with dH_2O, supplement with antibiotics for selection

V.I.VII Primers

Primer	Sequence	Source	Application
Hs_CENPA_1_SG	Cat N° = QT00001057	Qiagen	RT-qPCR
Hs_DUSP2_1_SG	Cat N° = QT00199794		
Hs_CD70_1_SG	Cat N° = QT00998340		
Hs_ZBP1_1_SG	Cat N° = QT00029631		
Hs_JAG1_1_SG	Cat N° = QT00031948		
Hs_NEK2_2_SG	Cat N° = QT01668394		
Hs_RCBTB2_1_SG	Cat N° = QT00007021		
Hs_DHRS2_1_SG	Cat N° = QT00039760		
Hs_CKS2_1_SG	Cat N° = QT00014693		

Hs_CDC20_1_SG	Cat N° = QT00089558		
Hs_CXCL10_1_SG	Cat N° = QT01003065		
Hs_PTK2_1_SG	Cat N° = QT00057687		
Hs_CDKN3_1_SG	Cat N° = QT00014728		
Hs_IL4_1_SG	Cat N° = QT00012565		
Hs_IL2_1_SG	Cat N° = QT00015435		
Hs_PLK1_1_SG	Cat N° = QT00049749		
Hs_CCNI2_1_SG	Cat N° = QT01174698		
Hs_IL13_1_SG	Cat N° = QT00000511		
Hs_IL18RAP_1_SG	Cat N° = QT00036393		
Hs_TNFSF4_1_SG	Cat N° = QT00028658		
GAPDH rv	GGCATGGACTGTGGTCATGAG	AG Schindler	
GAPDH fw	TGCACCACCAACTGCTTAGC		
BamHI – Vpr(N)	GTAGGATCCATGGAACAAGCCCCAGAA		Cloning
NotI – Stop - Vpr(C)	TATGCGGCCGCTAGGATCTACTGGCT		
NotI – Vpr(C)	TATGCGGCCGCGATCTACTGGCTCCA		
BamHI – TCF7v1(N)	ATAGGATCCTGCCGCAGCTGGACTCC		
NotI – Stop – TCF7v1(C)	TATGCGGCCGCTAGAGCACTGTCATC		
NotI – TCF7v1(C)	TATGCGGCCGCAGCACTGTCATCGGA		
BamHI – TCF7v2(N)	GCCGGATCCTGTACAAAGAGACCGTC		
NotI – Stop - TCF7v2(C)	TATGCGGCCGCTAGAGCACTGTCATC		
NotI – TCF7v2(C)	TATGCGGCCGCGAGCACTGTCATCGGA		
Vpr Fw	ATGGAACAAGCCCCAGAAGA		Vpr sequence verification
Vpr Rv	CTAGGATCTACTGGCTCCAT		

V.I.VIII Plasmids

Plasmid	Description	Source
pVSV-G	Glycoprotein of Vesicular Stomatitis Virus	[140]
pBR-NL4-3 (WT)	X4-tropic HIV-1	[141]
pBR-NL4-3 (ΔVpr)	X4-tropic HIV-1 without functional Vpr	
psPAX2	2nd generation lentiviral packaging plasmid	Addgene #12259
pMD2.G	VSV-G envelope-expressing plasmid	Addgene #12260
pWPI		

pWPI HXB	Lentiviral vectors expressing HIV-1 Vpr variants as well as GFP as a reporter gene.	[142]
pWPI Vpr B_B13C		
pWPI Vpr B_18E		
pWPI Vpr C		
pWPI Vpr H		
pWPI Vpr D_lo		
pWPI Vpr D_sh		
pWPI Vpr N		
pWPI Vpr O		
pWPI Vpr P		
pWPI Vpr Q65L_P		
pWPI-NL4-3 Vpr Q65R		Cloned by Dr. Anthea Darius.
mCherry-C1	Vectors expressing C-terminal mCherry-tagged HIV-1 accessory proteins.	Cloned by Dr. Johannes Schmid.
pmCherry-C1 Vpr		NIH AIDS Reagent Program
pmCherry-C1 Vpu		Cloned by Dr. Herwig Koppensteiner
pmCherry-C1 Nef		Cloned by Dr. Sandra Dehn
pBR-NL4-3 (WT)-IRES-mCherry	Expression vector encoding X4-tropic HIV-1 and mCherry as a reporter gene.	Cloned by Dr. Herwig Koppensteiner
pBR-NL4-3 (ΔVpr)-IRES-mCherry	Expression vector encoding X4-tropic HIV-1 without functional Vpr and mCherry as a reporter gene.	This work
phmKGN-MC	Expression vector coding for the N-terminal fragment of the Kusabira Green protein upstream of a multiple cloning site.	MBL Life Science (Code Number AM-1100M)
phmKGC-MC	Expression vector coding for the C-terminal fragment of the Kusabira Green protein upstream of a multiple cloning site.	
phmKGN-MN	Expression vector coding for the N-terminal fragment of the Kusabira Green protein downstream of a multiple cloning site.	
phmKGC-MN	Expression vector coding for the C-terminal fragment of the Kusabira Green protein downstream of a multiple cloning site.	
pCONT-1	phmKGN-MN plasmid encoding the p50 partial domain from the NF-κB complex.	

pCONT-2	phmKGC-MN plasmid encoding the p65 partial domain from the NF-κB complex.	
phmKGN-MN-Vpr (NL4-3 P35A)	phmKGN-MN plasmids encoding various HIV-1 NL4-3-derived Vpr variants exhibiting a wide array of functionally-relevant polymorphisms.	This work
phmKGN-MN-Vpr (NL4-3 Q65R)		
phmKGN-MN-Vpr (NL4-3 R80A)		
phmKGN-MC-Vpr (NL4-3 WT)		
phmKGN-MC-Vpr (NL4-3 P35A)		
phmKGN-MC-Vpr (NL4-3 Q65R)		
phmKGN-MC-Vpr (NL4-3 R80A)		
phmKGC-MC-TCF7v1	phmKGC-MC plasmids encoding the two most commonly expressed variants of TCF7, long (v1) and short (v2).	
phmKGC-MC-TCF7v2		
phmKGC-MN-TCF7v2	phmKGC-MN plasmid encoding the long variant of TCF7.	
pcDNA3-HA-TCF7	Expression vector encoding N-terminal HA-tagged TCF7v1.	Addgene #40620, Donated by AG Sauter (Tübingen, Germany)
pCG-IRES-GFP	Empty expression vector encoding an independent IRES-controlled GFP expression reporter.	AG Schindler
pCG_Vpr-IRES-GFP	Expression vector encoding NL4-3-derived Vpr with an independent IRES-controlled GFP expression reporter.	
pCG_AU1-Vpr(Q65R)-IRES-GFP	Expression vector encoding NL4-3-derived Vpr mutants (Q65/R80A) with an N-terminal AU1 tag as well as an independent IRES-controlled GFP expression reporter.	
pCG_AU1-Vpr(R80A)-IRES-GFP		
pEYFP-N1	Expression vector encoding YFP.	Clontech (discontinued)
pEYFP-N1 NL4-3 Vpr	Expression vector encoding various N-terminal YFP-tagged Vpr variants exhibiting a wide array of functionally-relevant polymorphisms.	Cloned by Dr. Kristin Höhne
pEYFP-N1 VprWT Jörg		
pEYFP-N1_Vpr K27M		
pEYFP-N1_Vpr P35A		
pEYFP-N1 Vpr64-68A		
pEYFP-N1 VprQ65R		
pEYFP-N1 VprC76A		

pEYFP-N1 VprR80A		
pECFP-C1 DCAF1	Expression vector encoding C-terminal CFP-tagged DCAF1.	
pECFP-C1	Expression vector encoding CFP.	Clontech (discontinued)
peYFP-CFP	Expression vector encoding a YFP-CFP fusion protein.	Cloned by Dr. Carina Banning

V.I.IX Antibodies

Antibody	Description	Use	Dilution	Source
p24 ELISA coating antibody	Monoclonal mouse anti-HIV-1 p24 antibody	p24 ELISA	1:1000	EXBIO
p24 ELISA primary antibody	Polyclonal rabbit anti-HIV-1 p24 antibody	p24 ELISA	1:650	Eurogentec
p24 ELISA secondary antibody	Polyclonal goat anti-rabbit antibody (HRP-tagged)	p24 ELISA	1:2000	Dianova
Anti-BLIMP1 (PE)	Monoclonal (6D3) mouse anti-human BLIMP1 antibody (PE-tagged)	FC	1:50	BD Biosciences
Anti-HIV-1 core antigen (FITC)	Monoclonal mouse anti-HIV-1 p24 / core antigen (FITC-tagged)	FC	1:50	Beckman-Coulter
Anti-HIV-1 core antigen (RD1)	Monoclonal mouse anti-HIV-1 p24 / core antigen (RD1-tagged)	FC	1:50	Beckman-Coulter
Anti-human CD69 (BV421)	Monoclonal mouse anti-human CD69 antibody (Brilliant Violet 421-tagged)	FC	1:50	Biolegend
Anti-CD186 (PE/Dazzle594)	Monoclonal (K041E5) mouse anti-human CD186/CXCR6 (PE/Dazzle594-tagged)	FC	1:50	Biolegend
Anti-CD49 (PE)	Monoclonal (TS2/7) mouse anti-human CD49a (PE-tagged)	FC	1:50	Biolegend
Anti-CD103 (FITC)	Monoclonal (Ber-ACT8) mouse anti-human CD103 (FITC-tagged)	FC	1:50	Biolegend
Anti-cMyc (FITC)	Monoclonal (SH1-26 E7.1.3) mouse anti-human cMyc (FITC-tagged)	FC	1:50	Miltenyi Biotec
Anti-STAT5 (FITC)	Monoclonal (REA549) mouse anti-human STAT5 antibody (FITC-tagged)	FC	1:50	Miltenyi Biotec
Anti-HA.11 epitope	Monoclonal rat anti-HA.11 epitope antibody	WB	1:1000	Biolegend
Anti-Vpr serum	Polyclonal rabbit anti-Vpr (NL4-3; aa 1-50) serum	WB	1:1000	NIH AIDS Reagent Program

Anti-VprBP	Polyclonal rabbit anti-human DCAF1/VprBP antibody	WB	1:1000	Fortis Life Sciences
Anti-rabbit (IRDye 800CW)	Monoclonal goat anti-rabbit FC antibody (800CW-tagged)	WB	1:15000	LI-COR
Anti-rat (IRDye 800CW)	Monoclonal goat anti-rat FC antibody (800CW-tagged)	WB	1:15000	LI-COR

V.I.X Organisms & Cells

Cell line	Description	Source
HEK/293T	HEK/293T cells are a highly transfectable derivative of the primary human embryonal kidney cell line 293, additionally carrying a plasmid encoding a temperature-sensitive mutant of the SV-40 large T-antigen.	DSMZ ACC 635
U-2 OS (G3BP1-GFP)	An osteosarcoma-derived cell lineage with epithelial morphology, U-2 OS cells are adherent and transfectable, with this clone additionally expressing a GFP-tagged version of G3BP1.	Donated by AG Locker (Surrey, England)
Jurkat-Dual	Jurkat cells are a T cell leukemia-derived lineage growing in suspension. Jurkat-Dual cells, developed by Invivogen, express SEAP under the control of an IRF-responsive promoter, as well as Luciferase downstream of NF-κB activation.	Purchased from Invivogen, Donated by AG Sauter (Tübingen, Germany)
NEB10 beta	Competent *E. coli* derivative of the popular DH10B. This lineage is T1 phage-resistant and endonuclease I-deficient for high-quality plasmid preparations.	NEB C3019I

V.I.XI Consumables

Consumable	Supplier
Amersham Protran Western blotting membrane, nitrocellulose, pore size 0.2 µm	GE Healthcare
Assay 96-well plate, white, flat bottom	Costar
CELLSTAR 24-well culture plate	Greiner
CELLSTAR 6-well culture plate	Greiner
CoSTAR 12-well culture plate	Corning
Coverslips	MatTek
Cell culture flasks 250 mL (T75)	Greiner
Cell culture flasks 50 mL (T25)	Greiner

Cell culture plates 96 well U Bottom	Greiner
Neon Electroporation Tips, 10 µl	Invitrogen
LightCycler 480 Multiwell Plate 96, white	Roche
MaxiSorp flat-bottom 96-well plate	Thermo Fisher Scientific
Micropipettes, various capacities	Eppendorf / Gilson
Neubauer-improved counting chamber	Marienfeld
Pipette, graduated, sterile, 10 mL	Corning
Pipette, graduated, sterile, 5 mL	Corning
Reaction Tubes, 1.5 mL / 2 mL	Eppendorf
Tubes, sterile, 15 mL PP	Falcon
Tubes, sterile, 50 mL PP	Falcon

V.II Methods

V.II.I Polymerase chain reaction (PCR)

PCR was performed with the Q5 High-Fidelity DNA Polymerase in accordance to the manufacturer's protocol.

V.II.II Restriction digests

Plasmid integrity was verified by mixing 1 µg of plasmid DNA in the reaction buffer with two Fast Digest restriction enzymes (0.5 µl each) for 15 min at 37°C in a total volume of 20 µl.

For sub-cloning, 1 µg plasmid DNA in reaction buffer was mixed with two Fast Digest restriction enzymes (0.5 µl each) and 1 µl alkaline phosphatase in a total volume of 20 µl. Similarly, sufficient PCR product in reaction buffer was mixed with two Fast Digest restriction enzymes (0.5 µl each) in a total volume of 20 µl. These reactions were incubated for 15 min at 37°C.

V.II.III Agarose gel electrophoresis

DNA fragments were separated by electrophoresis in 1% agarose gels, which were prepared by adding agarose to the desired volume of 1x TAE buffer and heating until completely dissolved. After a short cooling time, 4% ethidium bromide was added to the mixture, and this solution was poured into a gel cassette bearing a comb with an appropriate number of wells. Once solidified, the gel was transferred into an agarose electrophoresis chamber and supplemented with sufficient 1x TAE buffer. DNA samples and 7 µl GeneRuler 1 kb Plus DNA Ladder were loaded into individual wells therein, and electrophoresis was performed at 80 V for 45-60 min.

V.II.IV DNA extraction from agarose gels

After separation, DNA bands corresponding to inserts, PCR products, or linearized plasmid vectors were cut out from agarose gels under UV irradiation. Thereafter, DNA fragments were purified using the NucleoSpin Gel and PCR Cleanup kit according to the manufacturer's instructions.

V.II.V Ligation

Ligation of linearized vectors and inserts digested with identical nucleases was performed using the T4 DNA ligase according to the manufacturer's instructions, employing a vector-to-insert molar ratio of at least 1:10.

V.II.VI Transformation of chemically-competent bacteria

Chemically competent *E. coli* cells were thawed on ice, after which either 1 µl purified plasmid or a whole ligation reaction was added. Upon incubation for 30 minutes on ice, bacterial cells were subjected to a 45-second heat shock at 42°C, after which they were cooled down on ice again for 2 min.

Bacteria were then plated on LB agar plates with appropriate antibiotics, or pre-incubated in 200 µl liquid medium for 1 h at 37°C.

V.II.VII Plasmid preparation

Plasmid preparation from *E. coli* suspension cultures was performed with the PureYield Plasmid Midiprep System and/or the QIAprep Miniprep Kit in accordance to each particular manufacturer's instructions. DNA concentration was assessed via microvolume absorbance spectrophotometry using the NanoDrop ND-1000 instrument.

V.II.VIII Plasmid sequencing

For sequence verification, 500 ng plasmid DNA and 5 µl of 5 µM primer were diluted in endotoxin-free water for a total volume of 15 µl per sample, after which they were sent to Eurofins (Germany) for Sanger sequencing. The results thereof were analyzed using Serial Cloner (v2.6).

V.II.IX Cultivation & storage of *E. coli*

E. coli was cultured overnight at 37°C, either on solid agar plates or in liquid LB medium under continuous shaking. To produce plasmids with high recombination tendencies, the incubation temperature was reduced to 30°C. Antibiotics were used for clonal selection. Competent bacterial cells and plasmid-bearing bacterial glycerol stocks were stored at -80°C.

V.II.X Cell culture

All mammalian cells were cultured at 37°C, 5 % CO_2, and 95 % humidity. Adherent cell lines were passaged using trypsin either twice or thrice weekly, depending on cell density. Suspension cell lines were passaged twice weekly. For a complete overview of the corresponding culture medium compositions, please refer to Table I.I.VI.

V.II.XI Isolation of primary $CD4^+$ T cells

Healthy donor-derived buffy coats were obtained from the ZKT (Center for Clinical Transfusion Medicine) Tübingen. Blood was extracted into a 50 ml tube, and a volume thereof was mixed with 1.75x volumes of PBS. 0.15x volumes of RosetteSep Human $CD4^+$ T Cell Enrichment Cocktail were added to the blood/PBS mixture and incubated for 20 min at RT. This final mixture was overlaid on 15 ml Ficoll-Paque reagent for gradient separation by centrifugation (45 min at 2200 RPM, without brake).

$CD4^+$ T cells aggregated as white clumps or as a fine layer in the interphase between the Ficoll-Paque reagent and the plasma phase. These lymphocytes were removed by pipetting and collected in a separate tube. After two washing steps with PBS, $CD4^+$ T cells were resuspended in culture medium (see Table 1.1.6), and the total culture volume was adjusted to achieve a cell concentration not higher than $2*10^6$ cells/ml.

V.II.XII Gene Knockouts / Knockdowns

Multiple reagents were employed to attempt target gene knockdown / knockout. Our CRISPR/Cas9-based approach first required the assembly of gRNAs, for which equal volumes of 80 µM tracrRNA and 80 µM crRNA were mixed, resulting in a 40pmol/µl RNA solution. Per sample, 300 pmol of this RNA admixture (7.5 µl) were carefully mixed with 150 pmol Cas9 nuclease (2.5 µl of a 61.8 µM stock) at RT, constantly agitating the liquid with the pipette's tip so as to avoid any precipitations. This final RNP solution was incubated for 15 min at 37°C, during which the PHA-stimulated primary $CD4^+$ T cells to be electroporated were washed twice with PBS. The cells were resuspended and electroporated in 10 µl batches using the Neon transfection kit, following the manufacturer's instructions and using three 10-millisecond pulses at 1600 V (for PHA-stimulated cells). Thereafter, the electroporated cells were transferred into a 24-well plate containing antibiotic-free growth medium. These cells were kept in culture and harvested at 96 hpt. Knockdowns employing FANA ASOs were carried out by transfecting 2 nmol ASOs for every 10^6 PHA-stimulated, IL-2-supplemented primary $CD4^+$ T cells. To this end, ASOs were supplemented directly to the serum-free medium, and cells were maintained in culture for 72 hours, whereupon they were harvested for further downstream processing.

V.II.XIII Transfections

Various reagents were employed for DNA transfection in adherent cell lines. To achieve optimal transfection efficiencies, only cell cultures with confluency between 50 % and 80 % were used. All protocols detailed in this section are designed for a single well of a 6-well plate and were thus upscaled as necessary in accordance to each experiment. Transfections employing JetPRIME were carried out according to the manufacturer's instructions. To transfect cells using the $Ca_3(PO_4)_2$ method, 5 µg DNA were first mixed with 13 µl of a 2 M $CaCl_2$ solution and sufficient dH_2O to achieve a total volume of 100 µl. This solution was diluted in a 1:1 ratio with 2x HBS buffer, which was carefully added dropwise, vortexed, and incubated for 15 min on ice. Thereafter, this transfection mix was added dropwise to the cells. Medium was changed at 16 hours post-transfection. For transfections employing PEI, 100 µl of a 10% PEI solution in OptiMEM were mixed with 100 µl of a second OptiMEM-based suspension containing 5 µg DNA. The mixture thereof was vortexed and incubated for 30 min at RT, after which it was carefully added dropwise to the cells. A medium change took place between 4 and 6 hours after transfection.

V.II.XIV Protein Co-Immunoprecipitation Assays

To assess protein-protein interactions, adherent cells were washed, detached, centrifuged at 800xg for 10 min at 4°C, and their supernatant was discarded. Thereafter, they were lysed in 250 µl CoIP lysis buffer (per sample). 30 µl thereof were harvested as an input control and supplemented with 6 µl 6x SDS loading buffer, with the remaining 220 µl of the lysate being pre-cleared by adding 25 µl Anti-Rabbit IgG IP beads per sample and incubating this suspension in a parafilm-sealed tube at 4°C for 30 min under constant inversion. Afterwards, the beads were removed by centrifugation (10,000xg for 3

min), and the supernatant was transferred to another tube with 1 µg of the corresponding primary antibody. This tube was sealed with parafilm and incubated at 4°C for 1 hour under constant inversion, after which 25 µl IP beads were added. The tube was resealed and further incubated at 4°C for 1 hour under constant inversion. Thereafter, the tube was centrifuged for 1 min at 10,000xg and the supernatant was removed, leaving only the beads. Samples processed in this manner were washed 2-3 times with 250 µl lysis buffer, and finally resuspended in 50 µl 6x SDS loading buffer. All lysates / input controls were vortexed and incubated for 10 min at 90-100°C, after which they were separated via SDS-PAGE electrophoresis as described below.

V.II.XV Proximity assays

Protein-protein interactions were additionally assessed with two different proximity assays: Kusabira Green & FACS-FRET. After subcloning the proteins of interest unto the corresponding Kusabira Green plasmids, the proximity assays were performed following the plasmid manufacturer's instructions. Shortly, HEK/293T cells were transfected with the corresponding KG plasmids using the $Ca_3(PO_4)_2$ method previously described. At 24 hpt, cells were harvested and analyzed by flow cytometry as described below, gating for all cells positive for $KG_{488/529}$ fluorescence. FACS-FRET assays were performed following the experimental protocol published by Banning et al [143]. Shortly, HEK/293T cells were transfected with the corresponding fluorophore-tagged protein expression plasmids using the $Ca_3(PO_4)_2$ method described above. At 24 hpt, cells were harvested and analyzed by flow cytometry, first gating for all cells positive for both $CFP_{405/450}$ and $YFP_{488/529}$ fluorescence whilst excluding false positive events stemming from YFP excitation by the 405nm laser. Afterwards, the FRET-positive population was defined by creating a gate excluding all cells transfected with YFP and CFP, which should theoretically elicit no $FRET_{405/529}$ signal. This gate would then contain the entirety of the sample transfected with a CFP-YFP fusion protein (FRET-positive control).

V.II.XVI SDS-PAGE & Western Blotting

Adherent cells were washed, detached, centrifuged at 800xg for 10 min at 4°C, and their supernatant was discarded. Thereafter, they were lysed in 250 µl Western Blot lysis buffer, supplemented with 6x SDS loading buffer, incubated for 10 min at 90-100°C, and directly loaded into SDS-polyacrylamide gels or stored at -20°C. The composition of the gels is detailed below:

Reagent	Separating gel		Stacking gel
	10 %	12 %	
Acrylamide Stock (30%)	3.4 ml	4 ml	0.67 ml
dH_2O	3 ml	2.4 ml	3 ml
Stacking gel Buffer	2.5 ml	2.5 ml	-
Separating gel Buffer	-	-	1.26 ml
10% SDS	100 µl	100 µl	50 µl
10% APS	100 µl	100 µl	50 µl
TEMED	5 µl	5 µl	5 µl

Polyacrylamide gels were placed into a complete electrophoresis unit filled with 1x SDS running buffer. 20 – 40 µl of each cell lysate and at least one well with 7 µl of SDS-PAGE Ruler protein ladder were loaded per gel. These were run at 120 V for 90 minutes, after which their contents were transferred unto a nitrocellulose membrane using the PROTEAN wet blotting system. To this end, a nitrocellulose membrane was soaked in 1x transfer buffer, and the SDS gel was assembled together with the nitrocellulose membrane between two blotting papers into the blotting cassette, avoiding the formation of air bubbles between them. The transfer was performed at 80 V for 90 minutes, after which the membrane was blocked under constant agitation for 30 min at RT in 10 ml of a TBS-based 5% milk powder solution. Thereafter, the membrane was washed with TBS and incubated under agitation in 5 ml of a similar TBS-based 5% milk solution containing the corresponding primary antibody at the desired concentration for either 1 hour at RT or overnight at 4°C. After three 10-minute washing steps of TBS-T, the membrane was again incubated in 5 ml of a TBS-based 5% milk solution containing the corresponding secondary antibody at the desired concentration for 1 hour at RT. Finally, membranes were washed again as before, and target protein detection was performed with the LI-COR Odyssey Fc imaging system. The images were processed using Image Studio (v6.0).

V.II.XVII Viral stock production & concentration

Native HIV-1 viral stocks were produced by transfecting HEK/293T cells with proviral vectors, employing the JetPRIME transfection protocol as previously described. Virus-containing supernatants were harvested at 32 hours post-transfection and employed for infection assays. VSV-G-pseudotyped HIV-1 viral stocks were generated in a similar manner, with proviral vectors being co-transfected with pVSV-G at a ratio of 10:1 using either the PEI or $Ca_3(PO_4)_2$ methods. Viral stocks were harvested at 48 hours post-transfection. Vpr-expressing VLPs were generated as described previously [144]. Multiple batches of viral production were employed, all of which underwent centrifugation at 3200xg for 10 min in order to clarify them from remaining cells and debris. Depending on the experiment, VSV-G-pseudotyped HIV-1 NL4-3 viral stocks underwent an additional concentration step, where the corresponding supernatants were overlaid on 20% sucrose and centrifuged for 4 hours at 20,000xg and 4°C. Afterwards, supernatants were withdrawn, and viral pellets were resuspended in infection medium.

V.II.XVIII p24 antigen quantification

To assess their p24 content, small volumes of virus-containing samples were simultaneously neutralized and diluted by incubating them in PBS with 10 % Triton X-100 for 30 min at 37°C, after which they were stored at 4°C until later use. p24 ELISA was performed as follows: a highly adsorbent 96-well immunoplate was coated with 10 µl/well of a 31 µg/ml monoclonal anti-p24 antibody solution at 4°C overnight. This plate was washed once with PBS-T, blocked with 100 µl/well of 10% FCS in PBS for 2 hours at 37°C, and washed three times with PBS-T. Concomitantly, a standard p24 concentration curve was prepared by serially diluting a 1 mg/ml HIV-1 p24 antigen solution with PBS-T, first 1:100

twice, and then 1:2 ten times. Previously lysed virion-containing samples were further diluted as needed, and 100 µl thereof were pipetted into the blocked immunoplate in duplicates, along with 100 µl of every standard dilution prepared. The plate was incubated at RT in a humid chamber overnight, washed thrice with PBS-T, and incubated with 100 µl/well of a serum-based polyclonal anti-HIV-1 p24 antibody solution for 1 hour at 37°C. Afterwards, the plate was washed thrice with PBS-T and incubated with 100 µl/well of a 0.4 µg/ml HRP-tagged goat anti-rabbit secondary antibody solution for 1 hour at 37°C. Thereafter, the plate was washed three more times and treated with 100 µl/well of SureBlue TMB 1-Component Microwell Peroxidase Substrate at RT for 5 minutes. The reaction was then stopped using 50 µl/well of 0.5 M H_2SO_4, and the absorbance of these solutions at λ_1 = 450 nm and λ_2 = 650 nm was measured with a Berthold TriStar2 S LB 942 multi-mode reader. p24 antigen concentrations of the analyzed samples were interpolated using the standard concentration curve as a reference. Absorbance data (for p24 quantification) was processed with the ICE software (v1.0.9.8)

V.II.XIX Infection Assays

Unstimulated primary $CD4^+$ T cells were seeded into 6-well plates ($6x10^6$ cells/well) or 96-U-well plates ($2.5x10^5$ cells/well), supplemented with 10 ng/ml IL-2, and either left unstimulated or treated with 1 µg/ml PHA. In accordance with the experimental setup, various samples were additionally treated with 10 ng/ml FK-506, 10 µM Ruxolitinib, or 10 µM SN-50. Afterwards, unconcentrated (800 ng p24/well) viral stocks were added to the cells and kept in culture for up to 96 hours post-infection, with supernatants and cells being harvested at various intervals within this timeframe. Cells were fixed for 20 min at RT using 2% PFA and transferred unto 96-U-well plates for intra- and extracellular marker staining, whilst supernatants were collected and stored at -80°C for p24 ELISA analysis.

3-day pre-stimulated primary $CD4^+$ T cells were seeded into 24-well plates ($3x10^6$ cells/well), supplemented with 10 ng/ml IL-2, and either left unstimulated or treated with 1 µg/ml PHA. Concentrated (7200 ng p24/ml) HIV-1 viral stocks were added to the cells and kept in culture up to 48 hours post-infection. Thereafter, cells were harvested by centrifugation, washed once with PBS, and an aliquot thereof (~$3x10^5$ cells) was employed to assess infection rates via flow cytometry. The remainder of the sample was employed for RNA extraction as detailed later. All primary $CD4^+$ T lymphocytes underwent a spinoculation step, being centrifuged for 45 min at 37°C and 300xg to maximize virus-cell contacts. Jurkat-Dual cells were seeded into 96-U-well plates ($7.5x10^4$ cells/well), after which viral stocks were directly added and incubated for up to 32 hours. Jurkat-Dual cell-derived supernatants were stored at -20°C for downstream biochemical assays.

U-2 OS (G3BP1-GFP) cells were seeded on circular coverslips in 12-well plates. Upon reaching the desired cell density, unconcentrated (800 ng p24/well) VSV-G-pseudotyped viral stocks were added and left in contact with the cells for the remainder of the corresponding experiment. Live cell imaging took place as described in the corresponding methods section.

V.II.XX Flow Cytometry

PFA-fixed cells were initially washed with FACS buffer (PBS + 1% FCS) and centrifuged for 5 min at 500xg. Cells were simultaneously stained and permeabilized, for which they were resuspended in 50-100 µl of 0.1% Triton X-100 in PBS containing the corresponding fluorophore-tagged antibodies in a ratio between 1:50 and 1:20. Cells were then incubated for 30 min at 4°C, after which they were centrifuged and washed with 150 µl FACS buffer three more times. Afterwards, they were resuspended in FACS buffer and directly measured after the last washing step. All measurements were performed using a MACS Quant VYB Analyzer. Flow cytometric analyses were performed using FlowLogic (v8.3)

V.II.XXI RNA isolation & reverse transcription

Total RNA was isolated from cells with the RNeasy Mini Kit in accordance to the manufacturer's instructions. RNA was eluted from the column twice, each time adding 30 µl RNase-free water to the column membrane, incubating for 1 min, and centrifuging as indicated by the protocol. RNA concentration and purity were estimated via microvolume absorbance spectrophotometry using the NanoDrop ND-1000 instrument. 1.2 µg RNA were employed for cDNA synthesis with the QuantiTect Reverse Transcription Kit following the manufacturer's protocol.

V.II.XXII RT-qPCR

RT-qPCR reactions were prepared in triplicates, both for housekeeping genes as well as for the analyzed genes of interest. Per reaction, 5 ng of synthesized cDNA were mixed with 6 pmol of the corresponding QuantiTect Primer and 10 µl of Luna Universal qPCR Master Mix according to the manufacturer's instructions, for a total volume of 20 µl/reaction in nuclease-free water. RT-qPCR measurements were carried out using a Light Cycler 480 instrument, using a protocol consisting of an initial denaturation step (10 min at 95°C), followed by 45 amplification cycles (10 s at 95°C / 15 s at 55°C / 15 s at 72°C with fluorescence data acquisition at λ = 522 nm). Geometric means of the resulting Ct values were employed as input to calculate relative gene expression values using the $2^{-\Delta\Delta Ct}$ method [145]. RT-qPCR data was processed using the LightCycler 480 Software (v1.5.1.62).

V.II.XXIII Microscopy & Live Cell Imaging

For immunofluorescence, $1.5x10^5$ HEK/293T cells were seeded on poly-L-lysine-coated circular coverslips in 12-well plates. Upon reaching the desired cell confluency, they were transfected as previously described and supplemented with MG-132 when required. At 48 hours post-transfection, these cells were washed with IF buffer, fixed with 2% PFA for 15 min at RT, washed again, permeabilized with 0.02% saponin in PBS for 10 min at RT, and stained with 300 µl DAPI solution (1:20,000) for 10 min at RT. The slides were washed once again, rinsed with deionized water, dried by capillarity, and left to air dry completely at RT. Finally, these slides were mounted on a glass microscopy slide using 7 µl of VectaShield mounting medium. Mounted slides were sealed using glitter-free nail polish and dried again overnight. Wide field fluorescence microscopy of these samples was

carried out using an Observer.Z1 microscope outfitted with an Apotome2 optical sectioning device. Analysis of the produced images was performed using the Zen Desk software.

For live cell imaging, U-2 OS cells were seeded on uncoated circular coverslips in 24- or 96-well plates. Upon reaching the desired cell confluency, they were infected or transfected as previously detailed. At 24 hpi, they were treated with various concentrations of $NaAsO_2$ for 1 hour, after which their medium was changed and the cells were transferred into an IncuCyte S3 Live-Cell Analysis System. Live cell imaging experiments were performed employing the 20x objective, with cultures being incubated at 37°C, 5 % CO_2, and 80-90 % humidity. Visualization of the cells in question took place every 3 hours for up to 96 hours. Live cell imaging data was analyzed using the IncuCyte software (2022B Rev2).

V.II.XXIV Luciferase & SEAP Assays

Luciferase and SEAP activity in Jurkat-Dual cell-derived supernatants was assessed using the QUANTI-Luc 4 Lucia/Gaussia Detection Reagent and the QUANTI-Blue solutions, respectively. In either case, the manufacturer's protocol was followed. Luminescence and SEAP activity was measured on white 96-F-well plates using either a Berthold TriStar² S LB 942 or a Cytation3 multi-mode reader.
Luminescence data was analyzed using the Gen5 (v3.12) or ICE (v1.0.9.8) software packages. Absorbance data was processed with ICE (v1.0.9.8).

V.II.XXV Bioinformatic analysis of RNA Sequencing data

Unprocessed datasets (FASTQ files) generated by RNA sequencing of samples transferred by Dr. Anthea Darius to the c.ATG core facility (now NCCT Tübingen, Germany) were processed using the analytical pipeline developed by Dr. Rishikesh Lotke (AG Sauter). Briefly, FASTQ files were uploaded to the Galaxy web platform, and the public server at *usegalaxy.org* was used to perform differential expression analyses employing the DESeq2 (v1.40.2) package therein [146]. The resulting data was manually curated using the following cutoff criteria: q value < 0.05; adjusted p-value < 0.05; Base mean > 100; log2 fold change > 0.45 and < -0.45. Processed datasets were afterwards used as input for gene ontology enrichment analysis using enrichGO within clusterProfiler (v4.10.1).

V.II.XXVI Statistical analyses and figure generation

Statistical analyses were performed using GraphPad Prism (v10.1.1) and Microsoft Excel. Figures were generated using GraphPad Prism (v10.1.1), CorelDraw 2024 (v25.0.0.230), ggplot2 (v3.5.0), EnhancedVolcano (v1.20.0), enrichplot (v1.22.0), as well as with Biorender.com, Microsoft PowerPoint, and Microsoft Excel.

VI Results

VI.I Vpr does not activate ISGs or NF-κB in Jurkat-Dual cells

Preliminary work by Dr. Anthea Darius delved into the effect multiple primary Vpr alleles possess on intracellular signaling within HIV-1 target cells. This same approach was further employed to study whether Vpr induces NF-κB or ISG activation. To this end, unconcentrated lentiviral stocks expressing multiple Vpr alleles were used to infect Jurkat-Dual cells, and the supernatants thereof were probed for secreted luciferase (NF-κB reporter) and SEAP (IRF reporter) content. As seen in Fig. 1, Vpr failed to induce the activation of the NF-κB (Fig. 1A) and IRF pathways (Fig. 1B), as none of the transduced sample supernatants exhibited an increase in Luciferase / SEAP activity in comparison to the GFP transduction control.

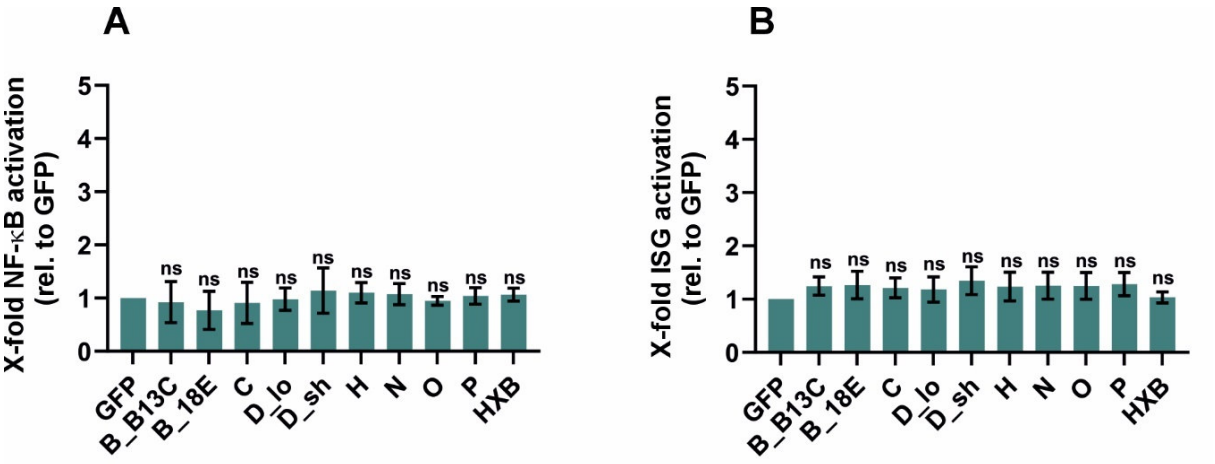

Figure 1. Vpr does not activate ISGs or NF-κB in Jurkat-Dual cells. Jurkat-Dual cells were infected with Vpr-expressing lentivirus stocks. (A) NF-κB and (B) ISG transcriptional activation was indirectly measured at 32 hpi as a function of reporter protein production via Luciferase and SEAP assays, respectively. Various primary HIV-1 Vpr isolates of groups M (clades B, C, D, and H), N, O, and P were compared to that of the laboratory-adapted virus HxB [142]. Statistics were calculated using a one-way ANOVA coupled to Šidák's multiple comparisons test (normalized to pWPI-only GFP). $\alpha = 0.05$; ns = not significant. Shown are the mean and SEM values of three independent experiments.

VI.II Vpr does not upregulate T_{RM} markers in primary resting $CD4^+$ T cells

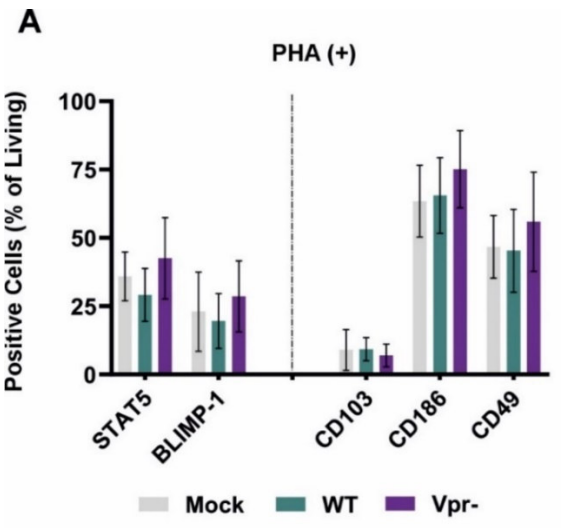

Figure 2. Vpr does not elicit an increase in the expression of various T_{RM} markers in primary resting $CD4^+$ T cells. Primary $CD4^+$ T cells were infected with highly concentrated VSV-G-pseudotyped HIV-1 viral stocks. (A) depicts the proportion of the total cell population expressing the indicated intracellular (left) and surface (right) protein markers at 72 hpi under the corresponding infection condition. Statistical analyses were performed using a two-way ANOVA coupled to Šidák's multiple comparisons test. $\alpha = 0.05$. Shown are mean and SEM values for three independent experiments.

Vpr has recently been implicated in establishing a tissue residency-like phenotype upon infecting resting memory T cells [147], reflected by the upregulation of markers and TFs connected with the JAK-STAT, NF-AT, and NF-κB pathways. To explore whether this also takes place in a less specialized T cell population, highly concentrated HIV-1 NL4-3 viral stocks with or without a functional *vpr* ORF were used to infect unstimulated bulk primary CD4⁺ T cells from healthy donors, harvested at 72 hpi and analyzed by flow cytometry. The results thereof (Fig. 2A) indicate that Vpr failed to induce a significant increase in the proportion of the cell population positive for STAT5, Blimp-1, CD103, CD186, or CD49, ruling out the establishment of a T_{RM} phenotype in primary resting CD4⁺ T cells.

VI.III Inhibiting NF-AT, but not NF-κB or JAK-STAT signaling, diminishes Vpr's ability to support HIV-1 infectivity

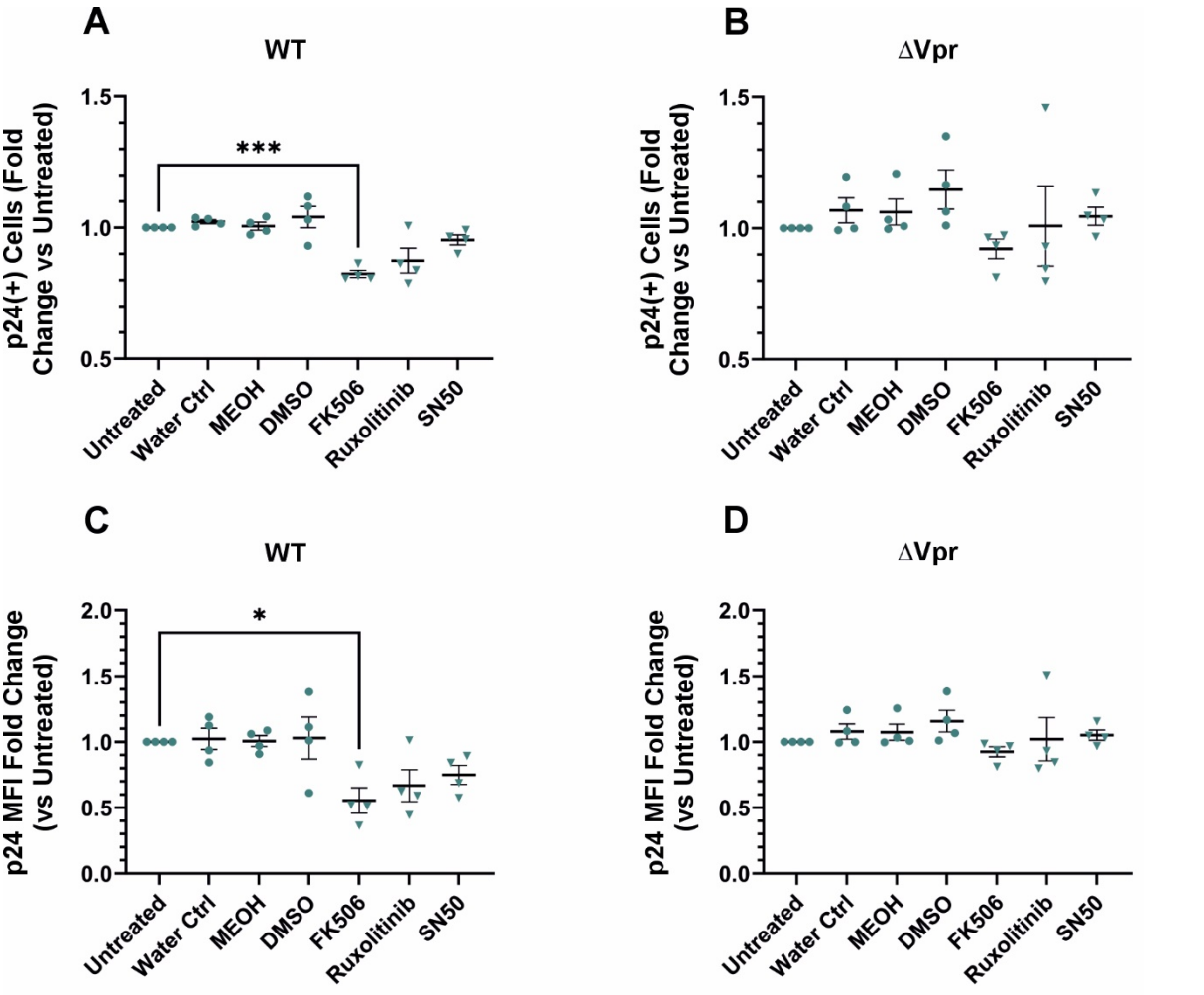

Figure 3. Vpr relies on NF-AT but not NF-κB or JAK-STAT signaling to aid HIV-1 productive infection. CD4⁺ T cells were simultaneously stimulated with PHA, infected with VSV-G-pseudotyped HIV-1 viral stocks, and treated with 10 ng/ml FK-506 (NF-AT inhibitor), 10 μM Ruxolitinib (JAK-STAT inhibitor), or 10 μM SN-50 (NF-κB inhibitor). (A) and (B) depict the relative infection rates attained at 48 hpi by WT and ΔVpr viruses, respectively. (C) and (D) indicate the relative intracellular p24 MFI values measured via flow cytometry in CD4⁺ T lymphocytes infected with HIV-1 WT and ΔVpr, respectively. All the aforementioned values were normalized to Mock. Statistical analyses were performed using a one-way ANOVA coupled to a multiple comparisons test using Dunnett's statistical hypothesis (normalized to Untreated control). $\alpha = 0.05$; * = $p < 0.05$; *** = $p < 0.001$. Shown are the mean and SEM values of four independent experiments.

In order to help identify the signaling pathways Vpr relies on to aid productive infection, unconcentrated VSV-G-pseudotyped HIV-1 viral stocks, with or without a functional *vpr* ORF, were used to infect primary $CD4^+$ T cells from healthy donors. Concomitantly, these cells were stimulated with PHA and additionally treated with either 10 ng/ml FK-506 (NF-AT inhibitor), 10 μM Ruxolitinib (JAK-STAT inhibitor), or 10 μM SN-50 (NF-κB inhibitor), so as to target the specific signaling pathways in question. Infected cells were harvested at 48 hpi and analyzed via flow cytometry.

Fig. 3A showcases that, at this timepoint post-infection, only NF-AT inhibition had a statistically significant impact on the overall infection rates attained by HIV-1 WT. In the case of HIV-1 ΔVpr, the inhibition of the aforementioned signaling pathways did not result in a statistically significant decrease of infection rates (Fig. 3B). Analogously, NF-AT inhibition significantly impacted p24 MFI levels in $CD4^+$ T cells infected with HIV-1 WT, though this was not the case for the remainder of the tested signaling pathways (Fig. 3C). In HIV-1 ΔVpr-infected cells, none of the employed inhibitors caused a statistically significant shift in the measured p24 MFI levels (Fig. 3D).

VI.IV Vpr facilitates HIV-1 productive infection via NF-AT activation

Parting from the available evidence pertaining to its role in the HIV-1 life cycle, Vpr has been described to aid productive infection in multiple T-derived cell lines, but whether this phenomenon also takes place in primary $CD4^+$ T cells has remained thus far unclear. In order to explore how Vpr supports HIV-1 productive infection in its *in vivo* target population, native (i.e. non-VSV-G pseudotyped) HIV-1 NL4-3 viral stocks, with or without a functional *vpr* ORF, were used to infect primary $CD4^+$ T cells from healthy donors treated with PHA and/or FK-506, an NF-AT inhibitor. These infected cells and their corresponding supernatants were harvested every 24 hours for up to 4 days and analyzed via flow cytometry and p24 ELISA, respectively. Fig. 4 illustrates the results thereof, where panel 4A showcases how the infection rates attained by HIV-1 in PHA-stimulated $CD4^+$ T cells increase as a function both of time and Vpr presence, the latter granting HIV-1 a statistically significant edge in said parameter; that same effect was also observable as a clear increase in the p24 titers measured in the supernatants of these samples, bearing statistical significance at 72 and 96 hpi (Fig. 4D). Nevertheless, this phenomenon was completely trumped by the NF-AT inhibitor FK-506, causing infection rates (Fig. 4A) and p24 titers (Fig. 4D) to stagnate independently of Vpr presence and despite PHA stimulation. This was not the case for unstimulated T cells, where infection rates did not show a dependence on time, Vpr presence, or NF-AT inhibition whatsoever (Fig. 4B). Within PHA-stimulated samples, Vpr presence also correlated with a statistically significant increase in the total amount of $CD69^-$ cells in the total infected population at 72 and 96 hpi, whilst the opposite held true at 48 hpi (Fig. 4C).

Taken together, the results from Figs. 3 & 4 suggest a functional link existing between HIV-1 Vpr's ability to aid the establishment of a productive infection, and its capability to induce the activation and signaling effects of NF-AT.

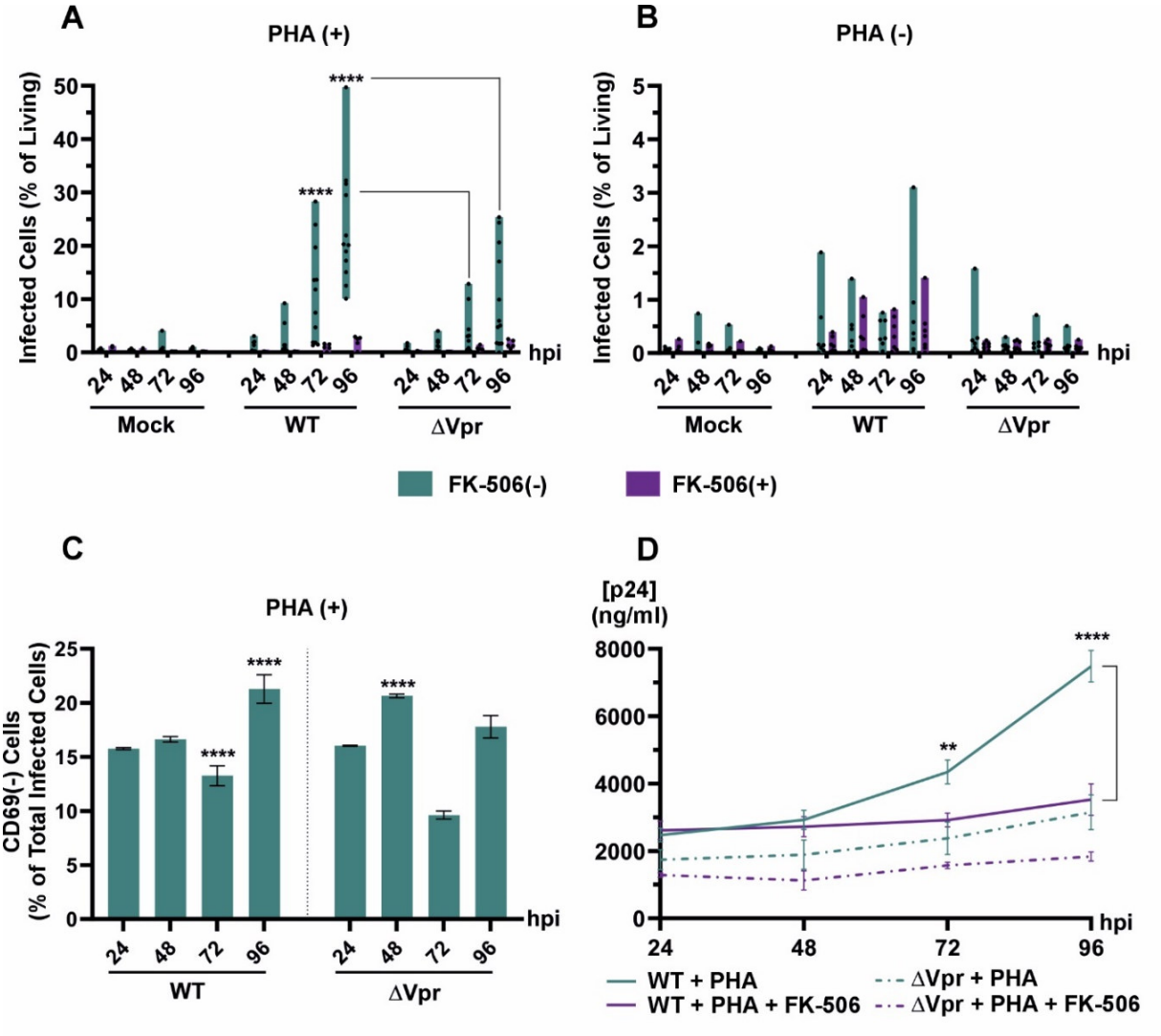

Figure 4. Inhibition of NF-AT abrogates Vpr-mediated enhancement of HIV-1 infection and p24 production in primary CD4⁺ T lymphocytes. Absolute infection rates of (A) PHA-stimulated and (B) unstimulated, FK-506-treated (10 ng/ml), HIV-1-infected CD4⁺ T cells at various time points post-infection (N = 5-12). (C) CD69⁻ cell percentage within the total infected population of FK-506(-) samples depicted in (A) (N = 5-12). (D) Supernatant p24 titers of PHA-stimulated, HIV-1-infected CD4⁺ T cells at various time points post-infection (N = 5-12). Statistical analyses for (A), (B), and (D) were performed using a three-way ANOVA with multiple comparisons testing, using Tukey's statistical hypothesis test. $\alpha = 0.05$; ** = $p < 0.01$; **** = $p < 0.0001$. Statistical analysis for (C) was performed using a two-way ANOVA coupled to a multiple comparisons test, using Tukey's statistical hypothesis test. $\alpha = 0.05$; **** = $p < 0.0001$.

VI.V Vpr exerts a transcriptionally dysregulating effect on NF-AT-controlled genes in primary CD4⁺ T cells

With the aim of exploring the potential effect Vpr exerts over the host cell transcriptome, the RNA-seq data Dr. Anthea Darius derived from HIV-1-infected (WT/ΔVpr) primary CD4⁺ T cells at 48 hours post-infection was analyzed in depth, taking advantage of various novel bioinformatic tools. Previously, the transcriptome profiling analysis performed at the Quantitative Biology Center Tübingen (QBic) employed the DESeq2 package to estimate variance-mean dependence in the aforementioned count data and test for differential gene expression based on a model using a negative binomial distribution, as originally postulated by Love and collaborators [146]. The resulting gene lists were ordered according to their Log_2 fold change value, and two such comparisons led to the identification of 672 Vpr-upregulated and 940 Vpr-downregulated elements, respectively. A follow-up gene ontology analysis

using Metascape [148] associated these DEGs with various key biological processes, such as cell cycle progression and cytokine production.

Following the analytic pipeline established by Dr. Rishikesh Lotke, the raw RNA-seq data was uploaded to the Galaxy web platform, and the public server at usegalaxy.org was employed to perform differential expression analyses using the DESeq2 package. The produced gene lists were refined by removing all entries with a Base mean value of zero, excluding elements undetected by the sequencing method. Additionally, type I errors were filtered out by applying a Benjamini-Hochberg correction with a q value of 0.05. The resulting PCA (Fig. 5A) revealed a consistent clustering pattern based on the infection status of the sample, with donor-dependent biological variability exerting a lesser influence on the overall predicted variance. Moreover, comparing samples according to infection status (Fig. 5B) indicated that HIV-1 WT induces notable transcriptomic alterations in primary T cells, as 5,859 out of 25,894 analyzed genes exhibited differential expression levels in comparison to Mock. Contrastingly, ΔVpr viruses induced a less pronounced transcriptional dysregulation in their host cells, with 3,682 genes showing signs of being differentially expressed when compared to Mock. As a consequence, comparing the hit list of HIV-1 WT against that of its Vpr-deficient counterpart allowed for the dissection of Vpr's transcriptional effect alone, with 2,363 genes appearing to be differentially expressed in a Vpr-dependent manner. These DEG lists were refined by excluding all genes with low expression levels (Base mean < 100) or unclear statistical significance (p-adj > 0.05), revealing that HIV-1 WT viruses cause the upregulation of 1,819 genes whilst downregulating 1,267 more (Fig. 5C). Vpr-deficient HIV-1 led to the upregulation of 1,113 and downregulation of 874 elements (Fig. 5C). Thus, Vpr was observed to be responsible for the upregulation of 574 and downregulation of 509 genes (Fig. 5C). These DEG lists were subjected to one more cutoff in order to filter out elements with less pronounced up-/downregulation (Log_2 Fold Change > 0.45 & < -0.45), and the results thereof were then compared against a list of NF-AT-controlled genes extracted from the Harmonizome 3.0 database. Fig. 6A illustrates the proportion of NF-AT-regulated elements in each of the depicted DEG lists, showing that 22.5 % of the overall analyzed entries correspond to this category. In contrast, 45.3 % of the genes dysregulated by HIV-1 WT (in comparison to Mock) are NF-AT-controlled, representing a statistically significant enrichment thereof. This result additionally revealed 46.5 % of all Vpr-dependent DEGs - 364 upregulated (33.6 %) and 140 downregulated (12.9 %) – to also be under NF-AT control. In order to distill the biological relevance from this highly processed Vpr-dependent DEG list, the EnrichGO package was employed to perform GO enrichment analysis. As illustrated by Fig. 6B, Vpr's transcriptionally dysregulating effect was predicted to compromise the normal function of a wide variety of biological processes, grouped into functional categories for visualization purposes. Therein, the categories "Signalling & Proliferation" and "Immune Function & Inflammation" appeared mildly upregulated, whilst three functional categories were starkly downregulated, namely "Ribosome Activity & Assembly", "Cytoskeleton & Organelle Activity", and "Cell Cycle Progression".

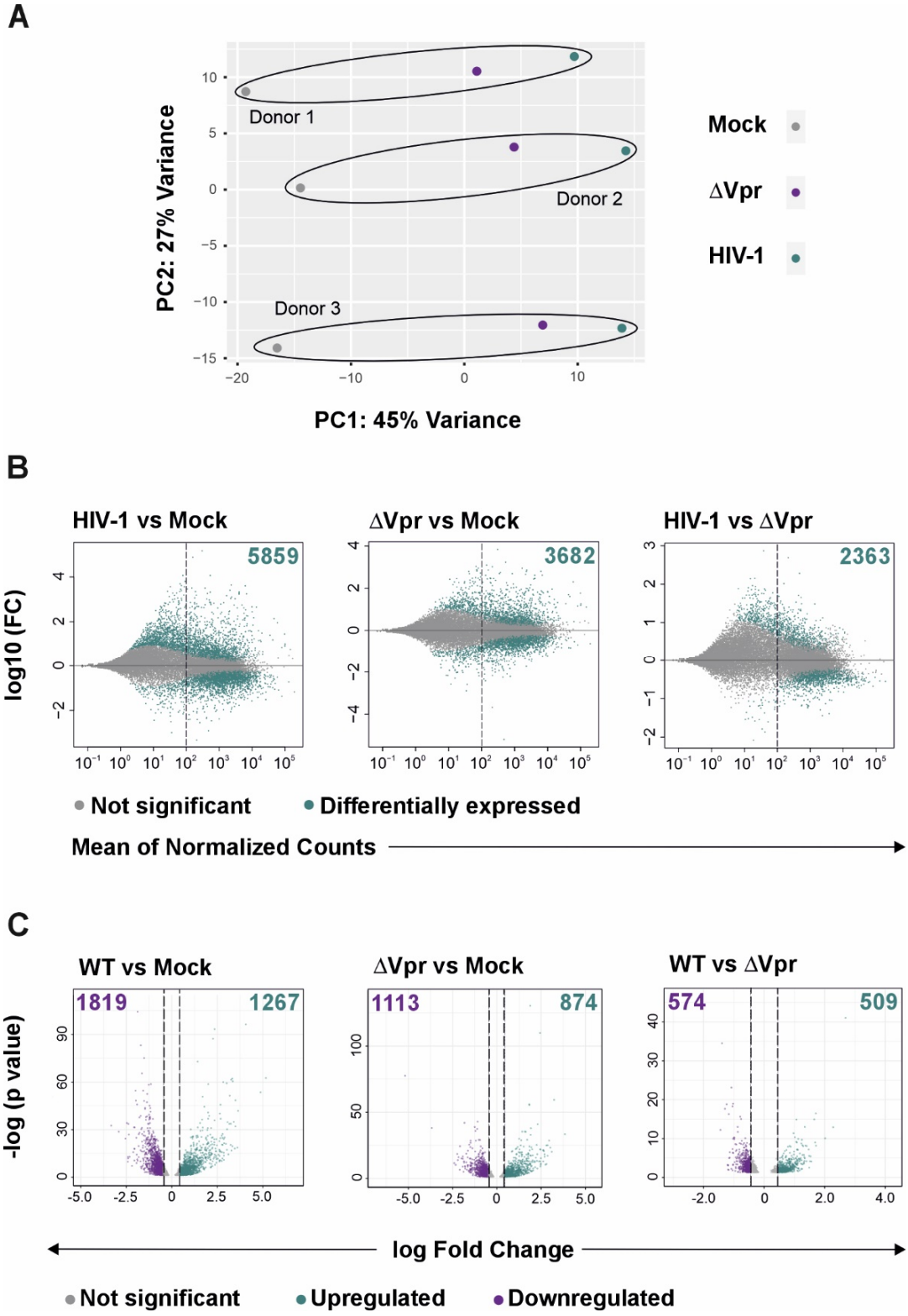

Figure 5. Vpr induces significant transcriptomic alterations in HIV-1-infected primary CD4+ T cells at 48hpi. (A) Principal component analysis plot indicating the main sources of variance for this experiment. (B) MA plot providing a global view of DEGs across infection conditions. Teal dots represent DEGs with a Base mean different from zero and a q value < 0.05 after applying a Benjamini-Hochberg correction. Teal numbers indicate the total number of DEGs in a given comparison before additional cutoff criteria were implemented. (C) Volcano plots depicting DEGs between infection conditions after applying the following cutoff criteria: p-adj < 0.05; Base mean > 100. Purple depicts downregulated genes (dots) and the total downregulated gene count (numbers). Teal depicts upregulated genes (dots) as well as the total upregulated gene count (numbers).

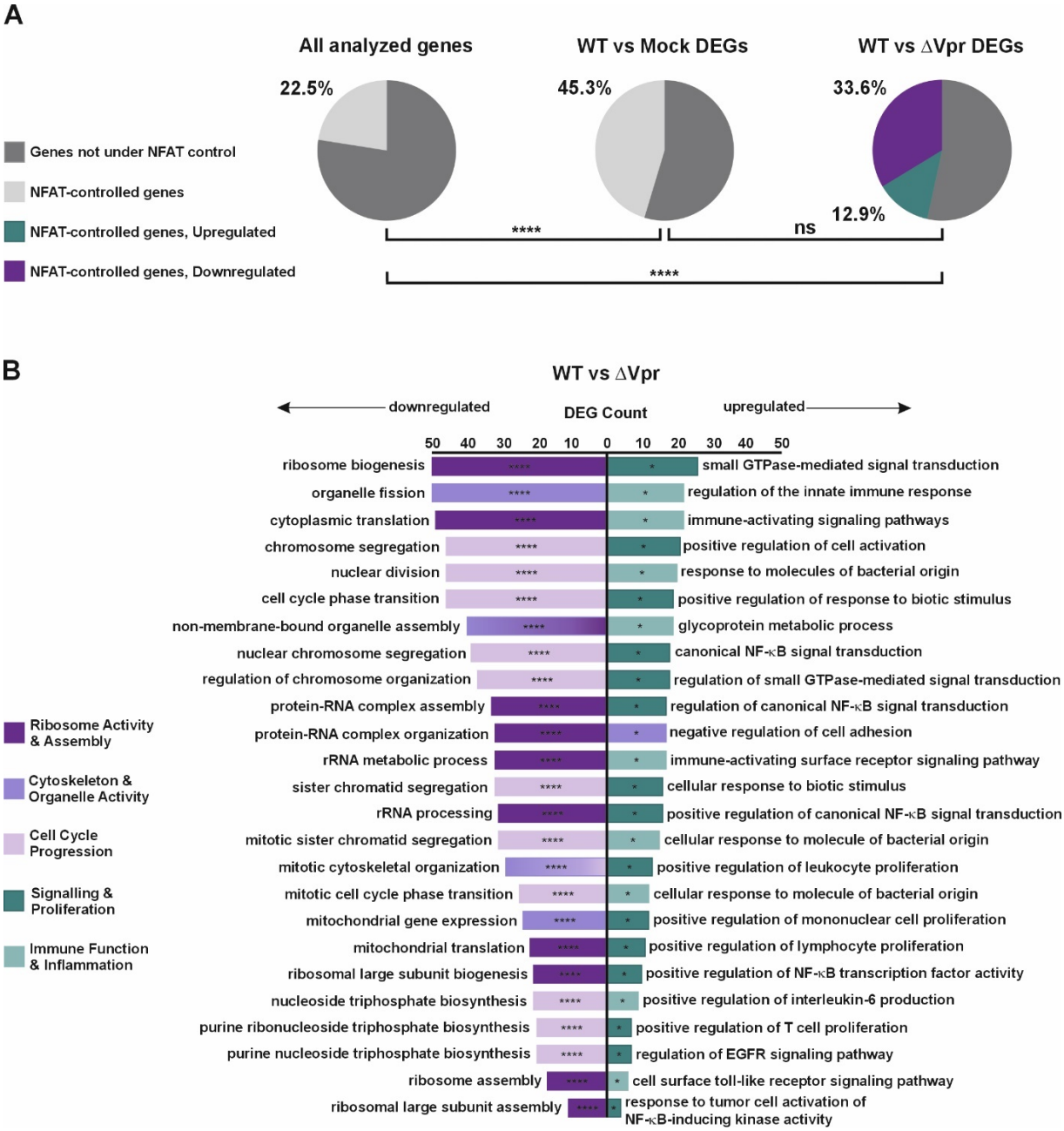

Figure 6. Vpr dysregulates NF-AT-controlled genes involved in diverse biological processes. (A) Pie charts depicting the percentage of NF-AT-controlled genes among various gene sets, based on a dataset of NF-AT-controlled genes extracted from the Harmonizome 3.0 database. Statistical significance was calculated using two-sided Fisher's exact tests independently for each comparison; **** = $p < 0.0001$. (B) Tornado plot depicting the top 25 up- and downregulated biological processes (GO terms) upon infection with HIV-1. Vpr suppresses ribosomal activity and assembly (dark purple), cell cycle progression (light purple), and cytoskeleton / organelle activity (lavender), whilst upregulating signaling and proliferation (dark teal) along with immune function and inflammation (light teal). This analysis was performed using EnrichGO, employing the DESeq2-processed RNA-seq results partly depicted in Fig. 5C as input. The hit list was subjected to the following cutoff criteria: adjusted p-value < 0.05, Base mean > 100, log2 fold change > 0.45 and < -0.45. * = $q < 0.1$; ** = $q < 0.01$; *** = $q < 0.001$; **** = $q < 0.0001$.

This gene ontology analysis was visualized in the form of CNET plots (Fig. 7), where a physiologically related gene network converges unto nodes representing relevant GO terms. Fig. 7A illustrates the top 10 BP GO terms upregulated by Vpr as teal nodes, 8 processes corresponding to the "Signalling & Proliferation" category, and the remaining being part of the "Immune Function & Inflammation" set. Fig. 7B depicts the top 10 BP GO terms downregulated by Vpr as purple nodes, including 6 and 4 elements of the "Cell Cycle Progression" and "Ribosome Activity & Assembly" categories, respectively.

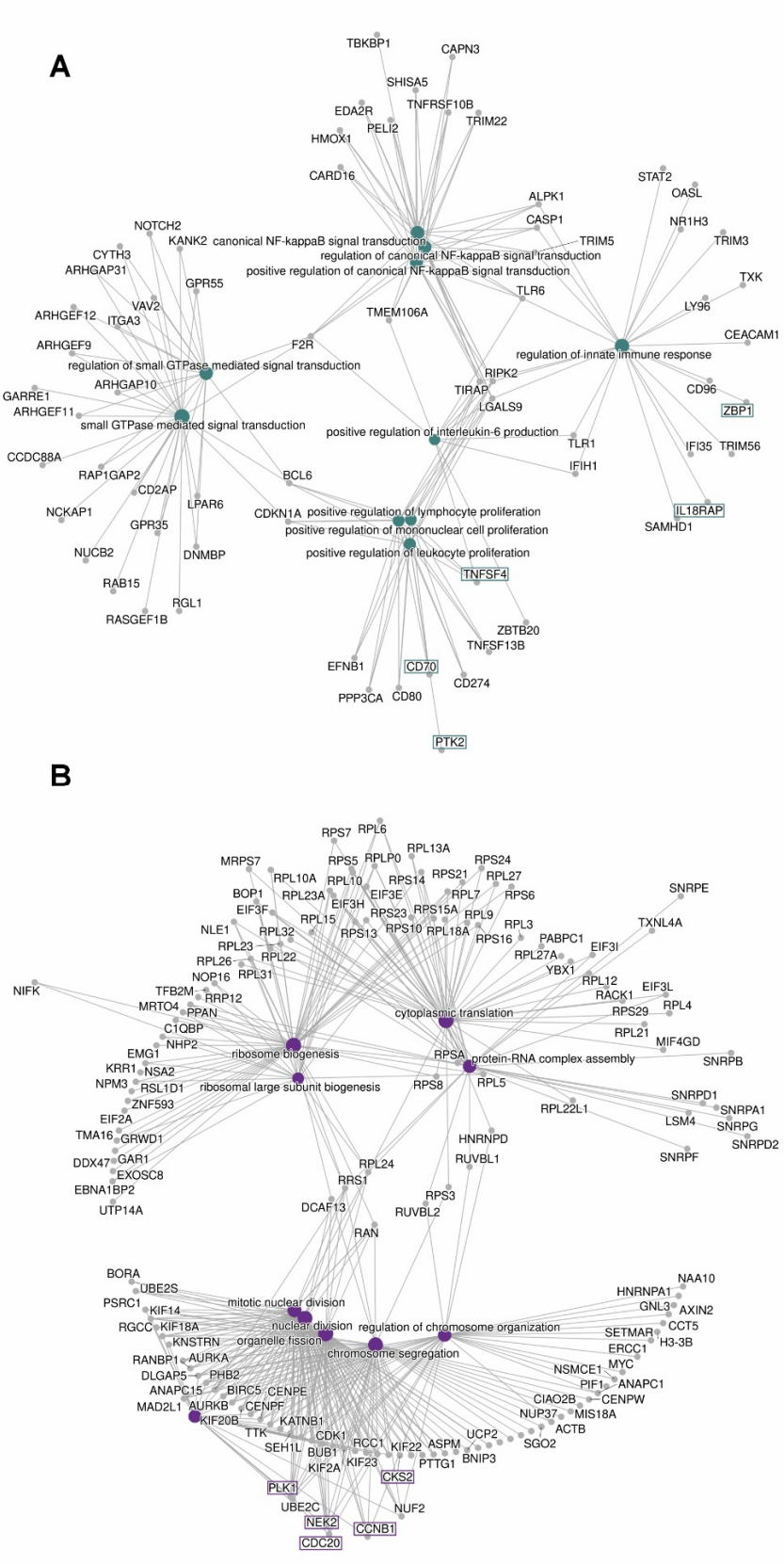

Figure 7. Vpr influences various key biological processes at the RNA level in stimulated CD4+ T cells. CNET plots depicting the top 10 (A, teal) upregulated / (B, purple) downregulated biological processes as nodes within the functional DEG network derived from the analysis illustrated by Fig. 5 (WT vs. ΔVpr). This analysis was performed using EnrichGO, employing the DESeq2-processed RNA-seq results partly depicted in Fig. 5C as input. The hit list was subjected to the following cutoff criteria: adjusted p-value < 0.05, Base mean > 100, log2 fold change > 0.45 or < -0.45. Gene hits analyzed by qPCR, as depicted in Fig. 8, are highlighted in purple (downregulated) or teal (upregulated).

From the EnrichGO-generated DEG list previously processed with all the aforementioned cutoff criteria, the top 70 up-/downregulated gene elements were selected and plotted on a waterfall plot - in teal and purple, respectively - according to their corresponding Log_2 Fold Change value (Fig. 8A). Within each category, a subset of affected genes, including both NF-AT-controlled (bold) and non-NF-AT-controlled (non-bold) elements, was chosen for further validation via qPCR. Fig. 8B illustrates the results for the upregulated gene subset, where HIV-1 WT was shown to significantly upregulate 6 out of these 8 targets at the RNA level in comparison to HIV-1 ΔVpr, these corresponding to NEIL1, TNFSF4, CXCL10, ZBP1, PTK2, and IL18RAP; CD70 and RBCTB2 did not show a statistically significant dysregulation, however. Analogously, Fig. 8C depicts the results of said qPCRs for the downregulated gene subset, where HIV-1 WT caused the statistically significant dysregulation of 4 out of 10 targets at the RNA level when compared to its Vpr-deficient counterpart, including CCNB1, CDC20, CENPA, and PLK1. Nevertheless, the remainder of this subset, i.e. DUSP4, NEK2, IL13, DUSP2, CDKN3, and CKS2, did not appear dysregulated. All in all, the results from Figs. 5-8 strongly suggest a direct link between Vpr's NF-AT activating phenotype and the transcriptional effects observed in WT-infected $CD4^+$ T cells.

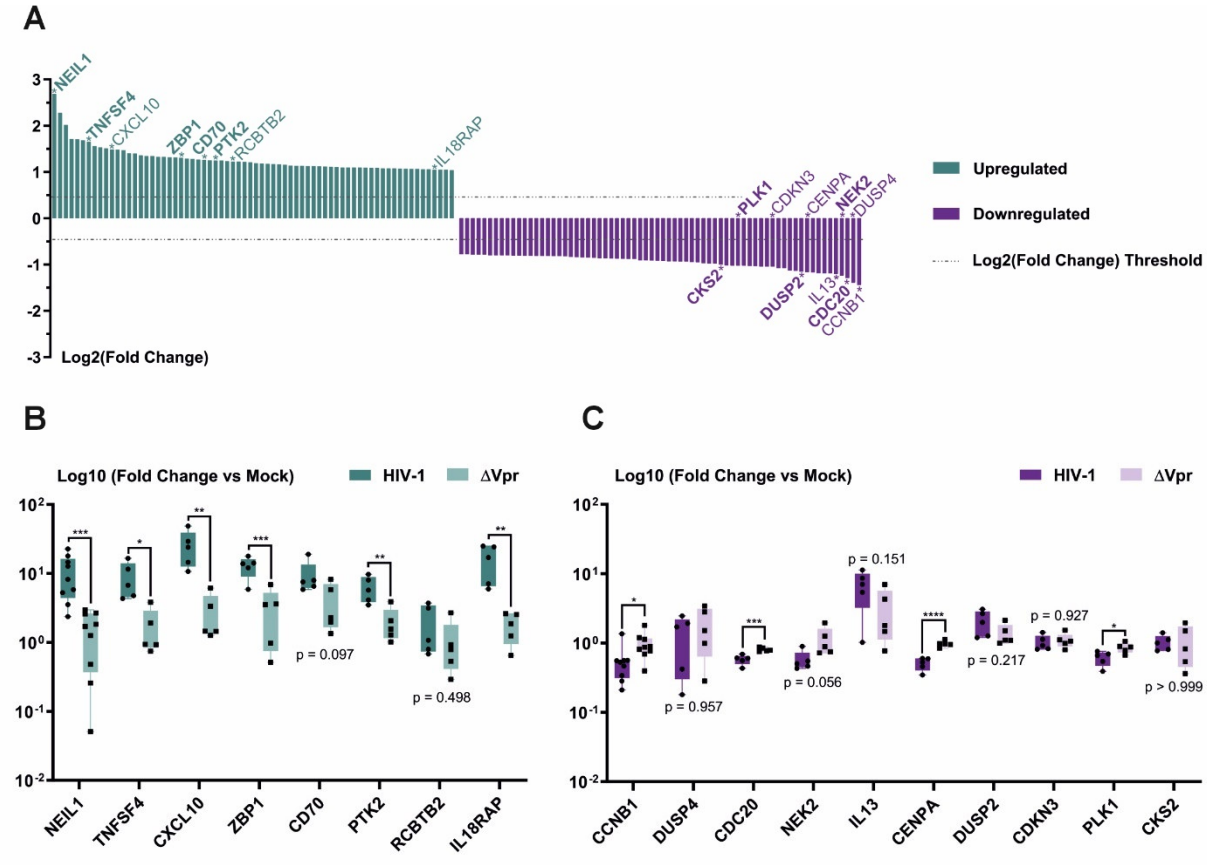

Figure 8. Vpr influences the RNA levels of multiple target genes in PHA-stimulated CD4+ T cells. (A) Waterfall plot depicting the top 70 genes significantly upregulated (teal) / downregulated (purple) by Vpr, ordered by log2 FC. Genes selected for validation via qPCR are labeled with asterisks and their corresponding gene symbol. NF-AT-controlled genes are highlighted in bold script, irrespective of their dysregulation status. qPCR analysis of selected upregulated (B) and downregulated (C) genes. Gene expression (normalized to mock) derived from the geometric mean of three replicate Cp values is shown. Statistical significance for each gene hit was calculated using a one-way ANOVA coupled to Šidák's multiple comparisons test (normalized to mock). $\alpha = 0.05$; * = $p < 0.05$; ** = $p < 0.01$; *** = $p < 0.001$; **** = $p < 0.0001$.

VI.VI Vpr does not establish a strong direct interaction with TCF7

In addition to its effect on the transcriptome, Vpr's effect on the proteome was also explored. Non-targeted proteomics performed by Dr. Anthea Darius on HIV-1-infected primary $CD4^+$ T cells at 48 hpi revealed a statistically significant decrease in the levels of several proteins theorized to be Vpr targets. TCF7, a transcriptional factor highly relevant towards immune function and development, was identified amongst them, and the present work sought to delve further into the relevance of this biological phenomenon. To this end, we first tested the hypothesis of Vpr and TCF7 interacting directly, for which HEK/293T cells were transfected using various plasmids encoding fluorophore-tagged versions of TCF7 and Vpr. At 48 hpi, the degree of interaction strength between said expression products was analyzed via two distinct proximity-based assays: Kusabira Green and FACS-FRET assay.

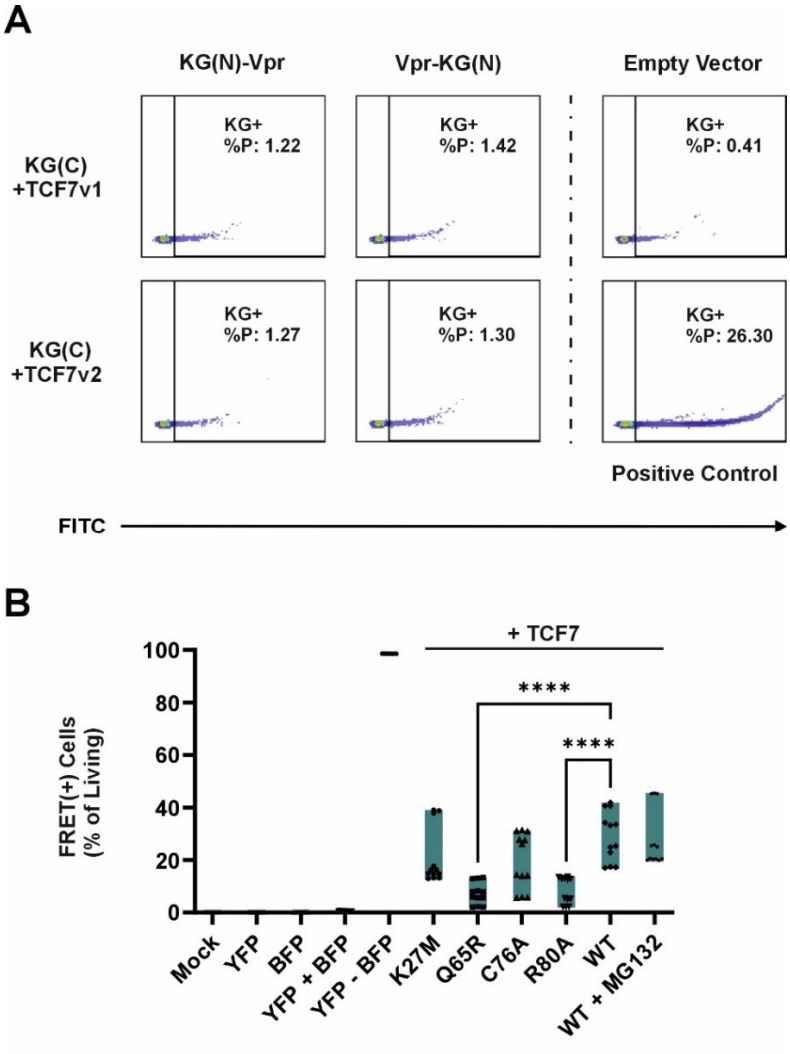

Figure 9. Direct Vpr-TCF7 interactions are of a relatively weak nature. HEK/293T cells were transfected with expression plasmids encoding the corresponding Vpr variant and/or the indicated interaction partner. (A) Kusabira Green assay results. Representative dot plots depicting the percentage of Kusabira Green fluorescence-positive cells within the living population under each experimental condition. (B) FACS-FRET results. Depicted is the proportion of the living cell population exhibiting FRET signal in each sample. Statistical significance was calculated using a one-way ANOVA coupled to Dunnet's multiple comparisons test. $\alpha = 0.05$; **** = $p < 0.0001$; N = 4.

Despite the cloning of Vpr and both studied TCF7 isoforms into the Kusabira Green system proving successful, the assay did not indicate a stark interaction occurring between Vpr and TCF7v1 nor

between Vpr and TCF7v2, as each of these tested pairs only yielded a ~1% increase in KG fluorescence-positive cells over that of the employed negative control, irrespective of whether the corresponding KG tag was present on the C- or N-terminus of the viral protein (Fig. 9A). Comparably, FACS-FRET results indicate that the interaction between Vpr WT and TCF7, whilst noticeable, is not particularly strong, as their corresponding FRET signal only comprises 40% of the positive control's signal. Employing MG132 to prevent the proteasomal degradation of TCF7 did not impact the strength of this interaction. Vpr mutants K27M and C76A, known for their reduced or absent NF-AT activation potential, respectively, exhibited a similar behavior, whilst the interaction between TCF7 and Q65R, a mutant unable to recruit DCAF1, as well as with R80A, a Vpr allele deficient in DCAF1-dependent target recruitment, showcased a statistically significant lower strength when compared to Vpr WT (Fig. 9B). The hypothesis of Vpr and TCF7 directly interacting was therefore explored from a different angle, employing a CoIP assay to this end. The results in Fig. 10 indicate that these two proteins, despite being successfully expressed (Fig. 10A), do not directly interact with one another, since a pulldown against HA-tagged TCF7 did not result in the coprecipitation of HIV-1 Vpr (Fig. 10B).

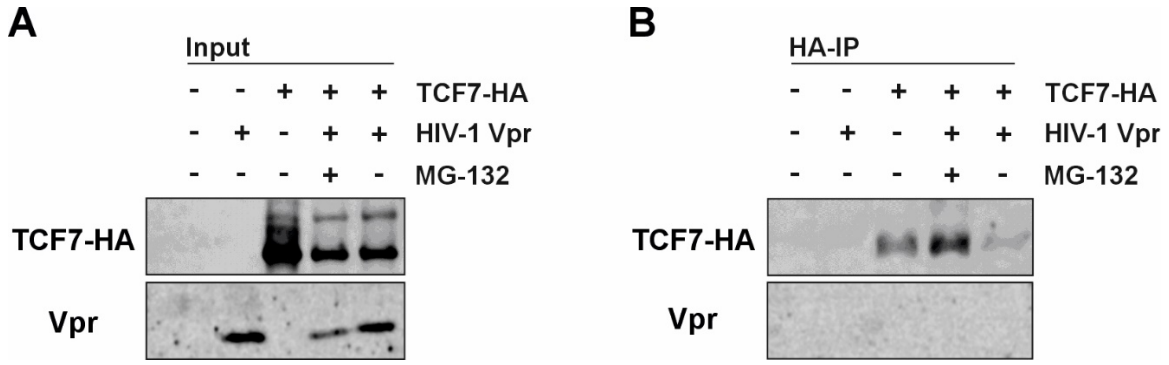

Figure 10: Vpr does not coprecipitate with TCF7. HEK/293T cells were transfected with pCG_IRES-GFP (Empty Control), pCG_DNA3-HA-TCF7 (TCF7-HA), and/or pCG_Vpr-IRES-GFP (HIV-1 Vpr). After a medium change, some samples were supplemented with MG132 (1 µM). At 48 hpt, cells were harvested and lysed as described in section V.II.XIV. Protein expression and interactions were analyzed via SDS-PAGE coupled to WB. Depicted are the WB results featuring Input (A) samples of the aforementioned lysates and their corresponding CoIPs (B), performed using Anti-Rabbit IgG IP beads (Rockland) and anti-HA (Rabbit) antibodies. TCF7 and HIV-1 Vpr were stained with anti-HA (rabbit) and anti-Vpr (mouse) antibodies, using the corresponding secondary antibody (see V.I.IX). N = 1.

VI.VII Vpr interacts indirectly with TCF7 via DCAF1

Considering the results of Fig. 9, it was hypothesized that the interaction between Vpr and TCF7 could instead take place through an intermediary protein. Since Vpr has been implicated in facilitating the degradation of multiple targets by recruiting DCAF1, the possibility of it bridging the Vpr-TCF7 interaction was explored using the samples presented in Fig. 10, as a pulldown against TCF7-HA would theoretically cause DCAF1 to coprecipitate if involved. Fig. 11 illustrates these results, with Fig. 11A illustrating the presence of endogenous DCAF1 in HEK/293T cell lysates, together with vector-expressed TCF7-HA and Vpr proteins. The results of the pulldown against TCF7-HA (Fig. 11B) reveal that DCAF1, though rather faintly, was present in every sample, irrespective of whether TCF7 and/or Vpr were additionally expressed. Nevertheless, DCAF1's signal was particularly accentuated in the sample containing TCF7, Vpr, and MG132, hinting towards a potential direct interaction.

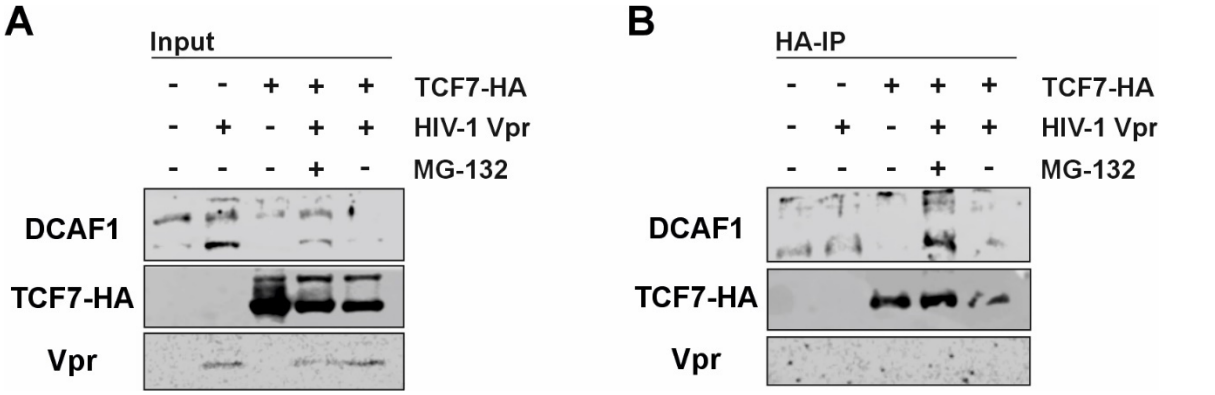

Figure 11: DCAF1 coprecipitates with TCF7. HEK/293T cells were transfected with pCG_IRES-GFP (Empty Control), pCG_DNA3-HA-TCF7 (TCF7-HA), and/or pCG_Vpr-IRES-GFP (HIV-1 Vpr). After a medium change, some samples were supplemented with MG132 (1 µM). At 48 hpt, cells were harvested and lysed as described in section V.II.XIV. Protein expression and interactions were analyzed via SDS-PAGE coupled to WB. Depicted are the WB results featuring Input (A) samples of the aforementioned lysates and their corresponding CoIPs (B), performed using Anti-Rabbit IgG IP beads (Rockland) and anti-HA (Rabbit) antibodies. TCF7, HIV-1 Vpr, and DCAF1 were stained against using the corresponding primary and secondary antibodies (see V.I.IX). N = 1.

To more specifically study whether DCAF1 bridges the interaction between TCF7 and Vpr, and in order to effectively remove unspecifically bound DCAF1 from the Anti-Rabbit IgG IP beads, a similar pulldown assay with an additional washing step was carried out against DCAF1. Further, this experiment featured the Vpr mutant Q65R, known for being unable to fully engage DCAF1 as an interaction partner [23]. The lysates generated in this experiment show that all the aforementioned interaction partners were present or successfully expressed according to the sample in question (Fig. 12A), and the subsequent pulldown (Fig. 12B) revealed that TCF7 coprecipitates with DCAF1 even in the absence of Vpr or MG132. All samples featuring both Vpr and TCF7 showcase a lower signal for the latter protein, an effect prevented by the use of MG132. Indeed, employing this proteasome inhibitor leads to the successful coprecipitation of both TCF7 and Vpr, revealing an indirect interaction between these two through DCAF1; only the Q65R Vpr mutant was unable to coprecipitate with DCAF1.

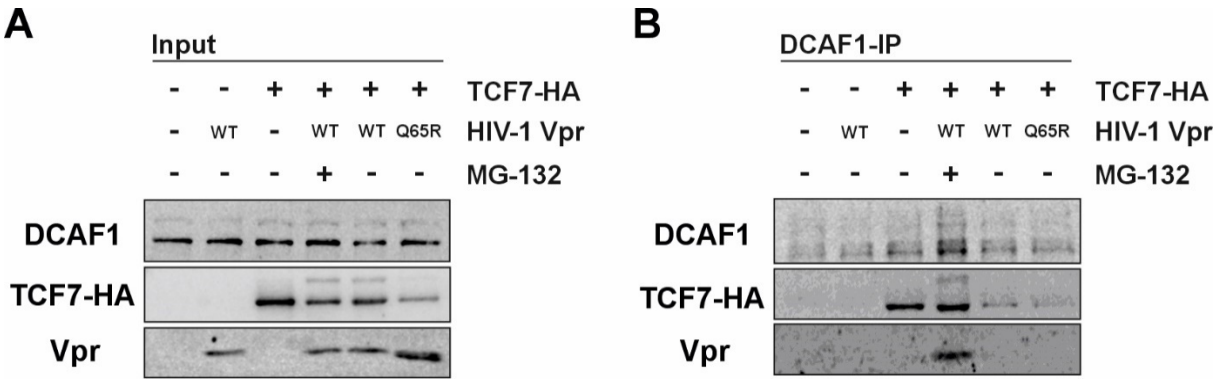

Figure 12: Vpr and TCF7 coprecipitate with DCAF1. HEK/293T cells were transfected with pCG_IRES-GFP (Empty Control), pCG_DNA3-HA-TCF7 (TCF7-HA), pCG_Vpr-IRES-GFP (HIV-1 Vpr WT), or pCG_AU1-Vpr(Q65R)-IRES-GFP. After a medium change, some samples were supplemented with MG132 (1 µM). At 48 hpt, cells were harvested and lysed as described in section V.II.XIV. Protein expression and interactions were analyzed via SDS-PAGE coupled to WB. Depicted are representative WB results featuring Input (A) samples of the aforementioned lysates and their corresponding CoIPs (B), performed using Anti-Rabbit IgG IP beads (Rockland) and anti-VprBP/DCAF1 (Rabbit) antibodies. TCF7, HIV-1 Vpr (WT/Q65R), and DCAF1 were stained against using the corresponding primary and secondary antibodies (see V.I.IX). N = 2.

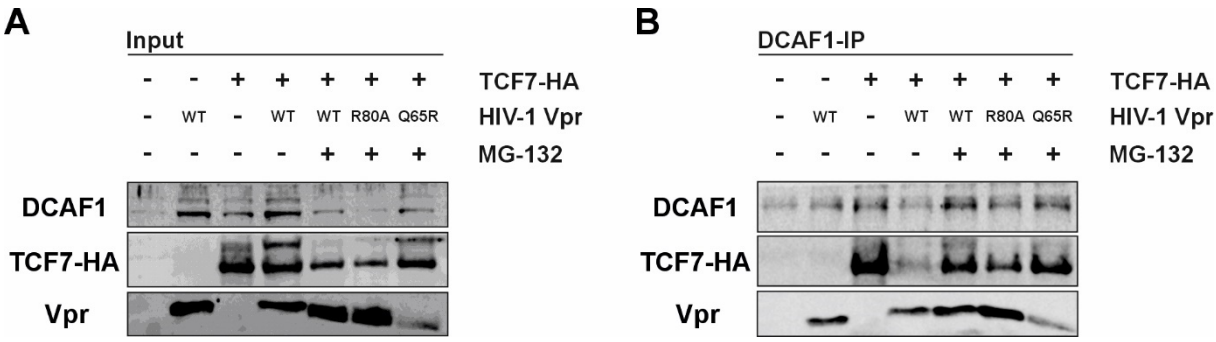

Figure 13: DCAF1 mediates an indirect Vpr–TCF7 interaction. HEK/293T cells were transfected with pCG_IRES-GFP (Empty Control), pCG_DNA3-HA-TCF7 (TCF7-HA), pCG_Vpr-IRES-GFP (HIV-1 Vpr WT), pCG_AU1-Vpr(Q65R)-IRES-GFP, or pCG_AU1-Vpr(R80A)-IRES-GFP. After a medium change, some samples were supplemented with MG132 (1 µM). At 48 hpt, cells were harvested and lysed as described in section V.II.XIV. Protein expression and interactions were analyzed via SDS-PAGE coupled to WB. Depicted are the WB results featuring Input (A) samples of the aforementioned lysates and their corresponding CoIPs (B), performed using Anti-Rabbit IgG IP beads (Rockland) and anti-VprBP/DCAF1 (Rabbit) antibodies. TCF7, HIV-1 Vpr (WT/Q65R/R80A), and DCAF1 were stained against using the corresponding primary and secondary antibodies (see V.I.IX). N = 1.

A third assay of this nature was performed using a similar experimental setup, but additionally included MG132(+) samples not only in the case of HIV-1 Vpr WT, but also for the Vpr mutants Q65R and R80A, the latter being a LTNP-associated Vpr variant notorious for its reduced cytopathicity [149] but nonetheless possessing WT-like DCAF1-recruiting capabilities [70]. Input samples for this experiment (Fig. 13A) demonstrate that DCAF1 was present in every sample to varying extents, and both TCF7 and all Vpr variants were expressed successfully. The corresponding CoIP samples (Fig. 13B) again showcase that TCF7 coprecipitates with DCAF1 both in the absence and in the presence of Vpr, with the signal for TCF7 also showing a qualitative decrease in the latter case. MG132(+) samples demonstrated that Vpr WT and R80A successfully coprecipitate with DCAF1 along with TCF7, whilst Vpr Q65R coprecipitated less markedly. Lastly, the sample containing Vpr only also showed that this protein coprecipitates with DCAF1 independently of the presence of other interaction partners.

VI.VIII DCAF1 and TCF7 colocalize in nucleoli

To identify the subcellular compartment where the Vpr-DCAF1-TCF7 interaction takes place, an IF setup featuring vector-expressed TCF7-mScarlet and DCAF1-YFP, along with untagged Vpr and 1 µM MG132, was carried out in HEK/293T cells. Qualitatively, the results thereof (Fig. 14A) indicate TCF7-mScarlet localizes to the nucleus, whilst DCAF1-YFP is present both in the nucleus as well as in the cytosol, though not in nucleoli. When co-expressed, red and green signals colocalized in the nucleus, though one of the two clearly dominates over the other, and no colocalization takes place in the nucleolus, an effect accentuated by the presence of Vpr. MG132, however, causes TCF7 and DCAF1 to colocalize in the nucleolus, this also being observed in the presence of Vpr. Employing Bravais-Pearson's correlation coefficient (Fig. 15) as a quantitative indicator for this phenomenon confirms a strong positive correlation for the colocalization of DCAF1-YFP and TCF7-mScarlet ($r = 0.65$), with MG132 boosting this effect ($r = 0.70$). Vpr notably weakens this positive correlation ($r = 0.44$), though the usage of MG132 rescues and further boosts TCF7-DCAF1's colocalization even in the presence of Vpr ($r = 0.67$).

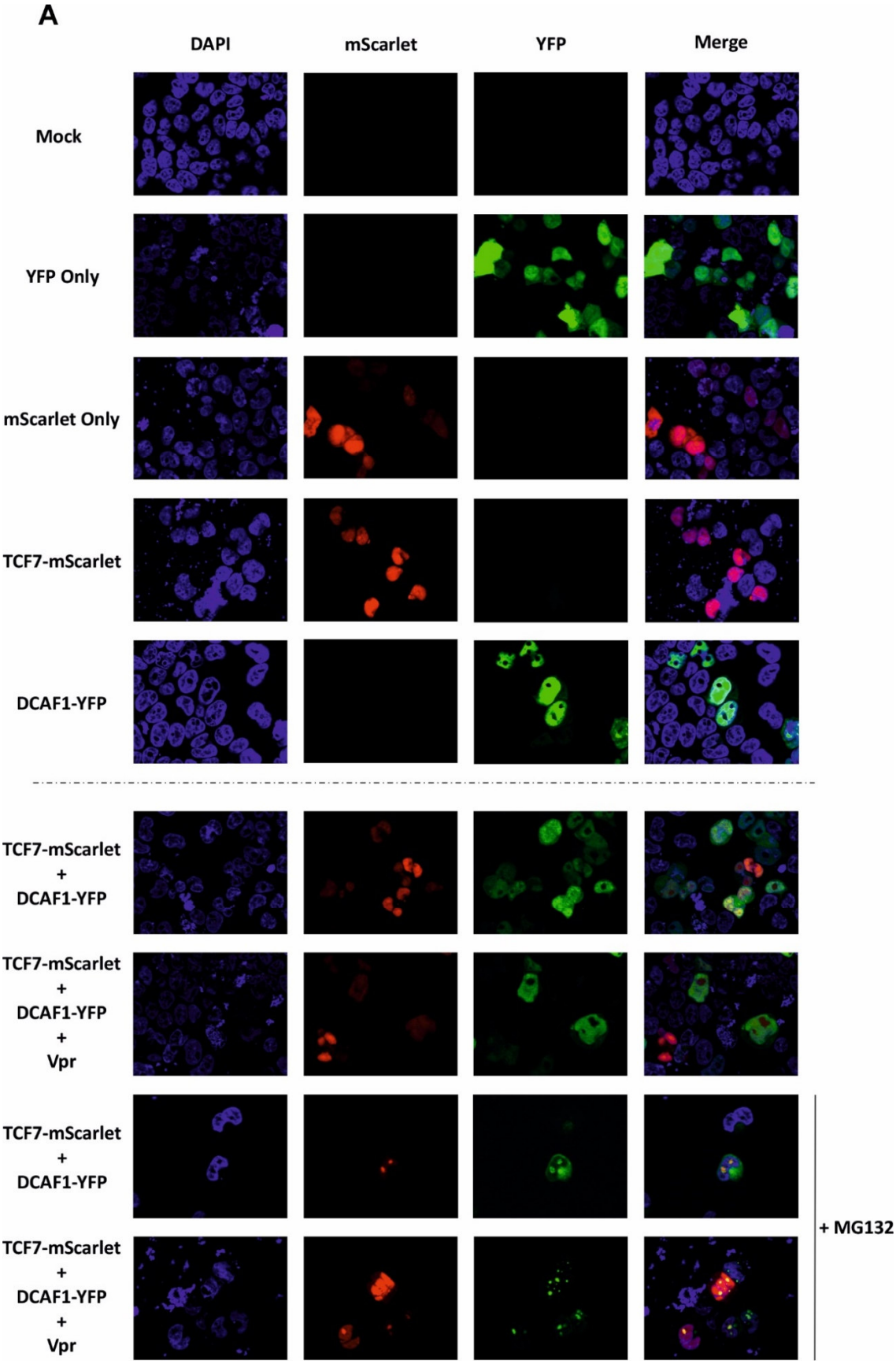

Figure 14: DCAF1 and TCF7 colocalize in the nucleolus. HEK/293T cells were transfected with plasmids encoding the indicated proteins. At 16 hpt, a medium change was carried out, whereupon the corresponding samples were treated with MG132 (1 μM). At 48 hpt, cells were fixed, treated with DAPI, mounted, and visualized as indicated in section V.II.XXIII. Red fluorescence (mScarlet) corresponds to tagged TCF7, green fluorescence (YFP) to tagged DCAF1, and blue fluorescence corresponds to DAPI (cell nucleus). (A) Representative results for the aforementioned assay are shown. N = 3.

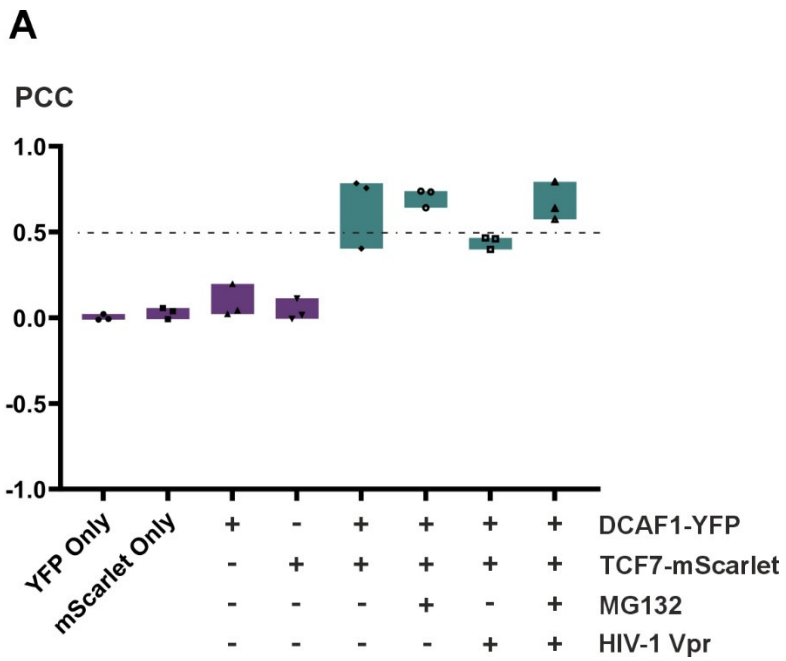

Figure 15: The colocalization of DCAF1 and TCF7 is abrogated by Vpr and strengthened by MG132. HEK/293T cells were transfected with plasmids encoding the indicated proteins. At 16 hpt, a medium change was carried out, whereupon the corresponding samples were treated with MG132 (1 µM). At 48 hpt, cells were fixed, treated with DAPI, mounted, and visualized as indicated in section V.II.XXIII (A) Bravais-Pearson's correlation coefficient (r) between the red (mScarlet) and green (YFP) fluorescence variables of the aforementioned experiment. The dotted line (r = 0.5) indicates the generally accepted threshold for a strong positive correlation. N = 3.

Altogether, the results from Figs. 9-13 point towards Vpr-mediated TCF7 degradation requiring an initial contact between DCAF1 and TCF7 that preempts the inclusion of Vpr in this tripartite interaction. Figs. 14 & 15 suggest this phenomenon occurs in the nucleus, particularly in nucleoli.

VI.IX Vpr does not disrupt the Wnt/β-Catenin signaling pathway in primary stimulated CD4⁺ T cells

Since TCF7's role as a transcriptional factor converges with the Wnt/β-Catenin signaling pathway at various TCF/LEF binding sites in the chromatin (WREs), we sought to explore whether Vpr's subversion of TCF7 affects this pathway in primary stimulated CD4⁺ cells. To this end, highly concentrated HIV-1 NL4-3 viral stocks, with or without a functional *vpr* ORF, were used to infect primary CD4⁺ T cells pre-stimulated for 3 days with PHA and additionally treated with 1 µM Tideglusib (β-Catenin activator) or 200 nM Adavivint (β-Catenin inhibitor). These were harvested at 72 hpi and analyzed via flow cytometry by staining against p24 and cMyc, a gene product whose expression is controlled by WREs, i.e. downstream of Wnt/β-Catenin signaling activation [150]. Fig. 16 reflects the results thereof, where infection status did not significantly impact infection rates, irrespective of whether the Wnt/β-Catenin signaling pathway was artificially activated or inhibited in the host cells (Fig. 16A). Within the bulk population, no statistically significant changes were detected in the cMyc MFI values when compared to Mock, indicating that neither HIV-1 WT nor HIV-1 ΔVpr affect the overall amount of expressed cMyc, independently of the activation status imparted to the Wnt/β-Catenin signaling pathway by the use of Tideglusib or Adavivint (Fig. 16B).

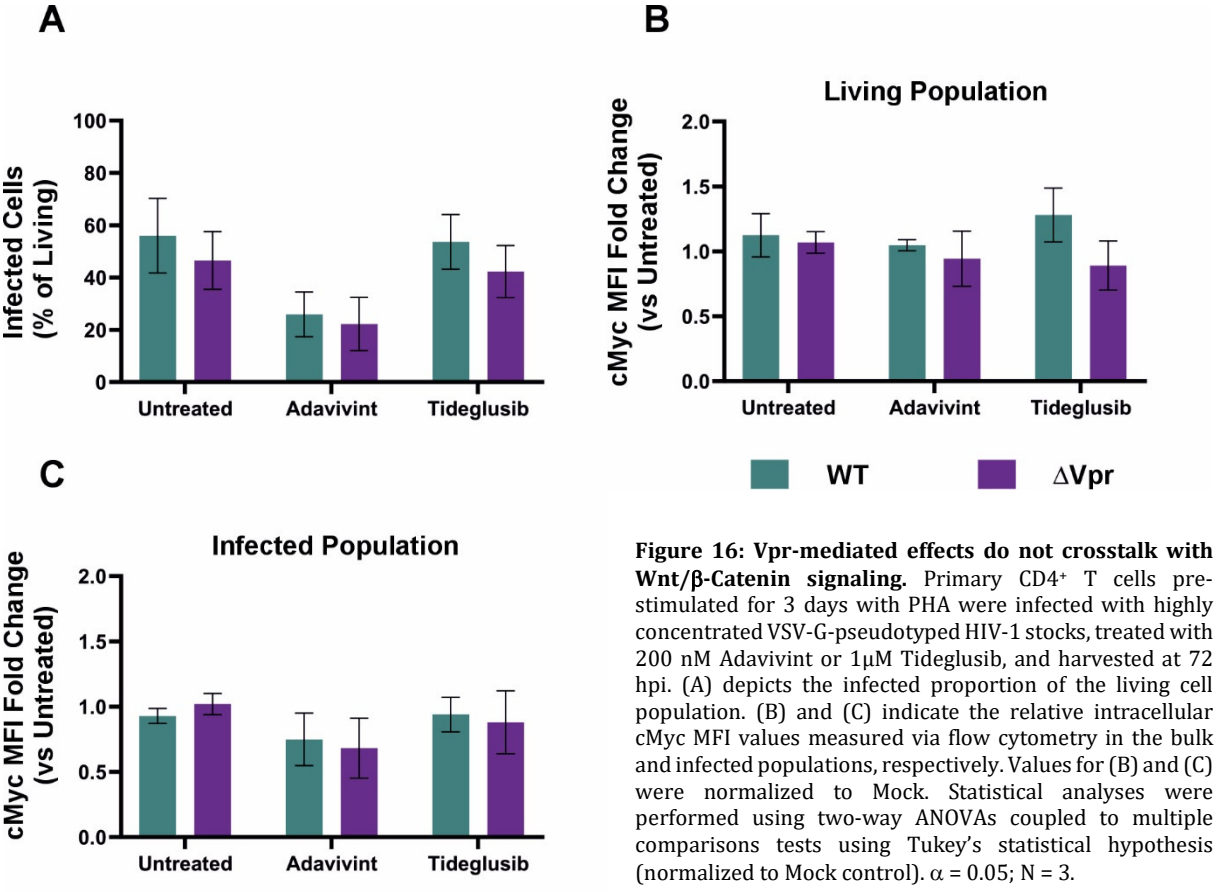

Figure 16: Vpr-mediated effects do not crosstalk with Wnt/β-Catenin signaling. Primary CD4⁺ T cells pre-stimulated for 3 days with PHA were infected with highly concentrated VSV-G-pseudotyped HIV-1 stocks, treated with 200 nM Adavivint or 1μM Tideglusib, and harvested at 72 hpi. (A) depicts the infected proportion of the living cell population. (B) and (C) indicate the relative intracellular cMyc MFI values measured via flow cytometry in the bulk and infected populations, respectively. Values for (B) and (C) were normalized to Mock. Statistical analyses were performed using two-way ANOVAs coupled to multiple comparisons tests using Tukey's statistical hypothesis (normalized to Mock control). $\alpha = 0.05$; N = 3.

In the exclusive case of HIV-1-infected cells, the MFI levels of cMyc did not differ in an infection status-dependent manner for any of the employed treatments, indicating that Vpr-mediated effects did not crosstalk with this signaling pathway under the studied experimental conditions (Fig. 16C).

VI.X Two different gene silencing approaches did not sufficiently impact TCF7 protein levels in primary CD4⁺ T cells

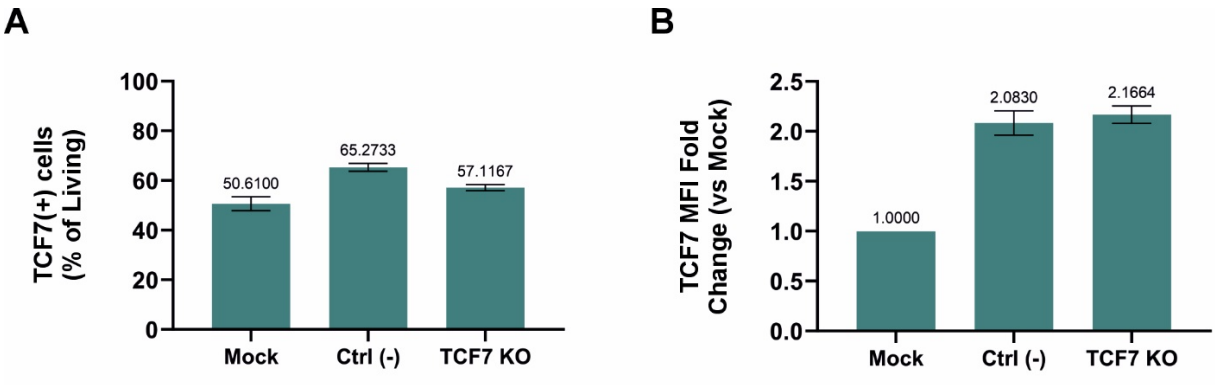

Figure 17. CRISPR/Cas9 gene editing against TCF7 did not alter the proportion of TCF7(+) lymphocytes. PHA-stimulated primary CD4⁺ T cells were electroporated with α-TCF7 CRISPR RNPs (as described in V.II.XII) and harvested at 96 for flow cytometric analysis. (A) depicts the TCF7(+) proportion of the living cell population. (B) indicates the relative intracellular TCF7 MFI values measured via flow cytometry in the bulk population. Values for (B) were normalized to Mock.

Considering the importance TCF7 possesses as a transcriptional factor towards T cell development, maturation, activation, and eventual differentiation, we sought to study the effects a TCF7 knockout / knockdown would exert over lymphocyte physiology in the context of HIV-1 infection. To this end, two different experimental approaches were employed: CRISPR gene editing and FANA ASO-mediated gene silencing.

The first approach, for which a protocol has been standardized in our group, consisted on the electroporation of PHA-stimulated CD4⁺ T cells (except for Mock) using self-assembled CRISPR RNPs, which were kept in culture and harvested at 96 hpt to be analyzed via flow cytometry. The results thereof indicate that the total amount of TCF7⁺ cells in the overall living population did not significantly decrease upon treatment in comparison to the corresponding negative control (Fig. 17A). Further, the relative abundance of TCF7 in treated cells did not differ from that of the negative control (Fig. 17B), though both of these samples did exhibit a twofold increase in the amount of said protein when compared to Mock.

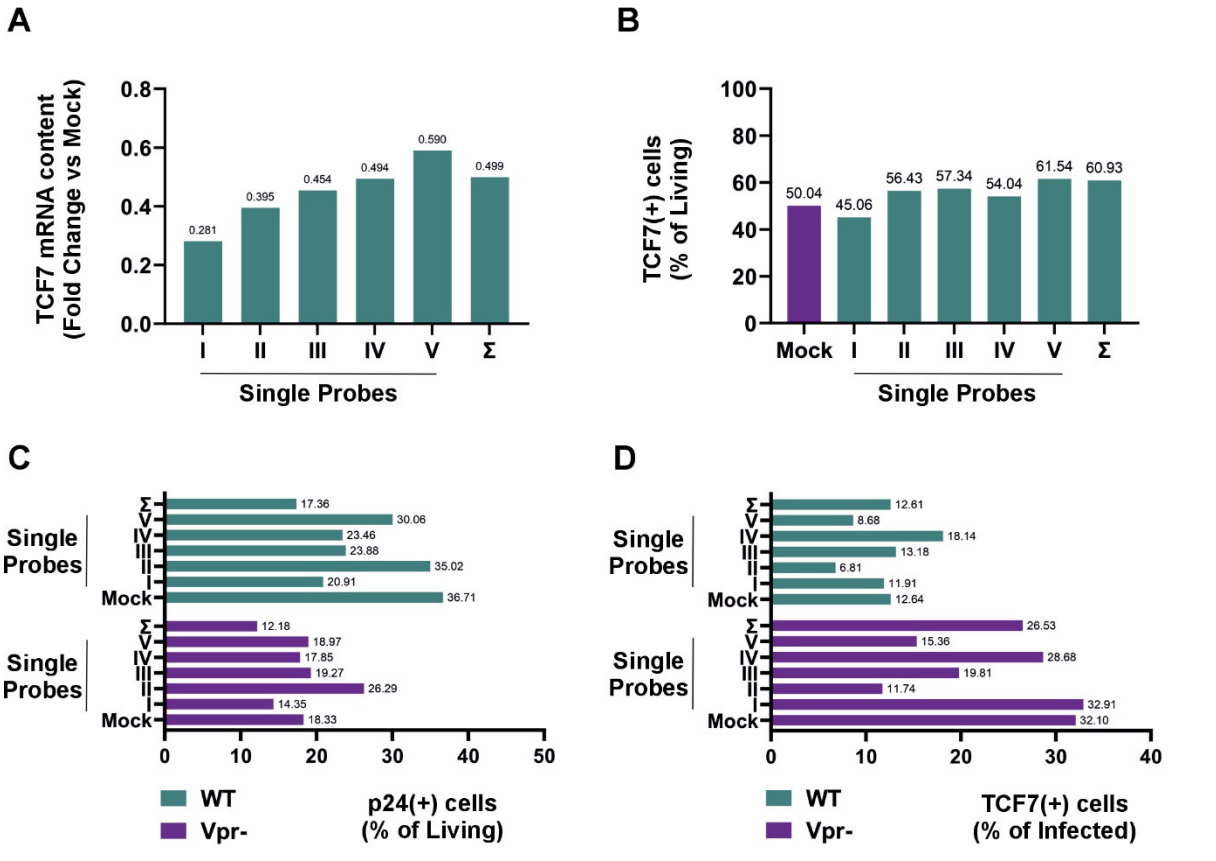

Figure 18. FANA ASO gene silencing against TCF7 depletes TCF7 mRNA levels. PHA-stimulated primary CD4⁺ T cells were transfected with various α-TCF7 FANA ASOSs (as described in V.II.XII) and partly harvested at 72 hpt for qPCR and flow cytometric analysis. Afterwards, they were infected with the indicated VSV-G-pseudotyped HIV-1 viral stocks and fully harvested at 48 hpi (120 hpt). (A) Relative TCF7 mRNA content of cells treated with various α-TCF7 FANA ASOs (normalized to Mock) at 72 hpt. (B) TCF7(+) proportion of the living cell population in each of the cell samples treated with various α-TCF7 FANA ASOs at 72 hpt. (C) Absolute infection rates of various ASO-treated CD4⁺ T cells infected with VSV-G-pseudotyped HIV-1 (WT/ΔVpr) as measured at 48 hpi (120 hpt) via flow cytometry. (D) TCF7(+) proportion of the infected cell population in each of the cell samples treated with various α-TCF7 FANA ASOs at 48 hpi (120 hpt).

The second approach to silence TCF7 was subsequently tackled, for which PHA-stimulated primary $CD4^+$ T cells were transfected using various α-TCF7 FANA ASOs. At 72 hpt, all the ASO probes employed heavily depleted the TCF7 mRNA content found in these cells in comparison to Mock, though an equimolar mixture of all 5 (Σ; 0.4 nmol / probe) did not exhibit an edge in terms of silencing efficacy (Fig. 18A). This notwithstanding, none of the ASO probes did significantly reduce the $TCF7^+$ proportion of the living cell population when compared with Mock. Infecting these cells using the indicated VSV-G-pseudotyped HIV-1 viral stocks led to the infection rates depicted in Fig. 18C, where WT viruses showcased a clear advantage in terms of infectiousness when compared to their Vpr-deficient counterparts; this effect was additionally reflected by the proportion of $TCF7^+$ cells within the infected population, where the presence of Vpr correlated with a decrease in TCF7 levels (Fig. 18D). Nonetheless, this approach was unable to fully deplete TCF7 in the target cell population, disallowing the possibility of studying the effects of its absence in the context of HIV-1 infection.

VI.XI Preliminary experiments exploring Vpr's role in the context of G3BP1-containing SG formation

G3BP1, another potential Vpr target protein identified through Dr. Anthea Darius' non-targeted proteomics, is best known for its role as an initiator of SG formation [151], a phase separation phenomenon intrinsically tied into RLR-mediated innate immunity against viral RNA. To this end, HIV-1 expression vectors encoding HIV-1 (with or without a functional *vpr* ORF) and mCherry as a reporter gene were subcloned and used to generate VSV-G-pseudotyped viral stocks in HEK/293T cells. In turn, these were used to infect U-2 OS cells stably expressing G3BP1-GFP for a timecourse experiment, where cells were harvested at 24 and 48 hpi for flow cytometric analyses. Fig. 19 shows the results thereof, where both WT and Vpr-deficient viruses exhibited a time-dependent increase in infection rates (Fig. 19A). Analogously, the dot plots in Fig. 19B illustrate the distribution of the virus-treated U-2 OS cell population at 24 hpi, where WT-infected cells showcased both higher infection rates and a higher mScarlet MFI than cells treated with the Vpr-deficient viruses.

In order to explore whether the putative Vpr-G3BP1 interaction plays a role in SG formation, a live cell imaging-based experimental setup using both the aforementioned G3BP1-GFP-expressing cells as well as the subcloned mScarlet reporter viruses was devised, additionally featuring the use of $NaAsO_2$ to artificially induce SG buildup [152]. After establishing a working $NaAsO_2$ concentration high enough to prime SG formation but low enough to allow for cell survival, this experiment was carried out multiple times, with $NaAsO_2$ treatment taking place at 24 hpi. Fig. 19C shows representative images thereof, with the chosen visualization timepoint corresponding to 36 hpi and 12 hours post-$NaAsO_2$ treatment. Therein, it is possible to observe that some U-2 OS cells accumulate G3BP1-containing SGs even in the absence of $NaAsO_2$, though the use of this inorganic reagent greatly boosts the formation of said structures.

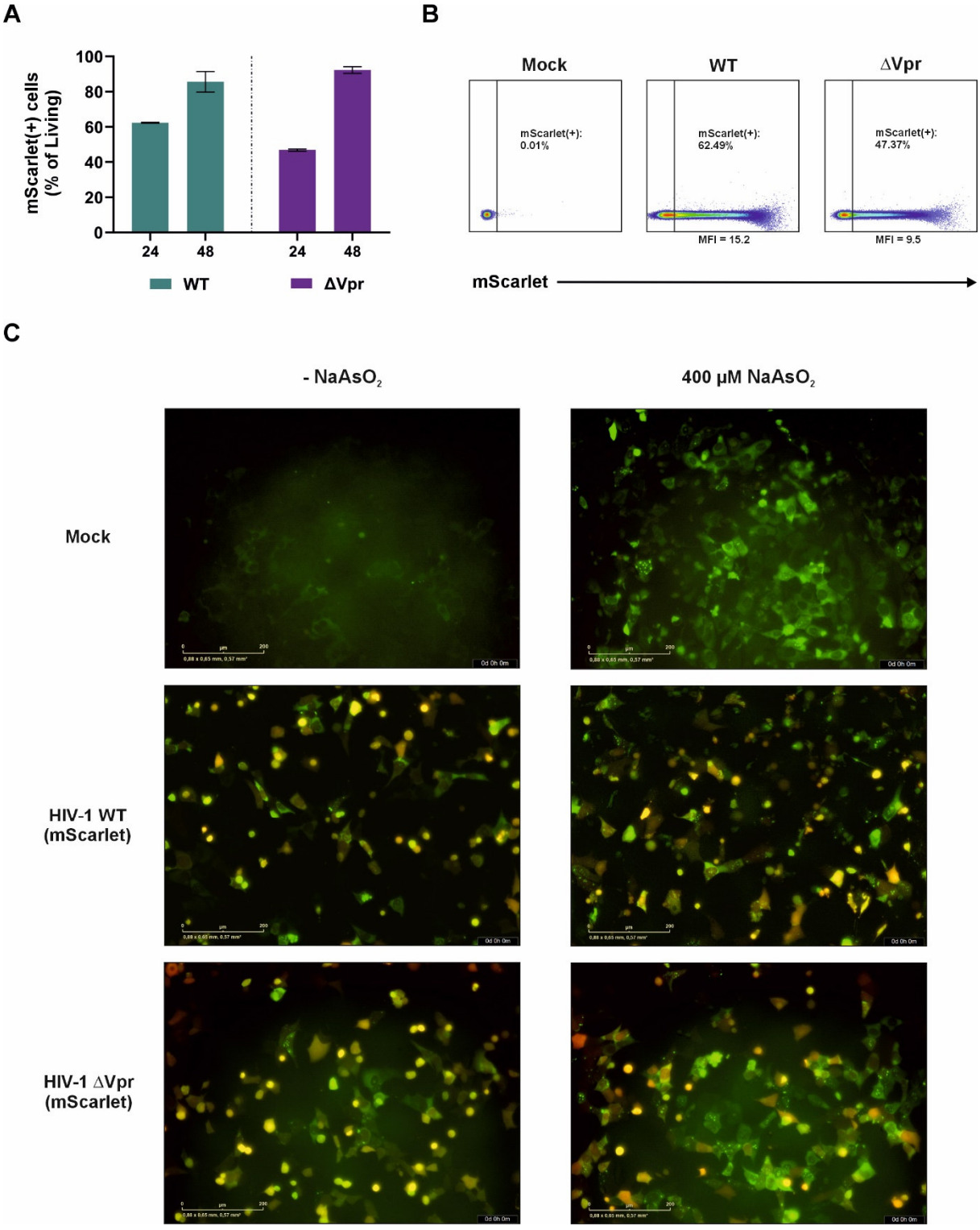

Figure 19. Preliminary assays exploring Vpr's role in the formation of G3BP1-containing SGs. VSV-G-pseudotyped viral stocks were generated by transfecting HEK/293T cells with HIV-1 (WT/ΔVpr)-encoding plasmids further expressing mScarlet as a reporter gene. These were employed to infect U-2 OS (G3BP1-GFP) cells, which were harvested at 24 and 48 hpi and analyzed via flow cytometry. (A) depicts the proportion of mScarlet(+) cells under both infection conditions at various timepoints. (B) shows representative dot plots for this experiment at 24 hpi. The corresponding average MFI values for both infection conditions are depicted underneath the corresponding dot plot. VSV-G-pseudotyped viral stocks were generated as described for (A) & (B), and employed to infect U-2 OS (G3BP1-GFP) cells. These cells were treated with 400 µM $NaAsO_2$ at 24 hpi, and visualized every 3 hours for 2 more days. (C) representative images of HIV-infected, $NaAsO_2$-treated U-2 OS (G3BP1-GFP) cells at 12 hpt (36 hpi). Green fluorescence corresponds to GFP-tagged G3BP1. Red fluorescence corresponds to the expression of reporter gene mScarlet in HIV-1-infected cells.

When treated with $NaAsO_2$, HIV-1 ΔVpr-infected U-2 OS cells qualitatively accumulated more SGs than their HIV-1 WT-infected counterparts, whilst Mock showcased the lowest amount thereof. However, the quantitative analysis of this data proved unfruitful, given how neither the Cytation-based nor the Incucyte-based counting algorithms could effectively distinguish between various intracellular structures and G3BP1-GFP-containing SGs. Independently thereof, these and other ImageJ-based counting algorithms reported a high level of red background fluorescence, further interfering with the identification of the infected cell subset in this assay.

VII Discussion

Four years after the Vpr ORF was initially identified by Ratner and colleagues [153], the first functional study aimed at elucidating its role within the HIV-1 life cycle concluded that Vpr is dispensable for infectivity, replication, and cytopathogenicity in lymphoid cell lines [154], though the possibility of it possessing subtle regulatory effects undetectable in their model cultures was not discarded by the authors either. Almost three decades later, Vpr's molecular physiology continues to puzzle the scientific community owing to the fact that it has been described to establish pleiotropic interactions with a broad spectrum of host cell components [15,16], but the exact mechanisms through which various of its attributed regulatory effects take place remain only partly characterized. The present work endeavored to advance the understanding of Vpr's impact on primary $CD4^+$ T cells within the context of HIV-1 infection, addressing previously unexplored scientific questions across various organizational levels, ranging from target protein degradation and signaling disruption to immune modulation and transcriptional reprogramming.

VII.I Vpr & the disruption of intracellular signaling

As beforehand alluded to, much research has been performed on the disruptive effect Vpr has on various signaling cascades within host T cells, with special emphasis put on those related to immune function, inflammation, proliferation, and survival. JAK-STAT, IFN, and NF-κB signaling, as drivers of such phenomena, have long been suspected of being targets for Vpr. To this end, various experiments were performed to study whether virion-delivered Vpr can actively induce these pathways, whilst other assays employed pathway-specific inhibitors to test if Vpr's support of productive infection would dwindle as a consequence thereof.

The JAK-STAT pathway, crucial towards proliferation and survival, is a signaling cascade suspected of playing a prime role in HIV-1 pathogenesis. Fig. 3A-D indicates that inhibiting this pathway at the JAK1/2 step with 10 μM Ruxolitinib in HIV-1-infected, PHA-stimulated primary $CD4^+$ T cells does not diminish infection rates or p24 MFI values at 48 hpi in a statistically significant manner. Nevertheless, the use of this inhibitor did slightly reduce both of these parameters in the case of WT-infected T cells (Fig. 3A & 3C), whilst cells infected with Vpr-deficient viruses remained largely unaffected (Fig. 3B & 3D). Further experiments carried out on resting (i.e. non-stimulated) $CD4^+$ T lymphocytes revealed that infection with highly concentrated viral stocks did not increase the proportion of the cellular population exhibiting a T_{RM}-like phenotype when compared to Mock (Fig. 2A). These results do not completely align with the existing literature, as a dependence on the JAK-STAT pathway could not be proven, despite other studies indicating that sub-micromolar Ruxolitinib concentrations suffice to inhibit HIV-1 replication in human leukocytes [155], including $CD4^+$ T cells [156]. Nevertheless, the aforementioned non-statistically significant trend in the reduction of infection rates and p24 MFI values exhibited by HIV-1 WT-infected T cells (Fig. 3A & 3C) could be an indicator of a disconnect between the studied phenomenon and the cell model employed. Indeed, the constitutive activation of

STATs in PBMCs and CD4+ T cells from individuals with progressive HIV disease was described in 1999 [157], with a novel study by Reuschl and colleagues demonstrating that Vpr is able to synergize with IL-7 signaling to ectopically activate STAT5, inducing a tissue residence-like phenotype upon delivery into memory CD4+ T cells [147]. This effect has been demonstrated to alter the epigenetic landscape of the host cell, pushing its phenotype towards polyfunctionality [158], though it requires the presence of additional leukocytes, such as non-cytolytic CD8+ cells [159] or activated macrophages [160]. Contrastingly, our experiments were performed on "bulk" CD4+ T cells and not in memory T cells, a subset seen to be preferentially infected by HIV-1 [147]. Additionally, our model is based on the culture of said isolated T cell population without the presence of other leukocytes, excluding a crucial element of JAK-STAT stimulation in the context of infection [159,160]. As such, follow-up experiments ought to more holistically integrate said physiologically relevant elements in order to better represent the conditions under which the interaction between JAK-STAT signaling and Vpr action takes place, with particular emphasis being placed on choosing the appropriate T lymphocyte subset as a host for infection.

Particularly in the case of the IFN pathway, the results presented in Fig. 1B indicate that none of the various Vpr alleles tested activated this signaling cascade in Jurkat-Dual cells at 32 hpi, as no reporter ISG activation could be detected. Though IRF1 and IRF2 have been shown to play an early role in the HIV-1 life cycle by upregulating the transcriptional activity of the viral LTR through their binding sites therein [161], IRF activation is canonically associated with the expression of myriad genes linked to inflammation and host defense [162], with IRF3 serving as a central node for various innate immune defense systems, such as cGAS-STING, TLR3, and RLRs [163]. This result falls in line with the existing literature, where it has been shown that Vpr trumps the activation of IFN signaling by eliciting the proteasomal degradation of IRF3 in Jurkat T cells and PBMCs [109]. Additionally, Vpr has been demonstrated to negate the possibility of IRF3 localizing to the nucleus by sequestering and degrading KPNA1 in primary CD4+ T cells [87], collaborating with Vpu in reducing the overall intracellular levels of this immune transducer [164]. As such, future experiments ought to corroborate the proteasomal degradation of IRF3 and its homologues in primary T cells, so as to establish the mechanistic basis thereof in a more physiologically-representative context. This could be achieved with HIV-1 infection experiments employing WT and Vpr-deficient viruses, where cultured lymphocytes would be treated with the proteasomal inhibitor MG-132 in order to assess a potential interaction between Vpr, DCAF1, and IRF3 through co-immunoprecipitation assays. This phenomenon could be indirectly studied by stimulating the Jurkat-Dual model with the double-stranded RNA analogue poly(I:C) whilst concomitantly challenging it with HIV-1, in order to observe whether Vpr presence causes a decrease in ISG reporter activity.

Tightly coupled to IFN signaling, the NF-κB pathway is known to be triggered as a consequence of PRR engagement and thus plays a pivotal role in the induction of both innate as well as adaptive immunity [165]. The results presented in Fig. 1A indicate that none of the tested Vpr alleles upregulated this

signaling cascade at 32 hpi in Jurkat-Dual cells. Additionally, treating HIV-1-infected, PHA-stimulated, primary $CD4^+$ T cells with 10 μM SN-50, an NF-κB nuclear translocation inhibitor, did not reduce infection rates (Fig. 3A-B) nor p24 MFI values (Fig. 3C-D) at 48 hpi in a statistically significant manner, irrespective of Vpr presence. The mechanism whereby HIV-1 Vpr manipulates this particular pathway remains a hotly debated topic, as the available body of evidence tends to be inconsistent and sometimes contradictory [166]. HIV-1 has evolved various mechanisms to avoid triggering NF-κB-coupled innate immune defenses, such as fully maintaining the integrity of the viral nucleocapsid up until its docking unto the nuclear pores [167,168]. However, the newest advances in this field converge on the premise of HIV-1 manipulating NF-κB signaling in a highly time-dependent fashion, as its induction poses a transcriptional advantage during the early stages of the viral life cycle, but inhibiting it later on is also crucial towards preventing the activation of innate immunity [169]. The results presented in Fig. 4C could support this hypothesis, as the proportion of $CD69^-$ cells within the $p24^+$ population of PHA-stimulated primary T lymphocytes peaked at 48 hpi in the case of Vpr-deficient viruses, but the presence of Vpr delayed the statistically significant downregulation of this NF-κB-dependent [170] early activation marker to 72 - 96 hpi. Since an increase in CD69 expression has been demonstrated to be detectable as early as 2 hours after initial TCR engagement [171], afterwards decreasing in accordance to the immunological milieu the cells find themselves in, the aforementioned result could be suggestive of Vpr facilitating a more gradual decline in NF-κB signaling shutdown, allowing eventual immune evasion without compromising the survivability of the infected host cells. *Ex vivo* data supports this notion, as it has been observed that primary $CD4^+$ T cells from HIV^+ patients exhibit significantly lower CD69 levels upon PHA stimulation, an effect particularly marked on non-responders to HAART [172].

An elegant study by Murray and colleagues aimed to estimate the time required for HIV-1 to complete all the separate stages of its life cycle through the administration of various individual antiviral drugs *in vivo* [173]. The results thereof indicate that a complete round of virion export amounts to an average of 52 hours: 33 hours between virion delivery and the completion of RT, 4.6 hours before vDNA successfully integrates, 6.8 hours until viral production finalizes, and 7.6 hours for said viral progeny to propagate. This study also pointed out that RT takes place up to three times faster in T-derived cell lineages [174], meaning the duration of a single viral generation would comprise a minimum of 30 hours under such conditions. In light of these findings, considering our usage of more physiologically akin primary T lymphocytes, and according to the NF-κB modulation timeline postulated by Kirchhoff and collaborators [169], the experimental results herein presented decidedly correspond to a late timepoint within the viral life cycle. As such, neither the lack of Vpr-associated NF-κB activation nor the absence of an SN-50-mediated reduction in productive infection would contradict the available literature, though future experiments ought to capitalize on all the aforementioned knowledge to continue exploring whether Vpr actively participates in the modulation of NF-κB signaling, especially since virion-delivered Vpr is perfectly poised to play a dysregulating role during the first round of viral transcription, i.e. 12 to 16 hpi.

All in all, additional research is necessary to better comprehend how Vpr modulates various host cell signaling pathways in parallel to support HIV-1 in establishing a productive infection. Though previously investigated [109,175], various steps in the Vpr-mediated suppression of IFN signaling still warrant validation in a physiologically relevant model, such as $CD4^+$ T lymphocytes or *ex vivo* lymphoid tissue. Further, the role of Vpr in Kirchhoff's [169] theory of HIV-1's dual-edged NF-κB modulation ought to continue being explored at the molecular level, with particular emphasis put on covering the timepoints comprising early LTR transcription, ideally in a similarly relevant biological model. Finally, implementing some of the newest advances in immune system modeling, such as engineered organoids or microfluidic chips mimicking the pluricellular structure and function of lymph nodes [176], will help overcome the limitations posed by the use of monotypic bulk $CD4^+$ T cell cultures in researching Vpr's leverage of the JAK-STAT pathway.

VII.II Vpr & the activation of NF-AT

First described in 2003 [177], Vpr-mediated NF-AT activation is a phenomenon presumed to alter the expression of multiple genes implicated in the establishment of a distinctive T cell phenotype exhibited during HIV-1 infection. Using unstimulated primary $CD4^+$ T lymphocytes, Höhne and collaborators demonstrated that virion-delivered Vpr enhances HIV-1 productive infection and promotes the activation of NF-AT, in parallel employing the NF-AT inhibitor FK-506 to corroborate that trumping this process does lead to a decrease in LTR transcription, G_2/M cell cycle arrest, early T cell activation, and overall productive HIV-1 infection [112]. However, very little further evidence exists describing a link between Vpr activity and NF-AT signaling in the context of HIV-1 infection. In order to confirm and further build on this knowledge, experiments employing the indirect NF-AT inhibitor FK-506 were carried out on activated primary $CD4^+$ T cells, aiming to assess how NF-AT activity impacts viral productivity and spread at various timepoints.

The results thereof indicate that, at 48 hpi, the infection rates (Fig. 3A) and p24 MFI values (Fig. 3C) attained by VSV-G-pseudotyped WT HIV-1 suffer a statistically significant decrease as a consequence of NF-AT inhibition, an effect not observed for Vpr-deficient HIV-1 viruses (Fig. 3B & 3D). Analogously, experiments employing native (i.e. non-VSV-G-pseudotyped) virus stocks show that the statistically significant advantage HIV-1 WT virions exhibit at 72 and 96 hpi against their Vpr-deficient counterparts in terms of infection rates and p24 titers (Fig. 4A & 4D) is completely abrogated upon NF-AT inhibition. Together, these results confirm that Vpr's ability to support a productive infection in stimulated $CD4^+$ T lymphocytes is indeed NF-AT dependent, agreeing with the existing literature in this field. However, none of the aforementioned differences could be observed in unstimulated T cells (Fig. 4B), either owing to an inherent biological variability across blood donors, or mayhap suggesting that the early (4 hpi) Vpr-mediated activation of NF-AT described by Höhne et al. [112] is later reflected in parameters not considered by the results presented in this thesis. To paint a more complete picture of Vpr's role in unstimulated T lymphocytes, future experiments ought to consider not only multiple

timepoints, but also explore potential virus-induced phenomena at various levels of biological organization, including transcriptomic, proteomic, and metabolomic effects. In addition, the experiments here presented made exclusive use of FK-506 as an NF-AT inhibitor, which indirectly achieves its effect by binding the immunophilin protein FKBP12 to preempt calcineurin activation [110]. Inherently, this mechanism may give way to stark off-target effects at the metabolic and signaling levels, potentially affecting a broader calcineurin-regulated gene set instead of just those genes whose regulation is determined by NF-AT. In order to complement these findings, a similar experimental setup could be employed to study whether more selective NF-AT inhibitors, including C17, MRD37, and CNBR3 [178], are capable of eliciting an effect comparable with that of FK-506, drawing parallels with the results herein presented.

Interestingly, the disparity across experiments regarding the timepoints at which the statistically significant Vpr-dependent effects herein described are first observed could be a consequence of the difference between viral entry mechanisms triggered by the employed viral stocks. In T cells, VSV-G-pseudotyped HIV-1 virions have been demonstrated to possess 20- to 130-fold higher infectivity in comparison to native viruses and additionally follow a different strategy regarding docking, entry, and payload delivery [179]. As such, follow-up assays should take this knowledge into consideration, as pseudotyped viruses could also affect intracellular signaling differently from native HIV-1.

VII.III Vpr & transcriptional dysregulation

Another strategy employed by HIV-1 to modify the intracellular conditions of its host is the alteration of its transcriptional landscape. A recent study comprehensively demonstrated that virion-delivered Vpr is sufficient to induce wide-ranging transcriptional alterations in primary $CD4^+$ T cells as early as 4.5 hpi, a signature that echoes unto later timepoints and precedes the triggering of ISGs, potentially dampening their activation [180]. Indeed, previous work by Dr. Anthea Darius (in collaboration with QBic Tübingen) pointed towards Vpr disrupting various physiological processes in primary HIV-1-infected T cells at 48 hpi, and the present work recapitulated this data to carry out a more in-depth analysis, taking stricter cutoff criteria into consideration.

As described in the results section, the PCA plot generated by the DESeq2 analysis (Fig. 5A) indicates that the largest contributor of variance across samples corresponds to infection status, with the second largest being donor identity itself. After applying a cutoff for entries with a Base mean value of zero, the results from Fig. 5B demonstrate that Vpr is responsible for the dysregulation of 2363 genes, corresponding to 40% of the total DEGs (5859) disrupted by HIV-1 as a whole. In contrast to the analysis presented by Bauby et al. [180], the proportion of genes we found to be dysregulated specifically by Vpr at 48 hpi did not amount to the majority of those differentially expressed by HIV-1. However, our dataset was generated using only the NL4-3 HIV-1 strain, whilst their experimental approach employed HIV-1_{IIIB} instead. Additionally, their meta-analysis compiled other transcriptomic datasets

generated using multiple HIV-1 varieties, including the primary isolates CH293, CH007, and STCO1 [181], as well as the $HIV_{89.6}$ [182] and HIV-1 NL4-3 [183] strains. Despite NL4-3 and IIIB both being CXCR4-tropic and similarly pathogenic towards peripheral T cells [30], various differences have been observed between their downstream effects, for example, in terms of JAK/STAT activation [184] or HERV-K induction [185]. The discrepancy between HIV-1 strains, coupled to the variance inherent to the use of donor-derived primary T lymphocytes, may thus account for the dissimilarities observed across both studies.

A further cutoff for entries with a Base mean value below 100 and a p-adjusted value below 0.05 led to the refinement of our Vpr-associated DEG list (Fig. 5C), encompassing only the most reliably dysregulated elements. From the remaining 1083 hits, 46.5% thereof were revealed to be under NF-AT control (Fig. 6A), and the EnrichGO analysis performed on this gene list indicated that most of the upregulated genes could be associated with innate immunity and signaling (Fig. 6B & 7A), whilst the downregulated hits correspond to various physiological processes including translation, cell cycle progression, and organelle activity (Fig. 6B & 7B). The qPCR assays (Fig. 8B-C) performed to validate the affliction of various entries from the top 70 up/downregulated gene list (Fig. 8A), however, did evidence a degree of discrepancy when compared to the transcriptomic data, particularly in the case of genes observed to be downregulated (Fig. 8C). Those dissimilarities may not only stem from the biological variability associated with using of donor cells not corresponding to the transcriptomic dataset, but also from the fact that some of the presented qPCR data compile repeat results generated by two independent experimental operators, adding to the statistical variance observed. Further, every data point corresponds to an independent infection assay, meaning that unequal infection rates can lead to varying degrees of quantitative dysregulation. These differences notwithstanding, the results discussed above do validate and expand Dr. Darius' aforementioned Metascape analysis (not shown) whilst resonating with the existing literature in the field, reiterating that HIV-1's widespread transcriptomic effects lead to the upregulation of innate immunity [182] and the downregulation of genes associated with ribosome biogenesis, protein translation [181], and cell cycle progression [180]. Notably, not only were we able to confirm Vpr's crucial involvement in the transcriptional takeover of the host cell [180], but our findings establish an unprecedented connection between two hallmark Vpr activities: transcriptional dysregulation and NF-AT induction.

Intriguingly, a novel study by Clark and colleagues revealed that primary HIV-1-infected memory T lymphocytes exposed to antiretroviral therapy possess a transcriptomic signature similarly favoring survival, proliferation, and HIV-1 silencing [186], highlighting how future efforts – coupled to the use of more representative immune modeling – stand to profit from the knowledge herein generated in order to thoroughly describe the transformation of the host cell transcriptome over the course of HIV-1 infection. Eventually, this could help explain how HIV-1 hijacks T cell diversification to generate its elusive reservoir populations [187], paving the way towards the development of a cure for HIV-1. Further, persistent NF-AT activation without AP-1 cooperation during chronic lymphocyte stimulation has

been identified as a key factor in driving an exhaustion-like phenotype in $CD4^+$ and $CD8^+$ T cells alike [111,188–191], decreasing TCR signaling sensitivity [189] whilst upregulating inhibitory receptors such as PD-1, LAG-3, and TIM-3 [190,192,193], as well as exhaustion-maintaining factors, such as NR4A and TOX/TOX2 [189,194–198]. As such, future studies could part from the herein presented data to mechanistically explore whether Vpr-mediated NF-AT activation plays a role in HIV-1's hallmark induction of $CD4^+$ lymphocyte exhaustion, ideally placing attention on other physiological factors influencing this phenomenon, such as the epigenetic program or stimulation status of the T cell subset used for the infection assays in question.

VII.IV Vpr & the selective remodeling of the host's proteome

Using Vpr to selectively hijack the cell's protein degradation machinery is a well-documented strategy employed by HIV-1 to establish a favorable intracellular milieu whilst overcoming several obstacles posed by innate immunity. In 2019, a study performed in CEM-T4 cells revealed that most of the proteomic changes observed in HIV-infected cells can be attributed to Vpr, resulting in widespread target protein degradation [24]. This, coupled with the publication of a functional proteomic atlas of infected primary $CD4^+$ T lymphocytes [27], has helped explain the molecular basis of many Vpr-attributed *in vivo* phenotypes. In agreement with these findings, Dr. Anthea Darius' non-targeted proteomic assays (not shown) unveiled a cohort of proteins whose abundance was significantly reduced at 24 and 48 hpi in the presence of Vpr, and the present work aimed to delve deeper into the mechanism behind the depletion of certain such targets, chiefly TCF7 and G3BP1.

First, we explored the mechanism whereby TCF7 is degraded by Vpr, employing both Kusabira Green and FACS-FRET assays to test whether Vpr interacts directly with its target in a highly-transfectable HEK/293T cell model. The results presented in Fig. 9A did not support this theory, as the studied Vpr-TCF7 pairs yielded no significant increase in the KG^+ population, and in no case did this increase amount to more than $1/20^{th}$ of the signal generated by the positive control. Since low transfection efficiencies could be cited as a reason for this method not working, FACS-FRET was employed instead. Fig. 9B shows that the FRET signals for all Vpr-TCF7 pairs were markedly weaker than for the positive control, indicating that both of the fluorophore-bearing proteins under scrutiny are separated by a distance within the 10-100 Å range, albeit clearly outside the 30-60 Å Förster radius [199]. In addition, the results shown in Fig. 10 also indicate that Vpr did not coprecipitate with TCF7, further confirming that Vpr does not establish a direct protein-protein interaction with this target.

In light of these findings, and given how Vpr can hijack the essential E3 ubiquitin ligase substrate adapter DCAF1/VprBP to elicit the proteasomal degradation of numerous targets, including HLTF [38,44–46], Exo1 [43], MCM10 [200], and CENP-A [201], we pondered whether this could also be the case for TCF7. To test this idea, we sought to first analyze the same CoIP samples as in Fig. 10, as even if the pulldown against TCF7 did not uncover an interaction with Vpr, DCAF1 could still be in direct contact with TCF7.

This reasoning was later revealed to be correct, as evidenced by the results depicted in Fig. 11, where both TCF7 and DCAF1 were observable in the blot. In this case, however, Vpr was not observed, possibly due to the various washing steps in the CoIP protocol having caused its disappearance. As such, this hypothesis was tested again, this time performing pulldown assays against DCAF1 in order to explore whether TCF7 and various Vpr mutants coprecipitate with this adaptor protein. The results thereof (Fig. 12B & 13B) indicate that TCF7 does interact with DCAF1 independently of Vpr, and the presence of WT Vpr lowered the overall levels of this protein unless MG-132 was employed. Both Vpr WT and the R80A mutant, but not the Q65R mutant, were able to coprecipitate with DCAF1 and TCF7, further highlighting that Vpr's DCAF1-binding capabilities are mechanistically relevant towards the completion of the tripartite interaction between these proteins. The immunofluorescence results (Fig. 14) and their corresponding quantification (Fig. 15), in turn, indicate that the interaction between TCF7 and DCAF1 took place in the nucleolus, as the concomitant expression of mScarlet- and YFP-tagged versions of these proteins, respectively, led to a pronounced colocalization therein (r = 0.65), an effect that was intensified by the decoupling of the proteasomal degradation pathway (r = 0.70). In accordance with the aforementioned CoIP results, the presence of Vpr led to a less pronounced TCF7-mScarlet signal, which was also reflected by a lower correlation coefficient with DCAF1-YFP (r = 0.44). Again, this effect was counteracted by the addition of MG-132 (r = 0.67).

The available literature in this field has established that Vpr-mediated protein degradation can follow one of two distinct pathways: either Vpr hijacks VprBP first and targets a substrate protein thereafter, as in the case of HLTF [46], UNG2 [23,39], and SMUG1 [39], or the interaction between VprBP and its target preempts the binding of Vpr, as observed for MCM10 [202] or TET2 [203]. Using all the information provided by our experiments, the Vpr-mediated degradation of TCF7 seems to follow the second pathway, as its binding to DCAF1 in the nucleolus happens independently of Vpr, and the addition of WT or R80A Vpr – but not Q65R Vpr - did reduce TCF7 levels noticeably. These observations are in line with the work previously performed by Dr. Darius, underscoring Vpr's role as a remodeler of the host's proteome. However, the CoIP results herein presented are of a purely qualitative nature, and future repetitions of this experiment ought to focus on quantifying this effect for it to become fully established. Further, the co-transfection of Vpr and TCF7 always led to visibly reduced levels of the latter protein, independently of MG-132 usage; this could point towards a transcriptional or translational bottleneck occurring in the HEK/293T cells, a factor that should be considered in follow-up experiments. In addition, subsequent efforts aimed at determining the precise subcellular localization of this tripartite interaction ought to consider that the aforementioned results, while broadly agreeing with Jurkat-derived proteomic evidence pinning TCF7 to the nucleolus [204], may diverge from the *in vivo* localization of this trans-acting regulator, as all the results pertaining to this complex protein assemblage were generated in HEK/293T cells. Considering TFC7's role as a chromatin-bound transcriptional factor in T cells [205] and Vpr's predominantly nuclear localization in the context of infection, as seen in PBMCs and primary $CD4^+$ T lymphocytes [206], the Vpr-DCAF1-TCF7 interaction would likely take place in a more chromatin-enriched nuclear sub-compartment. Further, the use of proteasomal inhibitor MG-

132, a compound reported to trigger cytotoxic effects in T cells [207] and cell lines alike [208], may not only impede the degradation of protein targets, but could also play a role in altering both their function and their distribution, as observed in U937 cells for AP-1, Ago2, TNF-R1, and IL-1R1, among others [209]. As such, studying this phenomenon in a more physiologically relevant model will prove crucial towards achieving a better understanding of TCF7 dynamics in the context of HIV-1 infection.

Even more intriguing than the Vpr-mediated degradation of TCF7 itself, researching the impact this phenomenon could exert on the physiology of HIV-1-infected T lymphocytes was the main objective of multiple follow-up experiments. First, PHA-stimulated primary $CD4^+$ T cells were infected with highly concentrated HIV-1 viral stocks to study whether Vpr's effect on TCF7 affects β-Catenin signaling, for which both an inducer and an inhibitor of this pathway, namely Tideglusib and Adavivint, were also employed. The results depicted by Fig. 16 indicate that the inhibition of this signaling cascade played a modest (albeit non-statistically significant) role in downmodulating infection rates, whilst its activation did not impact infection rates anyhow (Fig. 16A). cMyc, a well-established marker of β-Catenin activation [210–212], did not undergo a change in MFI values as a consequence of Tideglusib or Adavivint usage, neither in general (Fig. 16B) nor particularly in the infected fraction of the studied cell population (Fig. 16C), and no significant Vpr dependency could be observed in any of these cases. A limitation of the current study which may account for this result is the fact that endogenous cMyc was measured, and the levels of this protein are not exclusively dictated by Wnt/β-Catenin signaling, but also by the JAK/STAT pathway, amongst others [213]. A cellular model bearing a synthetic TCF/LEF construct with a reporter cMyc gene could facilitate the study of this phenomenon, as it would rule out the signaling interference elicited by parallel stimuli, including viral infection [214].

In parallel, two distinct experimental approaches were utilized to attempt the removal of TCF7 within primary $CD4^+$ T cells: CRISPR/Cas9 gene editing and FANA ASO gene silencing. The first method proved ineffective, as neither the overall proportion of $TCF7^+$ cells (Fig. 17A) nor the MFI values for this protein (Fig. 17B) were anyhow altered upon treatment. Nevertheless, the second method did successfully diminish TCF7's mRNA levels by up to 72% (Fig. 18A), even though the proportion of $TCF7^+$ cells was initially only reduced by a maximum of 5% (Fig. 18B). Upon exposure to HIV-1, Vpr presence exerted a clear positive effect on the infection rates achieved in these cells, although the effectiveness of the FANA ASO treatment did not correlate with this parameter (Fig. 18C). After both HIV-1 infection and ASO-KD, the proportion of $TCF7^+$ cells within the infected population shrank to an average of ~12% in the case of WT-exposed samples, compared to ~22.5% in the absence of Vpr (Fig. 18D), clearly showcasing the previously described negative impact Vpr exerts on TCF7 levels. However, the combined effects of ASOs and HIV-1 Vpr could not be further studied in the context of Wnt/β-Catenin signaling due to a combination of several factors, including the compounded cytotoxicity of both treatments, a notably reduced cell viability after various weeks of continuous culture, and a small sample size.

De novo TCF7 expression takes place mostly in immature $CD4^+$ $CD8^+$ thymocytes, where it collaborates with HEB and other members of the LEF/TCF family in defining the epigenetic profile of the developing T cell [215] whilst ensuring its survival [216]. For instance, TCF7 and HEB have been demonstrated to share ~7000 binding sites in the human genome, where they remodel the chromatin landscape to optimize the placement of various enhancer elements involved in modulating the activity of T cell development-relevant genes, such as *Tcra, Tcrb, Bcl2l1, CD4* and many more [215,217,218]. Notably, TCF7 has also been described to increase the chromatin accessibility of said loci through nucleosome displacement, with these showing a marked enrichment in activatory marks ($H_3K_4me_2/me_3$, H_3Ac, $H_3K_{27}Ac$) [215] despite TCF7's intrinsic HDAC activity [219]. However, TCF7 expression wanes as lymphocytes commit to more specialized roles [220–223], signifying that the turnover rate of this protein may be very low in mature $CD4^+$ T cells. As our experiments were performed on bulk $CD4^+$ T lymphocytes, the composition of this population could have been subjected to a high degree of inconsistency, as the abundance of naïve T cells within this fraction is dependent on myriad factors, including age, health status, and environmental influences [224,225]; this could eventually explain the relative unfruitfulness of the KO approaches employed, underscoring the necessity to search for a better-suited model where this phenomenon can be further explored.

As an example, TCF7 has been demonstrated to be of critical importance towards T_{FH} function, playing a central part in their differentiation, the establishment of immune memory [223], the activation of their antiviral response, and the sensitization of naïve $CD4^+$ T cells to their stimuli [226]. TCF7 also plays a central role in the physiology of $CD8^+$ T cells, where it is required for the maintenance of longevity, stemness, and proliferative capacity [227–229]. Additionally, TCF7 has been described to bridge the activation of the Wnt/β-Catenin pathway with the generation of memory $CD8^+$ T cells [230], and its presence has been demonstrated to be crucial for these lymphocytes to mount a sustained cytotoxic response against persistent viruses [231]. As such, the degradation of TCF7 in T_{FH} and $CD8^+$ T cells could trigger a multitude of detrimental effects, which, together, would highly resemble the exhaustion-like phenotype observed in the context of a productive HIV-1 infection, including features such as anergy, impaired memory formation, resistance towards activatory signals, reduced proliferation potential, diminished cytotoxic activity, and – as with various other bystander leukocyte subpopulations – highly accelerated rates of apoptosis [232–238]. Despite $CD8^+$ T cells not being a direct target for HIV-1 infection, and therefore ruling out the potential involvement of virion-delivered Vpr, the soluble counterpart of this viral accessory protein, frequently found in various immune compartments of HIV-1^+ patients [234,238,239], is able to penetrate into otherwise non-infectable leukocyte populations, including $CD8^+$ T cells [238].

To build upon this knowledge, future experiments ought to explore the effects of TCF7 degradation by either soluble Vpr in $CD8^+$ T cells or virion-delivered Vpr in follicular helper $CD4^+$ T cells, placing a particular emphasis on characterizing the alterations this protein exerts at the transcriptomic and

epigenetic levels, as this insight may prove essential towards understanding the establishment of T cell exhaustion during HIV-1 infection. In addition, future attempts to achieve an effective TCF7 KO/KD ought to capitalize on novel methodologies, such as the use of locked nucleic acid-modified single-stranded oligonucleotides, whose increased binding efficiency and thermal stability [240] allow for single base pair substitutions that can go unnoticed by the DNA mismatch repair machinery, whilst their operational simplicity and lack of additional components virtually eliminate potential toxicity issues in primary $CD4^+$ T cells [241].

As indicated by Dr. Darius' non-targeted proteomic data, another protein suspected to be an interaction partner for Vpr is the helicase G3BP1, better known for priming the formation of stress granules [151]. In order to explore the impact of this potential interaction on SG formation, an mScarlet-expressing variant of HIV-1 NL4-3 – with and without Vpr - was first subcloned to later perform preliminary infection assays on U2-OS cells stably expressing GFP-tagged G3BP1. At 24 hpi, mScarlet expression exhibited comparable intensities across both samples, pointing towards a successful delivery of the viral payload (Fig. 19B), though HIV-1 initially possessed a slightly competitive advantage in terms of spread over its Vpr-deficient counterpart. Nevertheless, both viral stocks eventually achieved infection rates of ~90% at the end of the measuring period (Fig. 19A). Upon infection, viral spread and stress granule formation were simultaneously tracked via live cell imaging, where a standard concentration of $NaAsO_2$ [242] was employed at 24 hpi to induce the formation of SGs in certain experimental samples.

As previously postulated, the measured samples exhibited a very high level of background red fluorescence, impairing the proper detection of the infected cell population in this assay. In order to address this issue, cells could be imaged whilst kept in phenol-free culture medium [243], and mScarlet could be replaced with mScarlet3 in the aforementioned viral constructs, as its quantum yield of ~70% would greatly increase overall signal brightness. Additionally, its enhanced acid resistance (pKa = 4.5) and faster maturation rate could aid in reducing background fluorescence by means of mitigating its mis-segregation and the diffusion of the signal into organelles such as lysosomes or endosomes [244]. Additionally, it was impossible to establish a quantitative correlation between the abundance of stress granules and Vpr presence under the experimental conditions herein chosen, as none of the employed algorithms could reliably differentiate SGs from other subcellular structures. This problem could be solved by processing the generated images with machine learning-based tools such as ilastik, which allow for the accurate distinction of SGs under less-than-ideal circumstances [119]. The output thereof could later be quantified using CellProfiler, enabling the possibility of drawing numerical conclusions from this data type [245]. Combining these approaches with further experiments aimed at evidencing the Vpr-mediated degradation of G3BP1 and its impact on SG-triggered antiviral signaling via RIG-I and MDA5 [246–248] will help further comprehend how Vpr supports the establishment of a productive infection through the subversion of innate immunity.

VIII Conclusions

The present work sought to explore the effects that Vpr exerts on its host cell at the protein and transcriptomic levels, as well as on various signaling pathways.

In line with the available literature, the herein presented results confirmed that Vpr does not trigger the IFN signaling cascade. Mimicking the effects observed at late HIV-1 infection timepoints, the NF-κB signaling pathway was similarly unaffected by the presence of Vpr, and artificially inhibiting its activation does not result in the dampening of HIV-1 infection. Contrary to expectations, however, inhibiting the JAK/STAT pathway did not impair HIV-1 spread.

Further agreeing with the available literature, this work corroborates Vpr's ability to activate NF-AT. The herein-performed bioinformatic analyses demonstrate how Vpr alone elicits the dysregulation of a multitude of genes, heavily influencing processes such as innate immunity, translation, cell cycle progression, and organelle activity. Importantly, this study revealed a functional link between Vpr-induced NF-AT activation and its broader transcriptomic effects, as nearly half (46.5%) of the most reliably dysregulated genes under Vpr's influence are controlled by NF-AT.

Mechanistically, Vpr was shown to co-opt the E3 ligase adapter DCAF1 to direct the chromatin remodeler TCF7 for proteasomal degradation. Nevertheless, this did not yield detectable alterations on Wnt/β-catenin signaling, as the pharmacologic modulation of this pathway yielded no effect in HIV-1–infected $CD4^+$ T cells. Various TCF7 depletion strategies only partially reduced its mRNA levels, but ultimately failed to ablate protein expression. Parallel work on G3BP1, a stress granule component, revealed technical challenges in monitoring SG dynamics during infection, leaving Vpr's role in SG disruption unresolved.

Altogether, this study highlights Vpr's ability to subvert host proteostasis, manipulate signaling networks, and remodel transcriptional programs to support the establishment of a productive HIV-1 infection in $CD4^+$ T lymphocytes.

IX Bibliography

1. Goff, S. Retroviridae. in *Fields Virology* (eds. Knipe, D. & Howley P) 1424–1473 (Lippincot Williams & Wilkins – Wolters Kluwer, Philadelphia, Pennsylvania, U.S.A., 2007).
2. Coffin, J., Hughes, S. & Varmus, H. Retroviridae. in *Virus Taxonomy: Ninth Report of the International Committee on Taxonomy of Viruses* 477–495 (Elsevier Academic Press, San Diego, California, U.S.A., 2011).
3. Myers, G. *et al.* Human Retroviruses and AIDS. A compilation and analysis of nucleic acid and amino acid sequences. (1993).
4. Takehisa, J. *et al.* Origin and Biology of Simian Immunodeficiency Virus in Wild-Living Western Gorillas. *J Virol* **83**, 1635–1648 (2009).
5. Sharp, P. M. & Hahn, B. H. The evolution of HIV-1 and the origin of AIDS. *Philosophical Transactions of the Royal Society B: Biological Sciences* vol. 365 2487–2494 Preprint at https://doi.org/10.1098/rstb.2010.0031 (2010).
6. Woodburn, B., Emery, A. & Swanstrom, R. Human Immunodeficiency Virus (Retroviridae). in *Encyclopedia of Virology (Fourth Edition)* vols 1–5 460–474 (Elsevier, 2020).
7. Van Heuverswyn, F. *et al.* Human immunodeficiency viruses: SIV infection in wild gorillas. *Nature* **444**, 164 (2006).
8. Santiago, M. L. *et al.* Simian Immunodeficiency Virus Infection in Free-Ranging Sooty Mangabeys (Cercocebus atys atys) from the Taï Forest, Côte d'Ivoire: Implications for the Origin of Epidemic Human Immunodeficiency Virus Type 2 . *J Virol* **79**, 12515–12527 (2005).
9. Marx, P. A., Alcabes, P. G. & Drucker, E. Serial human passage of simian immunodeficiency virus by unsterile injections and the emergence of epidemic human immunodeficiency virus in Africa. in *Philosophical Transactions of the Royal Society B: Biological Sciences* vol. 356 911–920 (Royal Society, 2001).
10. Murphy, R. L. & Phair, J. P. AIDS. *Compr Ther* **14**, 3–12 (1988).
11. Shafer, R. W. & Vuitton, D. A. Highly active antiretroviral therapy (Haart) for the treatment of infection with human immunodeficiency virus type 1. *Biomedicine & Pharmacotherapy* **53**, 73–86 (1999).
12. Morales, D. R., Moreno-Martos, D., Matin, N. & McGettigan, P. Health conditions in adults with HIV compared with the general population: A population-based cross-sectional analysis. *EClinicalMedicine* **47**, 101392 (2022).
13. Joint United Nations Programme on HIV/AIDS (UNAIDS). *Fact Sheet 2024: Latest Global and Regional HIV Statistics.* (2024).
14. Vogt, P. Historical introduction to the general properties of retroviruses. in *Retroviruses* (eds. Coffin, J., Hughes, S. & Varmus, H.) 1–26 (Cold Spring Harbor Laboratory Press, Cold Spring Harbor, New York, U.S.A., 1997).
15. Anderson, J. L. & Hope, T. J. HIV Accessory Proteins and Surviving the Host Cell. *Curr HIV/AIDS Rep* 47–53 (2004).

16. Laguette, N. & Benkirane, M. Shaping of the host cell by viral accessory proteins. *Front Microbiol* **6**, (2015).
17. Bukrinsky, M. & Adzhubei, A. Viral protein R of HIV-1. *Rev Med Virol* **9**, 39–49 (1999).
18. Li, L., Li, H. S., Pauza, D., Bukrinsky, M. & Zhao, R. Y. Roles of HIV-1 auxiliary proteins in viral pathogenesis and host-pathogen interactions. *Cell Res* **15**, 923–934 (2005).
19. Kmiec, D. *et al.* Vpu-mediated counteraction of tetherin is a major determinant of HIV-1 interferon resistance. *mBio* **7**, e00934-16 (2016).
20. Staudt, R. P. *et al.* Structure, function, and inhibitor targeting of HIV-1 Nef-effector kinase complexes. *Journal of Biological Chemistry* **295**, 15158–15171 (2020).
21. Li, Y. L. *et al.* The structural basis for HIV-1 Vif antagonism of human APOBEC3G. *Nature* **615**, 728–733 (2023).
22. Gonzalez, M. E. The HIV-1 vpr protein: A multifaceted target for therapeutic intervention. *Int J Mol Sci* **18**, (2017).
23. Wu, Y. *et al.* The DDB1-DCAF1-Vpr-UNG2 crystal structure reveals how HIV-1 Vpr steers human UNG2 toward destruction. *Nat Struct Mol Biol* **23**, 933–939 (2016).
24. Greenwood, E. J. D. *et al.* Promiscuous Targeting of Cellular Proteins by Vpr Drives Systems-Level Proteomic Remodeling in HIV-1 Infection. *Cell Rep* **27**, 1579-1596.e7 (2019).
25. Romani, B. & Cohen, É. A. Lentivirus Vpr and Vpx accessory proteins usurp the cullin4-DDB1 (DCAF1) E3 ubiquitin ligase. *Curr Opin Virol* **2**, 755–763 (2012).
26. Ahn, J. *et al.* HIV-1 Vpr loads uracil DNA glycosylase-2 onto DCAF1, a substrate recognition subunit of a cullin 4A-RING E3 ubiquitin ligase for proteasome-dependent degradation. *Journal of Biological Chemistry* **285**, 37333–37341 (2010).
27. Naamati, A. *et al.* Functional proteomic atlas of HIV infection in primary human CD4+ T cells. *Elife* https://doi.org/10.7554/eLife.41431.001 (2019) doi:10.7554/eLife.41431.001.
28. Schröfelbauer, B., Hakata, Y. & Landau, N. R. HIV-1 Vpr function is mediated by interaction with the damage-specific DNA-binding protein DDB1. *Proc Natl Acad Sci U S A* **104**, 4130–4135 (2007).
29. Bredbenner, K. & Simon, S. M. Vpr Co-assembles with Gag during HIV-1 Assembly. *bioRxiv* https://doi.org/10.1101/2020.03.23.004689 (2020) doi:10.1101/2020.03.23.004689.
30. Berkowitz, R. D. *et al.* CCR5-and CXCR4-Utilizing Strains of Human Immunodeficiency Virus Type 1 Exhibit Differential Tropism and Pathogenesis In Vivo. *J Virol* **72**, 10108–10117 (1998).
31. Berkowitz, R. D. *et al.* R5 Strains of Human Immunodeficiency Virus Type 1 from Rapid Progressors Lacking X4 Strains Do Not Possess X4-Type Pathogenicity in Human Thymus. *J Virol* (1999).
32. Duquenne, C. *et al.* The Two Human CXCR4 Isoforms Display Different HIV Receptor Activities: Consequences for the Emergence of X4 Strains. *The Journal of Immunology* **193**, 4188–4194 (2014).
33. Fouchier, R. A. M. & Malim, M. H. Nuclear Import of HIV-1 Preintegration Complexes. in *Advances in Virus Research* vol. 52 275–299 (Academic Press, 1999).

34. Fouchier, R. A. M. *et al.* Interaction of the Human Immunodeficiency Virus Type 1 Vpr Protein with the Nuclear Pore Complex. *J Virol* **72**, 6004–6013 (1998).
35. Müller, T. G., Zila, V., Müller, B. & Kräusslich, H.-G. Nuclear Capsid Uncoating and Reverse Transcription of HIV-1. *Annu Rev Virol* **9**, 261–284 (2022).
36. Cullen, B. & Hughes, H. Journey to the Center of the Cell. *Cell* **105**, 697–700 (2001).
37. Le Rouzic, E. & Benichou, S. The Vpr protein from HIV-1: Distinct roles along the viral life cycle. *Retrovirology* vol. 2 Preprint at https://doi.org/10.1186/1742-4690-2-11 (2005).
38. Hrecka, K. *et al.* HIV-1 and HIV-2 exhibit divergent interactions with HLTF and UNG2 DNA repair proteins. *Proc Natl Acad Sci U S A* **113**, E3921–E3930 (2016).
39. Wen, X., Klockow, L., Nekorchuk, M., Sharifi, H. J. & de Noronha, C. M. C. The HIV1 protein Vpr acts to enhance constitutive DCAF1-dependent UNG2 turnover. *PLoS One* **7**, (2012).
40. Schröfelbauer, B., Yu, Q., Zeitlin, S. G. & Landau, N. R. Human Immunodeficiency Virus Type 1 Vpr Induces the Degradation of the UNG and SMUG Uracil-DNA Glycosylases. *J Virol* **79**, 10978–10987 (2005).
41. Zhou, D. *et al.* The HIV-1 accessory protein Vpr induces the degradation of the anti-HIV-1 agent APOBEC3G through a VprBP-mediated proteasomal pathway. *Virus Res* **195**, 25–34 (2015).
42. Ajoge, H. O. *et al.* Antiretroviral APOBEC3 cytidine deaminases alter HIV-1 provirus integration site profiles. *Nat Commun* **14**, (2023).
43. Yan, J. *et al.* HIV-1 Vpr Reprograms CLR4 DCAF1 E3 Ubiquitin Ligase to Antagonize Exonuclease 1-Mediated Restriction of HIV-1 Infection. *mBio* **9**, e01732-18 (2018).
44. Lahouassa, H. *et al.* HIV-1 Vpr degrades the HLTF DNA translocase in T cells and macrophages. *Proc Natl Acad Sci U S A* **113**, 5311–5316 (2016).
45. Yan, J., Shun, M. C., Zhang, Y., Hao, C. & Skowronski, J. HIV-1 Vpr counteracts HLTF-mediated restriction of HIV-1 infection in T cells. *Proc Natl Acad Sci U S A* **116**, 9568–9577 (2019).
46. Zhou, X. *et al.* HIV-1 Vpr protein directly loads helicase-like transcription factor (HLTF) onto the CRL4-DCAF1 E3 ubiquitin ligase. *Journal of Biological Chemistry* **292**, 21117–21127 (2017).
47. Blanco-Rodriguez, G. *et al.* Remodeling of the Core Leads HIV-1 Preintegration Complex into the Nucleus of Human Lymphocytes. *J Virol* **94**, e00135-20 (2020).
48. Sapp, N. *et al.* HIV-1 Preintegration Complex Preferentially Integrates the Viral DNA into Nucleosomes Containing Trimethylated Histone 3-Lysine 36 Modification and Flanking Linker DNA. *J Virol* **96**, (2022).
49. Bhardwaj, V. *et al.* HIV-1 Vpr induces ciTRAN to prevent transcriptional repression of the provirus. *Sci Adv* **9**, (2023).
50. Forouzanfar, F. *et al.* HIV-1 Vpr mediates the depletion of the cellular repressor CTIP2 to counteract viral gene silencing. *Sci Rep* **9**, (2019).
51. Hofmann, S. *et al.* Dual role of the chromatin-binding factor PHF13 in the pre- and post-integration phases of HIV-1 replication. *Open Biol* **7**, (2017).

52. Rossi, F. *et al.* Connecting the Dots: PHF13 and cohesin promote polymer-polymer phase separation of chromatin into chromosomes. *bioRxiv* https://doi.org/10.1101/2022.03.04.482956 (2022) doi:10.1101/2022.03.04.482956.
53. Chung, H.-R. *et al.* PHF13 is a molecular reader and transcriptional co-regulator of H3K4me2/3. *Elife* **5**, (2016).
54. Nikolaitchik, O. A. *et al.* HIV-1 usurps transcription start site heterogeneity of host RNA polymerase II to maximize replication fitness. *Proc Natl Acad Sci U S A* **120**, (2023).
55. Dutilleul, A., Rodari, A. & Van Lint, C. Depicting HIV-1 transcriptional mechanisms: A summary of what we know. *Viruses* **12**, (2020).
56. Chen, J. *et al.* Transcriptome analysis of CD4+ T cells from HIV-infected individuals receiving ART with LLV revealed novel transcription factors regulating HIV-1 promoter activity. *Virol Sin* **38**, 398–408 (2023).
57. Thieu, K. P. *et al.* HIV-1 Vpr: Regulator of Viral Survival. *Curr HIV Res* **7**, 153–162 (2009).
58. McAllister, J. J. *et al.* Analysis of the HIV-1 LTR NF-κB-proximal Sp site III: Evidence for cell type-specific gene regulation and viral replication. *Virology* **274**, 262–277 (2000).
59. McAllister, J. J. *et al.* Altered recruitment of Sp isoforms to HIV-1 long terminal repeat between differentiated monoblastic cell lines and primary monocyte-derived macrophages. *Frontiers in Virology* **2**, (2022).
60. Goh, W. C., Manel, N. & Emerman, M. The human immunodeficiency virus Vpr protein binds Cdc25C: Implications for G2 arrest. *Virology* **318**, 337–349 (2004).
61. Goh, W. C. *et al.* HIV-1 Vpr increases viral expression by manipulation of the cell cycle: A mechanism for selection of Vpr in vivo. *Nat Med* **4**, 65–71 (1998).
62. Brasey, A. *et al.* The Leader of Human Immunodeficiency Virus Type 1 Genomic RNA Harbors an Internal Ribosome Entry Segment That Is Active during the G 2 /M Phase of the Cell Cycle. *J Virol* **77**, 3939–3949 (2003).
63. Andersen, J. L., Le Rouzic, E. & Planelles, V. HIV-1 Vpr: Mechanisms of G2 arrest and apoptosis. *Exp Mol Pathol* **85**, 2–10 (2008).
64. Zhang, F. & Bieniasz, P. D. HIV-1 Vpr induces cell cycle arrest and enhances viral gene expression by depleting CCDC137. *Elife* **9**, e55806-22 (2020).
65. Bruce, J. W., Bracken, M., Evans, E., Sherer, N. & Ahlquist, P. ZBTB2 represses HIV-1 transcription and is regulated by HIV-1 Vpr and cellular DNA damage responses. *PLoS Pathog* **17**, (2021).
66. Li, D., Lopez, A., Sandoval, C., Doyle, R. N. & Fregoso, O. I. HIV Vpr Modulates the Host DNA Damage Response at Two Independent Steps to Damage DNA and Repress Double-Strand DNA Break Repair. *mBio* **11**, e00940-20 (2020).
67. Nakai-Murakami, C. *et al.* HIV-1 Vpr induces ATM-dependent cellular signal with enhanced homologous recombination. *Oncogene* **26**, 477–486 (2007).
68. Laguette, N. *et al.* Premature activation of the SLX4 complex by Vpr promotes G2/M arrest and escape from innate immune sensing. *Cell* **156**, 134–145 (2014).

69. Zhou, X., Monnie, C., DeLucia, M. & Ahn, J. HIV-1 Vpr activates host CRL4-DCAF1 E3 ligase to degrade histone deacetylase SIRT7. *Virol J* **18**, (2021).
70. Byeon, I. J. L. *et al.* Structure of HIV-1 Vpr in complex with the human nucleotide excision repair protein hHR23A. *Nat Commun* **12**, (2021).
71. Chutiwitoonchai, N. *et al.* HIV-1 Vpr abrogates the effect of TSG101 overexpression to support virus release. *PLoS One* **11**, (2016).
72. Barbosa, J. A. F., Sparapani, S., Boulais, J., Lodge, R. & Cohen, É. A. Human Immunodeficiency Virus Type 1 Vpr Mediates Degradation of APC1, a Scaffolding Component of the Anaphase-Promoting Complex/Cyclosome. *J Virol* **95**, e0097120 (2021).
73. Zhao, L. *et al.* Vpr counteracts the restriction of LAPTM5 to promote HIV-1 infection in macrophages. *Nat Commun* **12**, (2021).
74. Stark, L. A. & Hay, R. T. Human Immunodeficiency Virus Type 1 (HIV-1) Viral Protein R (Vpr) Interacts with Lys-tRNA Synthetase: Implications for Priming of HIV-1 Reverse Transcription. *J Virol* **72**, 3037–3044 (1998).
75. Kleiman, L. tRNA Lys3 : The Primer tRNA for Reverse Transcription in HIV-1. *IUBMB Life* **53**, 107–114 (2002).
76. Meusser, B., Purfuerst, B. & Luft, F. C. HIV-1 gag release from yeast reveals ESCRT interaction with the gag N-terminal protein region. *Journal of Biological Chemistry* **295**, 17950–17972 (2020).
77. Chen, X. & Wang, X. The HIV-1 gag p6: a promising target for therapeutic intervention. *Retrovirology* vol. 21 Preprint at https://doi.org/10.1186/s12977-024-00633-2 (2024).
78. Varin, A. *et al.* Synthetic Vpr protein activates activator protein-1, c-Jun N-terminal kinase, and NF-κB and stimulates HIV-1 transcription in promonocytic cells and primary macrophages. *Journal of Biological Chemistry* **280**, 42557–42567 (2005).
79. Muthumani, K. *et al.* HIV-1 Vpr induces apoptosis through caspase 9 in T cells and peripheral blood mononuclear cells. *Journal of Biological Chemistry* **277**, 37820–37831 (2002).
80. Vogel, O. A., Forwood, J. K., Leung, D. W., Amarasinghe, G. K. & Basler, C. F. Viral Targeting of Importin Alpha-Mediated Nuclear Import to Block Innate Immunity. *Cells* **13**, 71 (2023).
81. Iwasaki, A. & Medzhitov, R. Regulation of Adaptive Immunity by the Innate Immune System. *Science (1979)* **327**, 291–295 (2010).
82. Wong, L. M. & Jiang, G. NF-κB sub-pathways and HIV cure: A revisit. *EBioMedicine* **63**, (2021).
83. Campbell, G. R., Bruckman, R. S., Chu, Y. L., Trout, R. N. & Spector, S. A. SMAC Mimetics Induce Autophagy-Dependent Apoptosis of HIV-1-Infected Resting Memory CD4+ T Cells. *Cell Host Microbe* **24**, 689-702.e7 (2018).
84. Ayyavoo, V. *et al.* HIV-1 Vpr suppresses immune activation and apoptosis through regulation of nuclear factor KB. *Nat Med* **2**, 1117–1123 (1997).
85. Chintala, K., Mohareer, K. & Banerjee, S. Dodging the Host Interferon-Stimulated Gene Mediated Innate Immunity by HIV-1: A Brief Update on Intrinsic Mechanisms and Counter-Mechanisms. *Front Immunol* **12**, (2021).

86. Kogan, M. *et al.* Inhibition of NF-κB activity by HIV-1 Vpr is dependent on Vpr binding protein. *J Cell Physiol* **228**, 781–790 (2013).
87. Khan, H. *et al.* HIV-1 Vpr antagonizes innate immune activation by targeting karyopherin-mediated NF-κB/IRF3 nuclear transport. *Elife* **9**, 1–29 (2020).
88. Liu, R. *et al.* HIV-1 Vpr stimulates NF-κB and AP-1 signaling by activating TAK1. *Retrovirology* **11**, (2014).
89. Liu, R. *et al.* HIV-1 Vpr activates both canonical and noncanonical NF-κB pathway by enhancing the phosphorylation of IKKα/B. *Virology* **439**, 47–56 (2013).
90. Liang, Z. *et al.* HIV-1 Vpr protein activates the NF-κB pathway to promote G2/M cell cycle arrest. *Virol Sin* **30**, 441–448 (2015).
91. Konrath, F., Willenbrock, M., Busse, D., Scheidereit, C. & Wolf, J. A computational model of the DNA damage-induced IKK/ NF-κB pathway reveals a critical dependence on irradiation dose and PARP-1. *iScience* **26**, (2023).
92. Sandoval, C. & Fregoso, O. I. HIV-1 Vpr-induced DNA damage activates NF-κB independent of cell cycle arrest and CRL4A DCAF1 engagement. *bioRxiv* https://doi.org/10.1101/2023.05.23.541990 (2023) doi:10.1101/2023.05.23.541990.
93. Takeuchi, O. & Akira, S. Innate immunity to virus infection. *Immunological Reviews* vol. 227 75–86 Preprint at https://doi.org/10.1111/j.1600-065X.2008.00737.x (2009).
94. Maheaswari, R., Sivasankar, K. & Subbarayan, S. Toll gates: An emerging therapeutic target. *Journal of Indian Society of Periodontology* vol. 18 686–692 Preprint at https://doi.org/10.4103/0972-124X.147398 (2014).
95. Hou, W. *et al.* Lambda Interferon Inhibits Human Immunodeficiency Virus Type 1 Infection of Macrophages. *J Virol* **83**, 3834–3842 (2009).
96. Liu, M. Q. *et al.* IFN-λ3 inhibits HIV infection of macrophages through the JAK-STAT pathway. *PLoS One* **7**, (2012).
97. Liu, M.-Q. *et al.* Combination antiretroviral therapy (cART) restores HIV-1 infection-mediated impairment of JAK-STAT signaling pathway. *Oncotarget* **8**, 22524–22533 (2017).
98. Nguyen, N. V., Tran, J. T. & Sanchez, D. J. HIV blocks Type I IFN signaling through disruption of STAT1 phosphorylation. *Innate Immun* **24**, 490–500 (2018).
99. Gargan, S. *et al.* HIV-1 Promotes the Degradation of Components of the Type 1 IFN JAK/STAT Pathway and Blocks Anti-viral ISG Induction. *EBioMedicine* **30**, 203–216 (2018).
100. Li, Z. *et al.* Role of TCF/LEF transcription factors in bone development and osteogenesis. *International Journal of Medical Sciences* vol. 15 1415–1422 Preprint at https://doi.org/10.7150/ijms.26741 (2018).
101. Al-Harthi, L. Interplay between Wnt/β-catenin signaling and HIV: Virologic and biologic consequences in the CNS. *Journal of Neuroimmune Pharmacology* vol. 7 731–739 Preprint at https://doi.org/10.1007/s11481-012-9411-y (2012).
102. Doumpas, N. *et al.* TCF / LEF dependent and independent transcriptional regulation of Wnt/β-catenin target genes . *EMBO J* **38**, (2019).

103. Kumar, A. *et al.* Active β-Catenin Signaling Is an Inhibitory Pathway for Human Immunodeficiency Virus Replication in Peripheral Blood Mononuclear Cells. *J Virol* **82**, 2813–2820 (2008).
104. Wortman, B., Darbinian, N., Sawaya, B. E., Khalili, K. & Amini, S. Evidence for Regulation of Long Terminal Repeat Transcription by Wnt Transcription Factor TCF-4 in Human Astrocytic Cells. *J Virol* **76**, 11159–11165 (2002).
105. Henderson, L. J., Narasipura, S. D., Adarichev, V., Kashanchi, F. & Al-Harthi, L. Identification of Novel T Cell Factor 4 (TCF-4) Binding Sites on the HIV Long Terminal Repeat Which Associate with TCF-4, β-Catenin, and SMAR1 To Repress HIV Transcription. *J Virol* **86**, 9495–9503 (2012).
106. Barbian, H. J. *et al.* β-catenin regulates HIV latency and modulates HIV reactivation. *PLoS Pathog* **18**, (2022).
107. Weiser, K., Barton, M., Gershoony, D., DasGupta, R. & Cardozo, T. HIV's Nef Interacts with β-Catenin of the Wnt Signaling Pathway in HEK293 Cells. *PLoS One* **8**, (2013).
108. Henderson, L. J., Sharma, A., Monaco, M. C. G., Major, E. O. & Al-Harthi, L. Human immunodeficiency virus type 1 (HIV-1) transactivator of transcription through its intact core and cysteine-rich domains inhibits wnt/β-catenin signaling in astrocytes: Relevance to HIV neuropathogenesis. *Journal of Neuroscience* **32**, 16306–16313 (2012).
109. Okumura, A. *et al.* HIV-1 accessory proteins VPR and Vif modulate antiviral response by targeting IRF-3 for degradation. *Virology* **373**, 85–97 (2008).
110. Lee, J. U., Kim, L. K. & Choi, J. M. Revisiting the concept of targeting NFAT to control T cell immunity and autoimmune diseases. *Front Immunol* **9**, (2018).
111. Maciá, F. *et al. Transcriptional Mechanisms Underlying Lymphocyte Tolerance Activation of the Cell-Intrinsic Mechanism of Lympho-Cyte Tolerance Is Closely Linked to the Cell-Surface Stimu-Lus Received. In Both T and B Cells, Combined Activation*. *Cell* vol. 109 http://www.cell.com/cgi/ (2002).
112. Höhne, K. *et al.* Virion encapsidated HIV-1 Vpr induces NFAT to prime non-activated T cells for productive infection. *Open Biol* **6**, (2016).
113. Riback, J. A. *et al.* Stress-Triggered Phase Separation Is an Adaptive, Evolutionarily Tuned Response. *Cell* **168**, 1028-1040.e19 (2017).
114. Molliex, A. *et al.* Phase Separation by Low Complexity Domains Promotes Stress Granule Assembly and Drives Pathological Fibrillization. *Cell* **163**, 123–133 (2015).
115. Onomoto, K., Yoneyama, M., Fung, G., Kato, H. & Fujita, T. Antiviral innate immunity and stress granule responses. *Trends in Immunology* vol. 35 420–428 Preprint at https://doi.org/10.1016/j.it.2014.07.006 (2014).
116. Boncella, A. E. *et al.* Composition-based prediction and rational manipulation of prion-like domain recruitment to stress granules. *Proc Natl Acad Sci U S A* **117**, 5826–5835 (2020).
117. Fomicheva, A. & Ross, E. D. From prions to stress granules: Defining the compositional features of prion-like domains that promote different types of assemblies. *International Journal of Molecular Sciences* vol. 22 1–19 Preprint at https://doi.org/10.3390/ijms22031251 (2021).

118. Markmiller, S. *et al.* Context-Dependent and Disease-Specific Diversity in Protein Interactions within Stress Granules. *Cell* **172**, 590-604.e13 (2018).
119. Freibaum, B. D. *et al.* Identification of small molecule inhibitors of G3BP-driven stress granule formation. *Journal of Cell Biology* **223**, (2024).
120. Millar, S. R. *et al.* A New Phase of Networking: The Molecular Composition and Regulatory Dynamics of Mammalian Stress Granules. *Chemical Reviews* vol. 123 9036–9064 Preprint at https://doi.org/10.1021/acs.chemrev.2c00608 (2023).
121. Kedersha, N. *et al.* G3BP-Caprin1-USP10 complexes mediate stress granule condensation and associate with 40S subunits. *Journal of Cell Biology* **212**, 845–860 (2016).
122. Guillén-Boixet, J. *et al.* RNA-Induced Conformational Switching and Clustering of G3BP Drive Stress Granule Assembly by Condensation. *Cell* **181**, 346-361.e17 (2020).
123. Matsuki, H. *et al.* Both G3BP1 and G3BP2 contribute to stress granule formation. *Genes to Cells* **18**, 135–146 (2013).
124. Freibaum, B. D., Messing, J., Yang, P., Kim, H. J. & Taylor, J. P. High-fidelity reconstitution of stress granules and nucleoli in mammalian cellular lysate. *Journal of Cell Biology* **220**, (2021).
125. Gilks, N. *et al.* Stress Granule Assembly Is Mediated by Prion-like Aggregation of TIA-1. *Mol Biol Cell* **15**, 5383–5398 (2004).
126. Reineke, L. C. & Lloyd, R. E. The Stress Granule Protein G3BP1 Recruits Protein Kinase R To Promote Multiple Innate Immune Antiviral Responses. *J Virol* **89**, 2575–2589 (2015).
127. Yang, W. *et al.* G3BP1 inhibits RNA virus replication by positively regulating RIG-I-mediated cellular antiviral response. *Cell Death Dis* **10**, (2019).
128. Rehwinkel, J. & Gack, M. U. RIG-I-like receptors: their regulation and roles in RNA sensing. *Nature Reviews Immunology* vol. 20 537–551 Preprint at https://doi.org/10.1038/s41577-020-0288-3 (2020).
129. Matz, K. M., Guzman, R. M. & Goodman, A. G. The Role of Nucleic Acid Sensing in Controlling Microbial and Autoimmune Disorders. in *International Review of Cell and Molecular Biology* vol. 345 35–136 (Elsevier Inc., 2019).
130. Li, W. *et al.* Cell Proteins TIA-1 and TIAR Interact with the 3′ Stem-Loop of the West Nile Virus Complementary Minus-Strand RNA and Facilitate Virus Replication. *J Virol* **76**, 11989–12000 (2002).
131. Michallet, M. C., Rota, G., Maslowski, K. & Guarda, G. Innate receptors for adaptive immunity. *Current Opinion in Microbiology* vol. 16 296–302 Preprint at https://doi.org/10.1016/j.mib.2013.04.003 (2013).
132. Valiente-Echeverría, F. *et al.* EEF2 and Ras-GAP SH3 domain-binding protein (G3BP1) modulate stress granule assembly during HIV-1 infection. *Nat Commun* **5**, (2014).
133. Rao, S. *et al.* HIV-1 NC-induced stress granule assembly and translation arrest are inhibited by the dsRNA binding protein Staufen1. *RNA* **24**, (2018).
134. Wickham, H. Data Analysis. in *Use R!* 189–201 (Springer, 2016). doi:10.1007/978-3-319-24277-4_9.

135. Yu, G. & Gao, C.-H. enrichplot: Visualization of Functional Enrichment Result. *R package version 1.28.4* (2025).
136. Yu, G. Thirteen years of clusterProfiler. *The Innovation* **5**, 100722 (2024).
137. Xu, S. *et al.* Using clusterProfiler to characterize multiomics data. *Nat Protoc* **19**, 3292–3320 (2024).
138. Wu, T. *et al.* clusterProfiler 4.0: A universal enrichment tool for interpreting omics data. *The Innovation* **2**, 100141 (2021).
139. Yu, G., Wang, L.-G., Han, Y. & He, Q.-Y. clusterProfiler: an R Package for Comparing Biological Themes Among Gene Clusters. *OMICS* **16**, 284–287 (2012).
140. Hiebenthal-Millow, K. & Kirchhoff, F. The most frequent naturally occurring length polymorphism in the HIV-1 LTR has little effect on proviral transcription and viral replication. *Virology* **292**, 169–175 (2002).
141. Rücker, E., Grivel, J.-C., Münch, J., Kirchhoff, F. & Margolis, L. Vpr and Vpu Are Important for Efficient Human Immunodeficiency Virus Type 1 Replication and CD4 + T-Cell Depletion in Human Lymphoid Tissue Ex Vivo . *J Virol* **78**, 12689–12693 (2004).
142. Pham, T. N. Q., Richard, J., Gerard, F. C. A., Power, C. & Cohen, É. A. Modulation of NKG2D-Mediated Cytotoxic Functions of Natural Killer Cells by Viral Protein R from HIV-1 Primary Isolates. *J Virol* **85**, 12254–12261 (2011).
143. Banning, C. *et al.* A flow cytometry-based FRET assay to identify and analyse protein-protein interactions in living cells. *PLoS One* **5**, (2010).
144. Belzile, J. P. *et al.* HIV-1 Vpr-mediated G2 arrest involves the DDB1-CUL4AVPRBP E3 ubiquitin ligase. *PLoS Pathog* **3**, 0882–0893 (2007).
145. Livak, K. J. & Schmittgen, T. D. Analysis of relative gene expression data using real-time quantitative PCR and the 2-ΔΔCT method. *Methods* **25**, 402–408 (2001).
146. Love, M. I., Huber, W. & Anders, S. Moderated estimation of fold change and dispersion for RNA-seq data with DESeq2. *Genome Biol* **15**, (2014).
147. Reuschl, A. K. *et al.* HIV-1 Vpr drives a tissue residency-like phenotype during selective infection of resting memory T cells. *Cell Rep* **39**, (2022).
148. Zhou, Y. *et al.* Metascape provides a biologist-oriented resource for the analysis of systems-level datasets. *Nat Commun* **10**, (2019).
149. Rajan, D., Wildum, S., Rü, E., Schindler, M. & Kirchhoff, F. Effect of R77Q, R77A and R80A changes in Vpr on HIV-1 replication and CD4 T cell depletion in human lymphoid tissue ex vivo. *AIDS* **20**, 831–836 (2006).
150. Cadigan, K. M. & Waterman, M. L. TCF/LEFs and Wnt signaling in the nucleus. *Cold Spring Harb Perspect Biol* **4**, (2012).
151. Zhang, K. *et al.* Stress Granule Assembly Disrupts Nucleocytoplasmic Transport. *Cell* **173**, 958-971.e17 (2018).
152. Yang, P. *et al.* G3BP1 Is a Tunable Switch that Triggers Phase Separation to Assemble Stress Granules. *Cell* **181**, 325-345.e28 (2020).

153. Ratner, L. *et al.* Complete nucleotide sequence of the AIDS virus, HTLV-III. *Nature* 277–284 (1985) doi:https://doi.org/10.1038/313277a0.
154. Dedera, D., Hu, W., Van der Heyden, N. & Ratner, L. Viral Protein R of Human Immunodeficiency Virus Types 1 and 2 Is Dispensable for Replication and Cytopathogenicity in Lymphoid Cells. *J Virol* **63**, 3205–3208 (1989).
155. Haile, W. B. *et al.* The Janus kinase inhibitor ruxolitinib reduces HIV replication in human macrophages and ameliorates HIV encephalitis in a murine model. *Neurobiol Dis* **92**, 137–143 (2016).
156. Gavegnano, C. *et al.* Ruxolitinib and tofacitinib are potent and selective inhibitors of HIV-1 replication and virus reactivation in vitro. *Antimicrob Agents Chemother* **58**, 1977–1986 (2014).
157. Bovolenta, C. *et al.* Constitutive Activation of STATs Upon In Vivo Human Immunodeficiency Virus Infection. *Blood* **94**, 4202–4209 (1999).
158. Ding, Z. C. *et al.* Persistent STAT5 activation reprograms the epigenetic landscape in CD4+ T cells to drive polyfunctionality and antitumor immunity. *Sci Immunol* **5**, (2020).
159. Mutascio, S. *et al.* CD8+ T cells promote HIV latency by remodeling CD4+ T cell metabolism to enhance their survival, quiescence, and stemness. *Immunity* **56**, 1132-1147.e6 (2023).
160. Kumar, N. A. *et al.* The role of antigen presenting cells in the induction of HIV-1 latency in resting CD4+ T-cells. *Retrovirology* **12**, (2015).
161. Battistini, A., Marsili, G., Sgarbanti, M., Ensoli, B. & Hiscott, J. IRF Regulation of HIV-1 Long Terminal Repeat Activity. *Journal of Interferon and Cytokine Research* **22**, 27–37 (2002).
162. Wang, L. *et al.* The multiple roles of interferon regulatory factor family in health and disease. *Signal Transduct Target Ther* **9**, 282 (2024).
163. Al Hamrashdi, M. & Brady, G. Regulation of IRF3 activation in human antiviral signaling pathways. *Biochem Pharmacol* **200**, (2022).
164. Doehle, B. P. *et al.* Vpu Mediates Depletion of Interferon Regulatory Factor 3 during HIV Infection by a Lysosome-Dependent Mechanism. *J Virol* **86**, 8367–8374 (2012).
165. Vallabhapurapu, S. & Karin, M. Regulation and function of NF-κB transcription factors in the immune system. *Annual Review of Immunology* vol. 27 693–733 Preprint at https://doi.org/10.1146/annurev.immunol.021908.132641 (2009).
166. Vanegas-Torres, C. A. & Schindler, M. HIV-1 Vpr Functions in Primary CD4+ T Cells. *Viruses* **16**, (2024).
167. Dharan, A. *et al.* KIF5B and Nup358 Cooperatively Mediate the Nuclear Import of HIV-1 during Infection. *PLoS Pathog* **12**, (2016).
168. Lelek, M. *et al.* Superresolution imaging of HIV in infected cells with FlAsH-PALM. *Proc Natl Acad Sci U S A* **109**, 8564–8569 (2012).
169. Heusinger, E. & Kirchhoff, F. Primate lentiviruses modulate NF-HIV, SIV, NF-κB, Nef, Vpu, Tat, LTRB activity by multiple mechanisms to fine-tune viral and cellular gene expression. *Front Microbiol* **8**, (2017).

170. López-Cabrera, M. *et al.* Transcriptional regulation of the gene encoding the human C-type lectin leukocyte receptor AIM/CD69 and functional characterization of its tumor necrosis factor-α-responsive elements. *Journal of Biological Chemistry* **270**, 21545–21551 (1995).
171. Cibrián, D. & Sánchez-Madrid, F. CD69: from activation marker to metabolic gatekeeper. *European Journal of Immunology* vol. 47 946–953 Preprint at https://doi.org/10.1002/eji.201646837 (2017).
172. Pitsios, C., Dimitrakopoulou, A., Tsalimalma, K., Kordossis, T. & Choremi-Papadopoulou, H. Expression of CD69 on T-cell subsets in HIV-1 disease. *Scand J Clin Lab Invest* **68**, 233–241 (2008).
173. Murray, J. M., Kelleher, A. D. & Cooper, D. A. Timing of the Components of the HIV Life Cycle in Productively Infected CD4 + T Cells in a Population of HIV-Infected Individuals . *J Virol* **85**, 10798–10805 (2011).
174. Donahue, D. A. *et al.* Stage-dependent inhibition of HIV-1 replication by antiretroviral drugs in cell culture. *Antimicrob Agents Chemother* **54**, 1047–1054 (2010).
175. Gargan, S. *et al.* HIV-1 Promotes the Degradation of Components of the Type 1 IFN JAK/STAT Pathway and Blocks Anti-viral ISG Induction. *EBioMedicine* **30**, 203–216 (2018).
176. Hammel, J. H., Cook, S. R., Belanger, M. C., Munson, J. M. & Pompano, R. R. Modeling Immunity in Vitro: Slices, Chips, and Engineered Tissues. *Annual Review of Biomedical Engineering* vol. 23 461–491 Preprint at https://doi.org/10.1146/annurev-bioeng-082420-124920 (2021).
177. Lahti, A. L., Manninen, A. & Saksela, K. Regulation of T cell activation by HIV-1 accessory proteins: Vpr acts via distinct mechanisms to cooperate with Nef in NFAT-directed gene expression and to promote transactivation by CREB. *Virology* **310**, 190–196 (2003).
178. Kitamura, N. & Kaminuma, O. Isoform-selective nfat inhibitor: Potential usefulness and development. *International Journal of Molecular Sciences* vol. 22 1–14 Preprint at https://doi.org/10.3390/ijms22052725 (2021).
179. Yu, D., Wang, W., Yoder, A., Spear, M. & Wu, Y. The HIV envelope but not VSV glycoprotein is capable of mediating HIV latent infection of resting CD4 T cells. *PLoS Pathog* **5**, (2009).
180. Bauby, H. *et al.* HIV-1 Vpr induces widespread transcriptomic changes in CD4+ T cells early postinfection. *mBio* **12**, e0136921 (2021).
181. Langer, S. *et al.* HIV-1 Vpu is a potent transcriptional suppressor of NF-kB-elicited antiviral immune responses. *Elife* **8**, (2019).
182. Sherrill-Mix, S., Ocwieja, K. E. & Bushman, F. D. Gene activity in primary T cells infected with HIV89.6: Intron retention and induction of genomic repeats. *Retrovirology* **12**, (2015).
183. Imbeault, M., Giguère, K., Ouellet, M. & Tremblay, M. J. Exon Level Transcriptomic Profiling of HIV-1-Infected CD4+ T Cells Reveals Virus-Induced Genes and Host Environment Favorable for Viral Replication. *PLoS Pathog* **8**, (2012).
184. Selliah, N. & Finkel, T. H. HIV-1 NL4-3, but not IIIB, inhibits JAK3/STAT5 activation in CD4+ T cells. *Virology* **286**, 412–421 (2001).

185. Li, X. *et al.* Infection by Diverse HIV-1 Subtypes Leads to Different Elevations in HERV-K Transcriptional Levels in Human T Cell Lines. *Front Microbiol* **12**, (2021).
186. Clark, I. C. *et al.* HIV silencing and cell survival signatures in infected T cell reservoirs. *Nature* **614**, 318–325 (2023).
187. Zhang, Y. *et al.* HIV-1 diversity in viral reservoirs obtained from circulating T-cell subsets during early ART and beyond. *PLoS Pathog* **20**, e1012526 (2024).
188. Blank, C. U. *et al.* Defining 'T cell exhaustion'. *Nat Rev Immunol* **19**, 665–674 (2019).
189. Martinez, G. J. *et al.* The Transcription Factor NFAT Promotes Exhaustion of Activated CD8+ T Cells. *Immunity* **42**, 265–278 (2015).
190. Shin, D. S. *et al.* Regulatory T cells suppress CD 4 + T cells through NFAT -dependent transcriptional mechanisms . *EMBO Rep* **15**, 991–999 (2014).
191. Soto-Nieves, N. *et al.* Transcriptional complexes formed by NFAT dimers regulate the induction of T cell tolerance. *Journal of Experimental Medicine* **206**, 867–876 (2009).
192. Chen, J. *et al.* NR4A transcription factors limit CAR T cell function in solid tumours. *Nature* **567**, 530–534 (2019).
193. Ames, R. Y., Ting, L. M., Gendlina, I., Kim, K. & Macian, F. The transcription factor NFAT1 participates in the induction of CD4+ T cell functional exhaustion during Plasmodium yoelii infection. *Infect Immun* **85**, (2017).
194. Yao, C. *et al.* Single-cell RNA-seq reveals TOX as a key regulator of CD8+ T cell persistence in chronic infection. *Nat Immunol* **20**, 890–901 (2019).
195. Khan, O. *et al.* TOX transcriptionally and epigenetically programs CD8+ T cell exhaustion. *Nature* **571**, 211–218 (2019).
196. Seo, H. *et al.* TOX and TOX2 transcription factors cooperate with NR4A transcription factors to impose CD8+ T cell exhaustion. *Proc Natl Acad Sci U S A* **116**, 12410–12415 (2019).
197. Scott, A. C. *et al.* TOX is a critical regulator of tumour-specific T cell differentiation. *Nature* **571**, 270–274 (2019).
198. Alfei, F. *et al.* TOX reinforces the phenotype and longevity of exhausted T cells in chronic viral infection. *Nature* **571**, 265–269 (2019).
199. Sekar, R. B. & Periasamy, A. Fluorescence resonance energy transfer (FRET) microscopy imaging of live cell protein localizations. *Journal of Cell Biology* vol. 160 629–633 Preprint at https://doi.org/10.1083/jcb.200210140 (2003).
200. Chang, H. *et al.* Distinct MCM10 proteasomal degradation profiles by primate lentiviruses Vpr proteins. *Viruses* **12**, (2020).
201. Zeitlin, S. G. *et al.* Uracil DNA N-glycosylase promotes assembly of human centromere protein A. *PLoS One* **6**, (2011).
202. Romani, B., Baygloo, N. S., Aghasadeghi, M. R. & Allahbakhshi, E. HIV-1 Vpr protein enhances proteasomal degradation of MCM10 DNA replication factor through the Cul4-DDB1[VprBP] E3 ubiquitin ligase to induce G2/M cell cycle arrest. *Journal of Biological Chemistry* **290**, 17380–17389 (2015).

203. Lv, L. *et al.* Vpr Targets TET2 for Degradation by CRL4 VprBP E3 Ligase to Sustain IL-6 Expression and Enhance HIV-1 Replication. *Mol Cell* **70**, 961-970.e5 (2018).
204. Jarboui, M. A. *et al.* Nucleolar Protein Trafficking in Response to HIV-1 Tat: Rewiring the Nucleolus. *PLoS One* **7**, (2012).
205. Niehrs, C. The complex world of WNT receptor signalling. *Nature Reviews Molecular Cell Biology* vol. 13 767–779 Preprint at https://doi.org/10.1038/nrm3470 (2012).
206. Iijima, S. *et al.* Nuclear localization of Vpr is crucial for the efficient replication of HIV-1 in primary CD4 + T cells. *Virology* **327**, 249–261 (2004).
207. Dybas, J. M. *et al.* Integrative proteomics reveals an increase in non-degradative ubiquitylation in activated CD4+ T cells. *Nat Immunol* **20**, 747–755 (2019).
208. Wu, H.-M., Wen, H.-C. & Lin, W.-W. *Proteasome Inhibitors Stimulate Interleukin-8 Expression via Ras and Apoptosis Signal-Regulating Kinase-Dependent Extracellular Signal-Related Kinase and c-Jun N-Terminal Kinase Activation*. *Am. J. Respir. Cell Mol. Biol* vol. 27 www.atsjournals.org (2002).
209. Ortiz-Lazareno, P. C. *et al.* MG132 proteasome inhibitor modulates proinflammatory cytokines production and expression of their receptors in U937 cells: Involvement of nuclear factor-κB and activator protein-1. *Immunology* **124**, 534–541 (2008).
210. Dose, M. *et al.* β-Catenin induces T-cell transformation by promoting genomic instability. *Proc Natl Acad Sci U S A* **111**, 391–396 (2014).
211. Grumont, R. *et al.* The Mitogen-Induced Increase in T Cell Size Involves PKC and NFAT Activation of Rel/NF-B-Dependent c-myc Expression unlike the essential role for Rel/NF-B during B cell ontogeny. *Immunity* **21**, (2004).
212. He, T. *et al.* Identification of c-MYC as a Target of the APC Pathway. *Science (1979)* **281**, (1998).
213. Hu, Q. *et al.* JAK/STAT pathway: Extracellular signals, diseases, immunity, and therapeutic regimens. *Frontiers in Bioengineering and Biotechnology* vol. 11 Preprint at https://doi.org/10.3389/fbioe.2023.1110765 (2023).
214. Ren, Z. *et al.* Syndecan-1 promotes Wnt/β-catenin signaling in multiple myeloma by presenting Wnts and R-spondins. *Blood* **131**, 982–994 (2018).
215. Emmanuel, A. O. *et al.* TCF-1 and HEB cooperate to establish the epigenetic and transcription profiles of CD4 + CD8 + thymocytes. *Nat Immunol* **19**, 1366–1378 (2018).
216. Ioannidis, V., Beermann, F., Clevers, H. & Held, W. The β-catenin-TCF-1 pathway ensures CD4 + CD8 + thymocyte survival. *Nat Immunol* **2**, (2001).
217. D'Cruz, L. M., Knell, J., Fujimoto, J. K. & Goldrath, A. W. An essential role for the transcription factor HEB in thymocyte survival, Tcra rearrangement and the development of natural killer T cells. *Nat Immunol* **11**, 240–249 (2010).
218. Huang, Z. *et al. Transcriptional Regulation of CD4 Gene Expression by T Cell Factor-1/-Catenin Pathway*. *The Journal of Immunology* vol. 176 http://journals.aai.org/jimmunol/article-pdf/176/8/4880/1219496/4880.pdf (2006).

219. Xing, S. *et al.* Tcf1 and Lef1 transcription factors establish CD8+ T cell identity through intrinsic HDAC activity. *Nat Immunol* **17**, 695–703 (2016).
220. Castrop, J. *et al.* The Human TCF-1 Gene Encodes a Nuclear DNA-Binding Protein Uniquely Expressed in Normal and Neoplastic T-Lineage Lymphocytes. *Blood* **86**, (1995).
221. Van De Wetering, M., Castrop, J., Korinek, V. & Clevers, H. Extensive Alternative Splicing and Dual Promoter Usage Generate Tcf-1 Protein Isoforms with Differential Transcription Control Properties. *Mol Cell Biol* **16**, 745–752 (1996).
222. Willinger, T. *et al. Human Naive CD8 T Cells Down-Regulate Expression of the WNT Pathway Transcription Factors Lymphoid Enhancer Binding Factor 1 and Transcription Factor 7 (T Cell Factor-1) Following Antigen Encounter In Vitro and In Vivo 1*. *The Journal of Immunology* vol. 176 http://journals.aai.org/jimmunol/article-pdf/176/3/1439/1217477/1439.pdf (2006).
223. Choi, Y. S. *et al.* LEF-1 and TCF-1 orchestrate TFH differentiation by regulating differentiation circuits upstream of the transcriptional repressor Bcl6. *Nat Immunol* **16**, 980–990 (2015).
224. Botafogo, V. *et al.* Age Distribution of Multiple Functionally Relevant Subsets of CD4+ T Cells in Human Blood Using a Standardized and Validated 14-Color EuroFlow Immune Monitoring Tube. *Front Immunol* **11**, (2020).
225. Bains, I., Antia, R., Callard, R. & Yates, A. J. Quantifying the development of the peripheral naive CD4 T-cell pool in humans. *Blood* **113**, (2009).
226. Wu, T. *et al.* TCF1 Is Required for the T Follicular Helper Cell Response to Viral Infection. *Cell Rep* **12**, 2099–2110 (2015).
227. Gattinoni, L. *et al.* Wnt signaling arrests effector T cell differentiation and generates CD8 + memory stem cells. *Nat Med* **15**, 808–813 (2009).
228. Im, S. J. *et al.* Defining CD8+ T cells that provide the proliferative burst after PD-1 therapy. *Nature* **537**, 417–421 (2016).
229. Zhou, X. *et al.* Differentiation and Persistence of Memory CD8+ T Cells Depend on T Cell Factor 1. *Immunity* **33**, 229–240 (2010).
230. Zhao, D.-M. *et al.* Constitutive Activation of Wnt Signaling Favors Generation of Memory CD8 T Cells. *The Journal of Immunology* **184**, 1191–1199 (2010).
231. Utzschneider, D. T. *et al.* T Cell Factor 1-Expressing Memory-like CD8+ T Cells Sustain the Immune Response to Chronic Viral Infections. *Immunity* **45**, 415–427 (2016).
232. Groux, H. *et al.* Activation-induced death by apoptosis in CD4+ T cells from human immunodeficiency virus-infected asymptomatic individuals. *Journal of Experimental Medicine* **175**, 331–340 (1992).
233. Lewis, D. E., Tang, D. S., Adu-Oppong, A., Schober, W. & Rodgers, J. R. Anergy and apoptosis in CD8+ T cells from HIV-infected persons. *Journal of Immunology* **153**, 412–20 (1994).
234. Hoshino, S. *et al.* HIV-1 Vpr induces TLR4/MyD88-mediated IL-6 production and reactivates viral production from latency. *J Leukoc Biol* **87**, 1133–1143 (2010).
235. Gougeon, M.-L. *et al.* Programmed Cell Death in AIDS-Related HIV and SIV Infections. *AIDS Res Hum Retroviruses* **9**, (1993).

236. Meyaard, L. *et al.* Programmed Death of T Cells in HIV-1 Infection. *Science (1979)* **257**, 1242 (1992).
237. Oyaizu, N. *et al.* Accelerated Apoptosis in Peripheral Blood Mononuclear Cells (PBMCs) From Human Immunodeficiency Virus Type-1 Infected Patients and in CD4 Cross-Linked PBMCs From Normal Individuals. *Blood* **82**, (1993).
238. Finkel, T. H. *et al.* Apoptosis occurs predominantly in bystander cells and not in productively infected cells of HIV-and SIV-infected lymph nodes. *Nat Med* http://www.nature.com/naturemedicine (1995).
239. Levy, D. N., Refaeli, Y., MacGregor, R. R. & Weiner, D. B. Serum Vpr regulates productive infection and latency of human immunodeficiency virus type 1. *Proc Natl Acad Sci U S A* **91**, 10873–10877 (1994).
240. Obika, S. *et al. Stability and Structural Features of the Duplexes Containing Nucleoside Analogues with a Fixed N-Type Conformation, 2'-O,4'-C-Methyleneribonucleosides*. *Pergamon Tetrahedron Letters* vol. 39 (1998).
241. Van Ravesteyn, T. W. *et al.* LNA modification of single-stranded DNA oligonucleotides allows subtle gene modification in mismatch-repair-proficient cells. *Proc Natl Acad Sci U S A* **113**, 4122–4127 (2016).
242. Yang, P. *et al.* G3BP1 Is a Tunable Switch that Triggers Phase Separation to Assemble Stress Granules. *Cell* **181**, 325-345.e28 (2020).
243. Ettinger, A. & Wittmann, T. Fluorescence live cell imaging. in *Methods in Cell Biology* vol. 123 77–94 (Academic Press Inc., 2014).
244. Gadella, T. W. J. *et al.* mScarlet3: a brilliant and fast-maturing red fluorescent protein. *Nat Methods* **20**, 541–545 (2023).
245. Freibaum, B. D., Messing, J., Yang, P., Kim, H. J. & Taylor, J. P. High-fidelity reconstitution of stress granules and nucleoli in mammalian cellular lysate. *Journal of Cell Biology* **220**, (2021).
246. Eiermann, N., Haneke, K., Sun, Z., Stoecklin, G. & Ruggieri, A. Dance with the Devil: Stress Granules and Signaling in Antiviral Responses. *Viruses* vol. 12 Preprint at https://doi.org/10.3390/v12090984 (2020).
247. Onomoto, K., Yoneyama, M., Fung, G., Kato, H. & Fujita, T. Antiviral innate immunity and stress granule responses. *Trends in Immunology* vol. 35 420–428 Preprint at https://doi.org/10.1016/j.it.2014.07.006 (2014).
248. Rozelle, D. K., Filone, C. M., Kedersha, N. & Connor, J. H. Activation of Stress Response Pathways Promotes Formation of Antiviral Granules and Restricts Virus Replication. *Mol Cell Biol* **34**, 2003–2016 (2014).

X List of Figures

XI Acknowledgements

First and foremost, I would like to acknowledge my principal supervisor, Prof. Dr. Michael Schindler, whose mentorship, advice, and rigorous scientific standards profoundly shaped the direction and quality of this research. His unwavering commitment to excellence has been invaluable at every stage of this endeavor, and I am deeply thankful for the opportunity to work in such an interesting and impactful academic discipline. This appreciation also extends to my secondary supervisor, Prof. Dr. Daniel Sauter, for his unreleting support throughout this journey. Further, I would like to thank the German Research Foundation (DFG), as having performed this study within the framework of the SPP1923 granted me access not only to their generous financial support, but also to many opportunities that have greatly enriched my skillset.

I am indebted to all the members of the Institute for Medical Virology at the University Hospital Tübingen for their collegiality, intellectual engagement, and technical assistance. The stimulating discussions and collective dedication within and across various research groups greatly enriched both the investigative process as well as my own personal and professional development. In particular, I would like to thank Dr. Rishikesh Lotke, whose expert bioinformatic know-how helped shape this research, both by establishing an analytic pipeline for our transcriptomic dataset, as well as by providing me the tools and expertise needed to attain the results achieved by this work.

To all the friends I have made along the way, both within and beyond academia, I extend a heartfelt recognition for your enduring companionship, understanding, and encouragement. Your kindness has been a constant source of strength and comfort, and knowing I do not walk alone sufficed for me to wake up every day with renewed motivation.

This work is also dedicated to my dear family, whose belief in me and my work, even when they did not understand it fully, sustained me through every challenge I faced along the way. Though far away, their love and encouragement have seen me through this journey, and I remain endlessly thankful for their sacrifices and their faith in my goals.

Finally, and above all, the most special thanks go to Iga, the love of my life. It has been a long time since the journey we embarked on separately brought us closely together, eventually leading us down separate but parallel paths. I could not be more grateful for the patience and understanding you have shown me, as well as the selfless love that characterizes my every interaction with you. I have come to grow not only as a scientist, but also as a partner and as a human, in no small measure due to you. The present work is a testament to the fact that love can endure every hardship, and I thank you for being my muse, my confidante, my North Star, and the best friend one could wish for. Ja miłuję cię na zawsze!